UNIVERSITEIT GENT

FACULTY OF SCIENCES

Department of Inorganic and Physical Chemistry
Research group L^3- Luminescent Lanthanide Lab

Synthesis of lanthanide-doped rare-earth vanadates for high-efficiency luminescent materials

Thesis submitted to obtain
the degree of Master of Science in Chemistry by

Micheline D'HOOGE

Academic year 2014 - 2015

Promoter: Prof. Dr. Rik Van Deun
Supervisor: Dr. Anna Kaczmarek

Department of Inorganic and Physical Chemistry
Research group L³- Luminescent Lanthanide Lab

Synthesis of lanthanide-doped rare-earth vanadates for high-efficiency luminescent materials

Thesis submitted to obtain
the degree of Master of Science in Chemistry by

Micheline D'HOOGE

Academic year 2014 - 2015

Promoter: Prof. Dr. Rik Van Deun
Supervisor: Dr. Anna Kaczmarek

Nederlandse samenvatting

Het doel van dit werk was om verschillende vanadaat materialen te synthetiseren via een mircogolf-geassisteerd synthesemethode. Met deze materialen zouden uiteindelijk core/shell deeltjes gemaakt worden, waarvan de core gedoteerd zou worden met een lanthanide ion. Deze core/shell structuur zou de emissie-intensiteit moeten verhogen. De vanadaat materialen waarmee gewerkt zou worden in deze thesis waren yttrium orthovanadaat (YVO_4), gadolinium orthovanadaat ($GdVO_4$) en lanthaan orthovanadaat ($LaVO_4$). Aangezien er vorig jaar in de L^3 groep iemand de synthese van YVO_4 al had geoptimaliseerd, weliswaar via een hydrothermale route met een autoclaaf, werden de reactie condities van dat werk gebruikt voor de microgolf-geassisteerde route. Gelijktijdig werden de andere vanadaat materialen ook gesynthetiseerd. Aangezien de pH condities bij $LaVO_4$ en $GdVO_4$ niet dezelfde waren als voor YVO_4, werd de invloed van de pH in de synthese op de fase en morfologie van de producten zo aangetoond. De producten werden via DRIFTS en XRD gekarakteriseerd.

Na verschillende reactiecondities getest te hebben, werden er voor de YVO_4 en $GdVO_4$ producten zuivere fasen bekomen. Deze werden via SEM gemeten om de grootte en de uniformiteit van de deeltjes te bepalen. Voor deze producten bleek dat de deeltjes niet uniform en klein genoeg zijn om tot core/shell structuren te verwerken. Voor de $LaVO_4$ producten bleek dat de gewenste tetragonale fase niet bekomen werd. De metastabiele tetragonale structuur wordt geprefereerd over de stabiele monokliene structuur, omdat de tetragonale structuur een betere gaststructuur is voor luminescerende lanthanide-ionen. De monokliene producten hadden ook niet de gewenste grootte en uniformiteit om te gebruiken in core/shell structuren. $LaVO_4$ gedoteerd met europium is het minst beschreven product in de literatuur. Daarom werd geopteerd om het monokliene product te doteren. Omdat de producten niet voldeden om te gebruiken voor core/shell deeltjes, werd het idee om core/shell deeltjes te gebruiken aan de kant geschoven.

De reactiecondities van het uitgekozen product werden herhaald voor het gedoteerde product. Deze reactiecondities voor dotering waren: 1 mmol lanthaannitraat, 1 mmol natriumorthovanadaat, 20 ml glycerol (dat als capping agent gebruikt werd), pH 4,

reactietemperatuur van 180°C en een reactietijd van 30 minuten. De gebruikte condities van het microgolf toestel waren ook steeds dezelfde: druk= 20 bar, power= 250W, high stirring en de powermaxx functie was uitgeschakeld.

Verschillende hoeveelheden Eu^{3+} ionen werden toegevoegd om te bepalen welke doterings-percentage de hoogste emissie intensiteit vertoonde. De hoeveelheden Eu^{3+} ionen waren: 2.5 wt%, 5 wt%, 10 wt%, 12.5 wt% en 15 wt%. Het product met 12.5 wt% Eu^{3+} vertoonde de hoogste emissie-intensiteit. Het doel was om deze intensiteit te verhogen. Aangezien het idee van core/shell structuren eerder verlaten werd, werden er andere ionen gecodoteerd (telkens werd er maar 1 extra ion gedoteerd). Deze ionen waren Gd^{3+}, Y^{3+} en Lu^{3+}. Deze ionen zouden voor geen extra transities in het product zorgen. Dr. Kaczmarek had in haar werk al ondervonden dat Gd^{3+} ionen de emissie-intensiteit verhoogden, maar de transitie van grond- naar aangeslagen toestand van Gd^{3+} overlapte met de ladingsoverdracht band van het vanadaat. Hierdoor kon er niet met exacte zekerheid bepaald worden dat deze transitie voor de verhoging in emissie-intensiteit zorgde. Om dit te kunnen nagaan werden er ook producten gemaakt met de andere ionen (deze hebben geen 4f-4f transities wegens hun electronenconfiguratie). Ook bij deze producten werd een verhoging in intensiteit opgemerkt. Dit is al een eerste indicatie dat de verhoging in intensiteit een gevolg is van een verandering van iongrootte (zowel Gd^{3+}, Y^{3+} en Lu^{3+} zijn kleiner dan Eu^{3+}). Ook werd er naar de vervaltijd van de aangeslagen toestand gekeken voor antwoorden. Er waren geen significante verschillen tussen de verschillende ionen. Ook dit is een indicatie dat de verhoging van emissie-intensiteit een gevolg is van de verschillen in gedoteerde iongrootte. Dit zorgt namelijk voor defecten in het kristalrooster. Het zouden dus deze defecten zijn die zorgen voor een verhoging in luminescentie-intensiteit.

SYNTHESIS OF LANTHANIDE-DOPED RARE-EARTH VANADATES FOR HIGH-EFFICIENCY LUMINESCENT MATERIALS

M. D'hooge[a], A. M. Kaczmarek[a], R. Van Deun[a]

[a] Department of Inorganic and Physical Chemistry, Ghent University, Ghent 9000, East-Flanders, Belgium

This work presents the microwave-assisted syntheses and characterization of YVO_4, $GdVO_4$ and $LaVO_4$. These vanadate materials are known to be excellent host materials for Ln^{3+} ions. No previous literature on the synthesis of microwave-assisted trivalent europium doped $LaVO_4$ was made available. To investigate any differences in phase and morphology, these doped materials were again characterized and compared with the undoped materials. Co-doping with trivalent gadolinium was performed to increase the luminescence intensity of the material

Introduction

More and more research is conducted on the luminescent properties of lanthanide-doped vanadate materials. Studies have shown that these materials are good host materials for trivalent lanthanide ions. These doped host materials are known for their wide range of applications. One of these host materials is the well-studied yttrium orthovanadate (YVO_4) (1). This host material has known use in many applications: some of these even used to have an everyday use, as host for Eu^{3+} ions in cathode ray tubes (CRT's) in colour television (2), while others are used in modern, more high-end equipment (as a host material for lasers when doped with Nd^{3+})(3). YVO_4 is a crystalline zircon-type material, which means that it has a tetragonal crystal structure. This material can either be synthesized in an acidic or basic environment. (4)

Gadolinium orthovanadate ($GdVO_4$) is another host material with a tetragonal crystal structure. As was the case for YVO_4, studies on the luminescent properties and behaviour have been conducted (5).

The last of the investigated host materials in this work is lanthanum orthovanadate ($LaVO_4$). The most stable crystal structure of $LaVO_4$ is the monazite-type (monoclinic). This monazite-type material is considered not to be suitable as a host material: studies have shown that the luminescent intensity of the monazite-type $LaVO_4$ is far less than the metastable zircon-type $LaVO_4$ (6). To the authors knowledge, no literature on the microwave-assisted synthesis of this zircon-type $LaVO_4$ has yet been published. Most of the reported literature on zircon-type $LaVO_4$ described a hydrothermal synthesis route to synthesize this material (6). It is suggested that metastable structures can be obtained using mild conditions.

Doping trivalent europium ions into the above mentioned host materials has been extensively studied in the past. To obtain a certain level of novelty, only the least studied host material has been used in this work, which is the lanthanum orthovanadate in the monoclinic phase. The main focus in this work is trying to increase the luminescent intensity of europium, which was incorporated into the crystal structure of nano-sized $LaVO_4$. It is known that nanoparticles of a material can have different properties than the bulk material. To obtain these nanoparticles, literature suggests the use of wet techniques (7-10). One idea to increase the luminescence intensity was by using core-shell particles. It was already shown that the intensity of lanthanide ions was increased when core-shell particles are used (11). For core-shell

structures, nano-sized, spherical, uniform particles are needed. In this work, the syntheses were optimized to obtain nano-sized particles, which was confirmed with SEM images. However, the particles were never uniform enough for using in core-shell structures. Therefore, other methods were necessary for improving the luminescence properties of these nanoparticles. It has been already reported that co-doping these materials with ions like Li^+ increases the luminescence intensity (12-16). Another ion, which can be used for co-doping is Gd^{3+}. Literature showed that the luminescence intensity of europium (Eu), samarium (Sm) and dysprosium (Dy) in doped tungstate material (Ln: Y_2WO_6 (Ln = Eu, Sm and Dy)) increased when the amount of Gd^{3+} ions increased (17).

Experimental

All of the synthesized products were both synthesized hydrothermally or via microwave techniques. This was done to see any effect on the phase and morphology if a different technique was used.

Used products

The products used in this work were yttrium nitrate ($Y(NO_3)_3 \cdot 6H_2O$, 99.9%, Sigma Aldrich), gadolinium nitrate ($Gd(NO_3)_3 \cdot 6H_2O$, 99.9%, Sigma Aldrich), lanthanum nitrate ($La(NO_3)_3 \cdot 6H_2O$, >98%, Acros Organics), lanthanum nitrate ($La(NO_3)_3 \cdot 6H_2O$, 99.9%, Merck), europium nitrate ($Eu(NO_3)_3 \cdot 6H_2O$, 99.9% Alfa Aesar), lutetium nitrate ($Lu(NO_3)_3 \cdot 6H_2O$, 99.9%, Sigma Aldrich), sodium orthovanadate (Na_3VO_4, 99.98%, Sigma Aldrich), ammonium orhtovanadate (NH_4VO_3, >99.0%, Sigma Aldrich), glycerol (99.9%, BDH Laboratory Supplies), nitric acid (69%, Merck), nitric acid (65%, Acros Organics), ammonia solution (28-30%, NH_3 basis), ethanol (96%, VWR Chemicals) and sodium hydroxide (pellets, Laborimpex).

Rare-earth Orthovanadate ($REVO_4$)

General synthesis. The synthesis of this material was adapted from Ndagsi's work (18). The general synthesis is as follows: 1 mmol of rare-earth nitrate hexahydrate (RE = Y, La, Gd)) was dissolved in 10 ml of distilled water. To this solution, a mixture of 20 ml glycerol (which acts as capping agent) and 10 ml distilled water was added. A separate solution of 1 mmol of sodium orthovanadate (Na_3VO_4) dissolved in 10 ml distilled was made and mixed with the rare-earth containing solution. This resulted in a pale yellow (when RE = Y) or milky white solution (when RE= La and Gd). On changing the pH value to lower or higher value with nitric acid and sodium hydroxide respectively, a bright yellow, clear (when pH was low) or a pale yellow, clear (when pH was higher than 6) solution was obtained. This solution was handled differently according to which technique was used.

Hydrothermal synthesis. The solution obtained from the general synthesis was transferred to an autoclave and placed into a furnace at 200°C for 24 hours. This solution was then left to cool naturally for 24 hours.

Microwave-assisted synthesis. The solution obtained from the general synthesis was transferred to a 35 ml microwave tube. A stirring rod was added to the tube and the tube was sealed with a plastic cap. This tube was placed into a microwave furnace. The settings on the microwave were the following and were unchanged for the different microwave-assisted syntheses of YVO_4: Power = 250 W, T = 180°C, high stirring = on and P = 20 bar.

After the complete synthesis (both synthesis routes), the obtained product was centrifuged at 7000 rpm for 5 minutes. The product was washed several times with both distilled water and ethanol. Afterwards, the product was heat treated at 900°C for 3 hours.

Doped and co-doped $LaVO_4$

The same procedure as for the undoped sample is followed, only here, a part of the amount of the $La(NO_3)_3 \cdot 6H_2O$ is replaced by $Eu(NO_3)_3 \cdot 6H_2O$, $Gd(NO_3)_3 \cdot 6H_2O$, $Y(NO_3)_3 \cdot 6H_2O$ or $Lu(NO_3)_3 \cdot H_2O$. The doping and co-doping synthesis is carried out in a microwave-assisted route. Centrifuging the Eu-doped samples was more difficult than the undoped sample. The doped samples were centrifuged at 9000 rpm for 10 minutes. The samples were washed several times with distilled water and ethanol. These samples were heat treated in the same way described in the synthesis of the undoped material.

Results and Discussion

YVO_4-morphology and phase

To analyse the samples, DRIFTS and XRD measurements were performed. Images of the sample were taken by SEM.

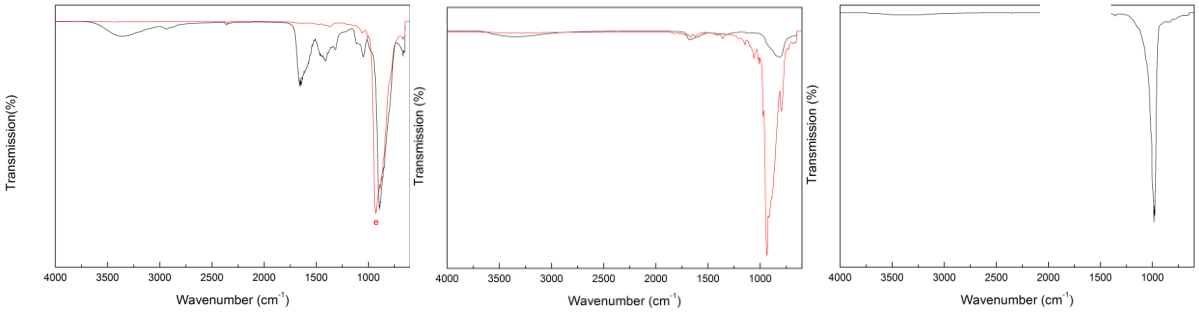

Figure 1. DRIFTS spectra (red is non-heat treated, black is heat treated) of a hydrothermal (left) and microwave-assisted product (middle and right). The middle spectra is of a sample where the vanadium source was sodium orthovanadate. The right spectra is of a sample were the vanadium source was ammonium metavanadate.

It is clear from Figure 1 that the non-heat treated samples contain more O-H vibrations than the heat treated samples (O-H vibration around 3400 cm^{-1} is attributed to water still present in the sample, the other peaks are O-H vibrations from glycerol). From the DRIFTS spectra, no distinction can be made between heat treated samples made via a hydrothermal or microwave-assisted route. No distinction can be made between the different sources of vanadium in the synthesis.

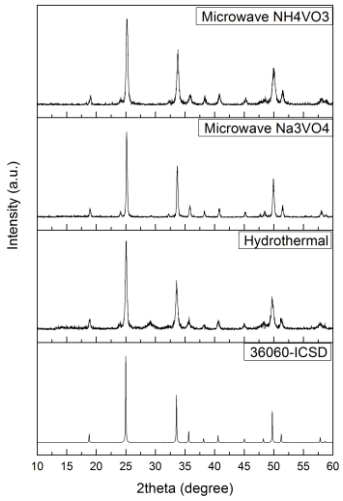

Figure 2. XRD diffractograms of a hydrothermal sample, microwave sample where the vanadium source was sodium orhtovanadate and a microwave sample were the vanadium source was ammonium metavandadate.

The XRD diffractograms of the samples are shown in Figure 2. All the samples have the same phase as the standard (36060-ICSD (19)), which has a tetragonal phase. This means that both the hydrothermal and microwave-assisted route give crystalline tetragonal YVO_4. To see any differences in morphology between the used source of vanadium, SEM images must be taken. The SEM images of the 2 samples can be seen in figure 3. Although the image of the ammonium metavanadate is lower in resolution (a lot of charge effects were present when measuring, therefore no better resolution was possible to obtain), it can be seen that both microwave-assisted synthesized products are nano-sized aggregates of spherical particles. The samples analysed by XRD and SEM were heat treated described in the experimental section.

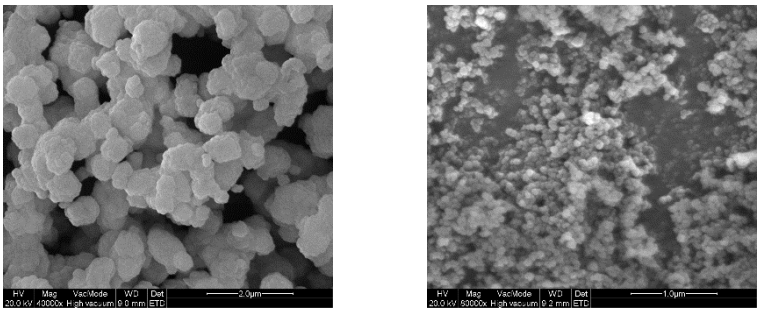

Figure 3. SEM images of the microwave-assisted synthesized products. Left: Na_3VO_4 as vanadium source. Right: NH_4VO_3 as vanadium source.

<u>$GdVO_4$-morphology and phase</u>

The same analyses for the YVO_4 samples were used on these materials. In Figure 4, the DRIFTS spectra are shown. Again, the heat treated samples show less peaks/contaminations than the non-heat treated samples. Again, DRIFTS does not show a significant difference between the hydrothermal and microwave-assisted synthesis route. No distinction between the 2 routes can be made with DRIFTS alone.

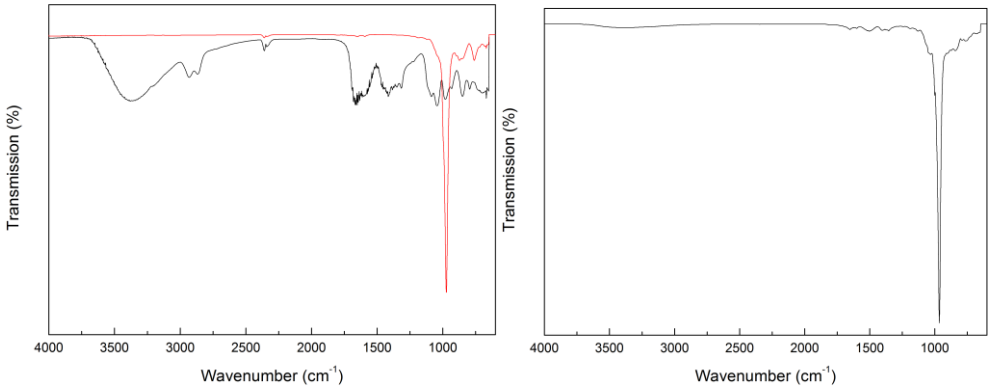

Figure 4. DRIFTS spectra of different $GdVO_4$ samples. Left: hydrothermal synthesis, non-heat treated (black) and heat treated (red). Right: microwave-assisted synthesis, heat treated.

To see a distinction, the XRD diffractograms were made. Figure 5 presents the XRD diffractograms for the samples whose DRIFTS spectra can be seen in Figure 4.

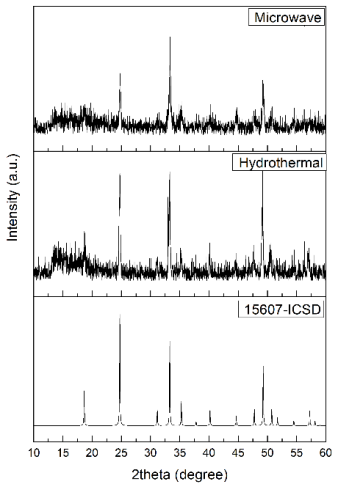

Figure 5. XRD diffractogram of a hydrothermally and microwave-assisted synthesized sample.

No significant difference can be seen in the XRD patterns. This means that the phase of the hydrothermally and microwave-assisted synthesized products are the same and have the same phase as the reference (15607-ICSD (20)). The goal for this thesis was to obtain nano-sized, spherical, uniform particles to create core/shell like structures. In order to obtain this, reaction conditions were changed. In Figure 6, SEM images of different reaction conditions are presented. When the pH changes from 7 to 10 and the amount of glycerol stayed the same (from left to middle in Figure 6), the particles tend to agglomerate more. When the pH stays 10 but the amount of glycerol changes from 20 ml to 0 ml (from middle to right in Figure 6), the material is no longer an aggregate of spherical particles. This proves that glycerol is an effective capping agent. Note that none of the obtained particles are qualified core/shell particles.

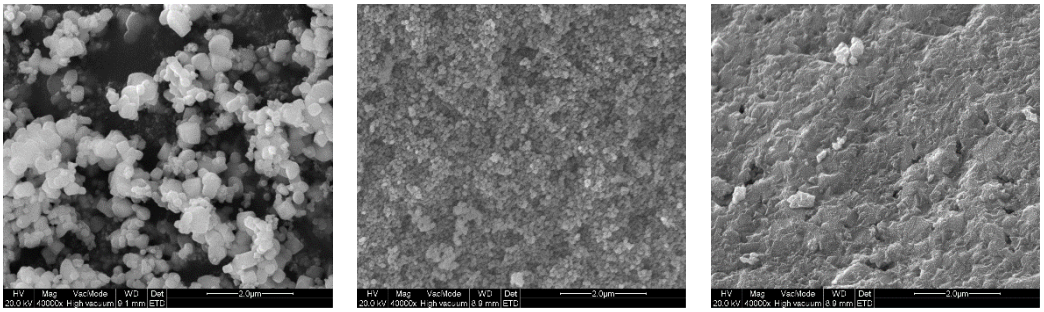

Figure 6. SEM images of: Left sample at pH 7, 20 ml glycerol. Middle sample at pH 10, 20 ml glycerol. Right sample at pH 10 and no glycerol. All SEM images had a magnification of x 40.000.

$LaVO_4$ - morphology and phase. The products were analyzed with DRIFTS and XRD. In Figure 7, DRIFTS spectra of the products are presented. Different reaction conditions (pH, reaction time, temperature) were changed in order to obtain the tetragonal $LaVO_4$. However, none of the obtained products had a tetragonal phase.

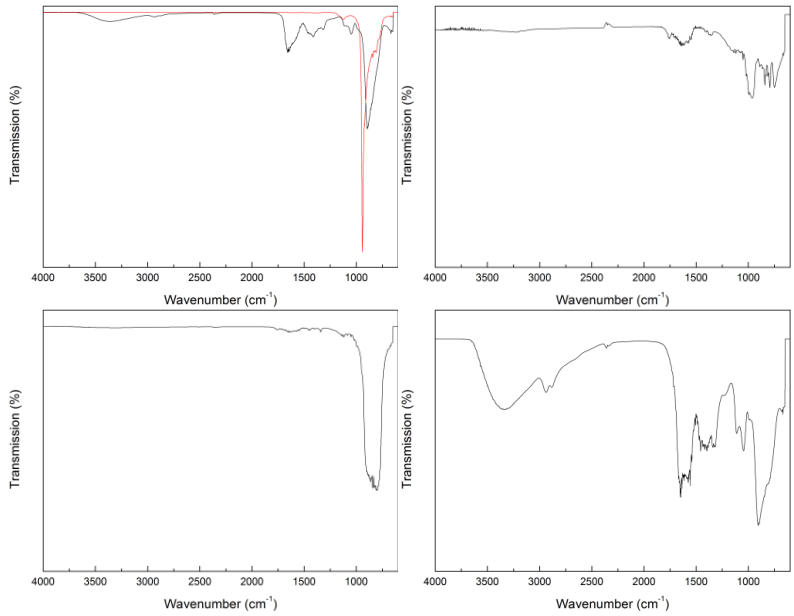

Figure 7. DRIFTS spectra of the different synthesized $LaVO_4$. Upper left = comparison between a heat treated at 900° C for 3 hours (red) and non-heat treated (black) sample. Upper right = microwave-assisted synthesized sample with pH 6 for 15 minutes. Bottom left = microwave-assisted sample with pH 4 for 30 minutes. Bottom right = non-heat treated microwave-assisted sample with pH 4 for 15 minutes.

The last samples in Figure 7 was synthesized without heat treatment to see if this would obtain a tetragonal phase. For a sample with pH 4, the DRIFTS spectra shows that the reaction needs to be longer than 15 minutes: a weak V-O stretch vibration peak is detected when the reaction only lasts 15 minutes (top right spectrum in Figure 7); if the reaction last longer (bottom left in Figure 7) the V-O stretch peak is much stronger, suggesting that the material is formed in a more pure way.

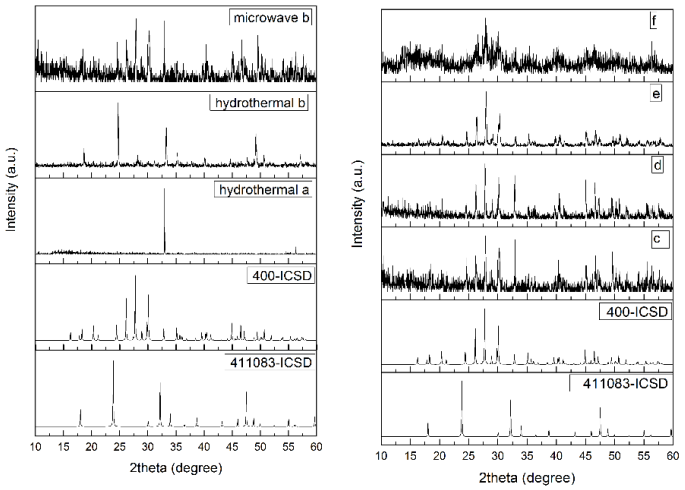

Figure 8. XRD spectra of the $LaVO_4$. Left: comparison of the methods used. The non-heat treated samples are denoted a and the heat treated (900°C for 3 hours) samples are denoted b. Right: microwave-assisted synthesized samples with different reaction conditions, c = pH 6 for 15 minutes, d = pH 4 for 15 minutes, e = pH 4 for 30 minutes and f = pH 4 for 30 minutes non-heat treated.

In Figure 8, XRD data of the samples is presented. The hydrothermal synthesis route shows more peaks belonging to the tetragonal phase (411083-ICSD (21)), as well as some peaks belonging to the monoclinic phase (400-ICSD (21)). For the microwave-assisted products, no tetragonal peaks can be detected. Note that the intense peak at $2\theta = 33$ in samples hydrothermal a, c and d are due to the sample holder of the XRD equipment. Since no tetragonal phase was formed, the sample chosen for doping with Eu^{3+} was sample c from Figure 8. This sample showed the best monoclinic XRD pattern. SEM images (see Figure 9) shows that he the monoclinic particles were not useable for core/shell like structures.

Eu-doped $LaVO_4$

Europium-doped $LaVO_4$ nanoparticles were the least investigated particles of the 3 vanadate materials in this work. It is for this reason that the focus lies on this material. To test which doping percentage gave the highest luminescence intensity, different doping percentages were used: 2.5 wt%, 5 wt%, 10 wt%, 12.5 wt% and 15 wt%.

Phase and Morphology. The phase and morphology of the doped samples are compared with the undoped sample to see if a significant change in either phase or morphology occurred. In Figure 9, the DRIFTS spectra of the doped and undoped samples are presented. It is clear that if the doping percentage increased up to 10 wt%, more glycerol peaks are present in the spectra. The V-O stretch bond is broadening as well. However, DRIFTS has shown that it is not a powerful tool to see the phase of the materials. To have a better comparison, the XRD diffractograms of the Eu-doped and undoped samples are presented in Figure 9. The XRD diffractograms of the Eu-doped samples resemble the diffractogram of the undoped sample quite well. This shows that no significant change in phase was detected. Only the doping percentages up to 10 wt% are shown.

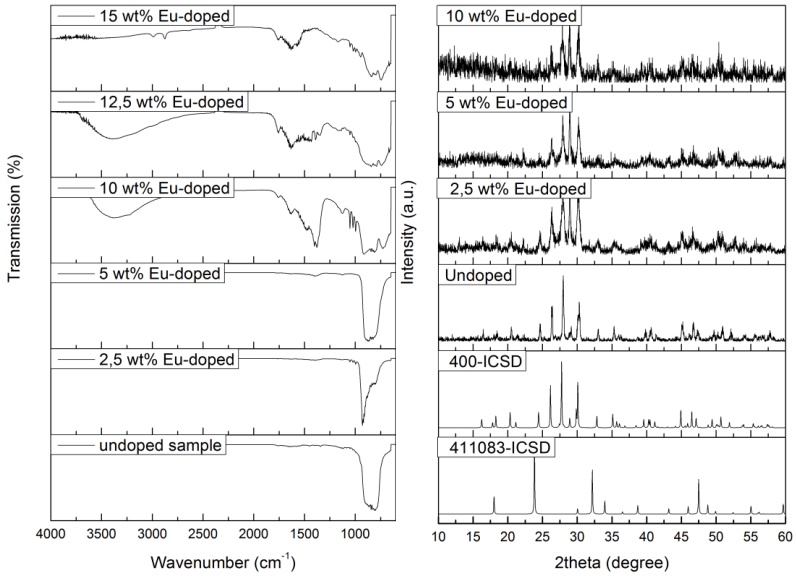

Figure 9. DRIFTS spectra of the Eu:$LaVO_4$ and undoped $LaVO_4$ samples (left) and the XRD diffractograms (right).

The morphology was investigated with SEM. Figure 10 presents the SEM images of the undoped and 10 wt% doped samples. Although the resolution of the doped sample is lower (due to charge effects on the sample), the magnification of the 2 images are the same. The SEM images in Figure 10 shows that the Eu-doped particles are smaller than the undoped particles.

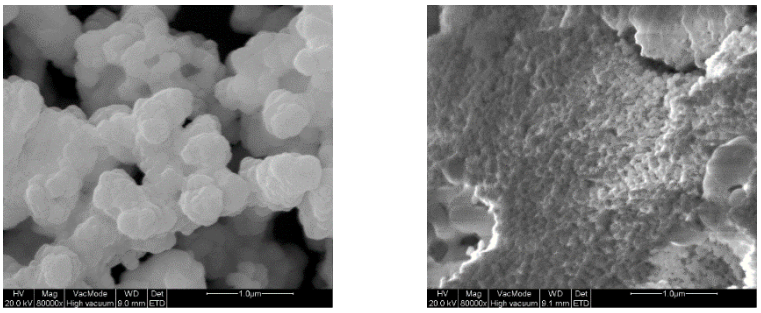

Figure 10. SEM images of the undoped (left) and 10 wt% Eu-doped sample.

Luminescence data. A comparison between the emission intensity and the luminescence decay time of the doped samples was made. The data showed that the 12,5 wt% Eu-doped sample has the highest emission intensity and luminescence decay time. The 12,5 wt% Eu-doped sample was chosen for further improvement of the luminescence intensity and decay time. The luminescence data can be found in Figure 11. The transition with the highest intensity is the $^5D_0 \rightarrow {}^7F_2$ transition, at around 614 nm. This leads to the emission of red light when the product is excited by a UV-lamp at a wavelength of 302 nm. This sample was co-doped with either Gd^{3+}, Y^{3+} and Lu^{3+} ions. In the work of Kaczmarek, it was shown that co-doping with Gd^{3+} ions can increase the emission intensity. However, the excitation peaks of Gd overlap with the V-O charge transfer band. Therefore, the increase in intensity cannot be attributed with certainty to the presence of Gd, it is possible that this increase in intensity is due to the change in size of the doped ions. To test this, the sample was also co-doped with Y or Lu ions. In Figure 12, the emission intensities of the co-doped samples are presented.

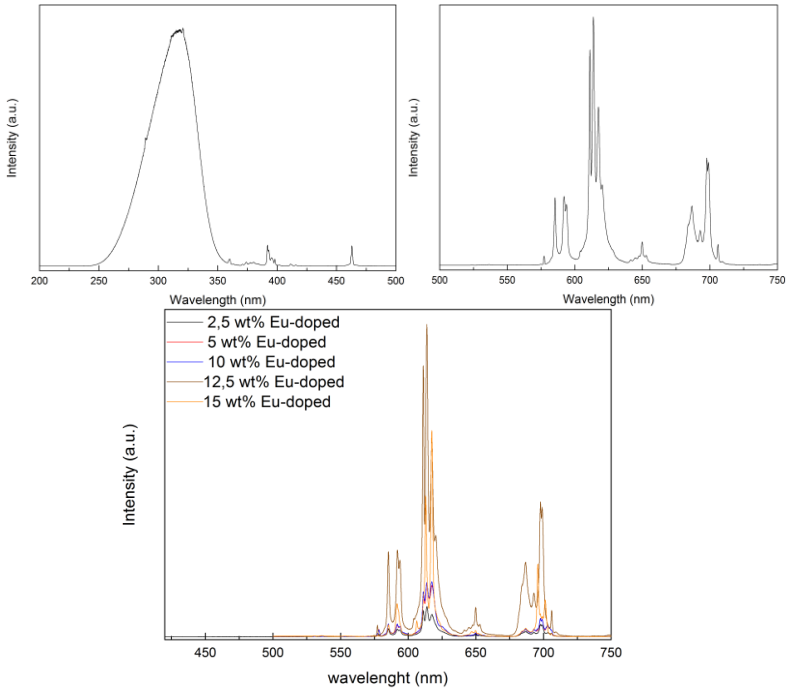

Figure 11. Excitation (upper left) and emission (upper right) spectra of the 12,5 wt% Eu-doped sample. Bottom: emission spectra of 2.5 wt% Eu-doped (black), 5 wt% Eu-doped (red), 10 wt% Eu-doped (blue), 12.5 wt% Eu-doped (brown) and 15 wt% Eu-doped (orange) samples.

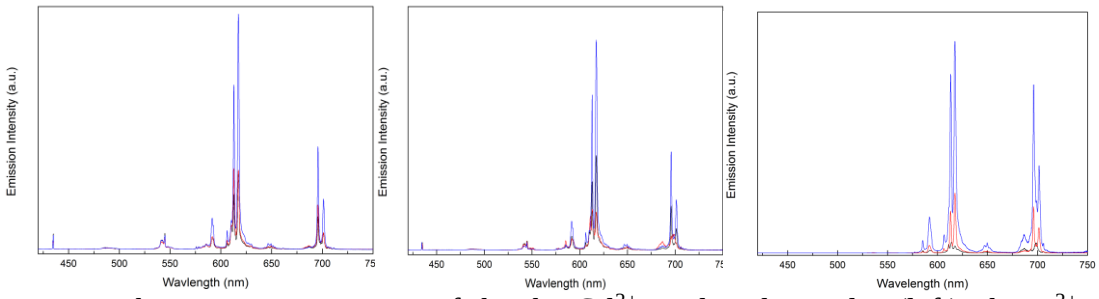

Figure 12. The emission spectrum of the the Gd^{3+} co-doped samples (left), the Y^{3+} co-doped samples (middle) and the Lu^{3+} co-doped samples: 2 wt% (black), 5 wt% (red) and 10 wt% (blue)

It is clear that the emission intensity increases for each different co-doped ion. This can suggest that the increase in emission intensity is an effect of the change in doped ion size. For further prove of this suggestion, the luminescent decay values are presented in Table 1.

TABLE I. Lifetime decay values.

Co-doped ion	**2 wt%**	**5 wt%**	**10 wt%**
Gd^{3+}	0.53 ms	0.50 ms	0.53 ms
Y^{3+}	0.49 ms	0.46 ms	0.46ms
Lu^{3+}	1.53 ms	0.53 ms	0.54 ms

Conclusions

From all the results, it is clear that the microwave-assisted synthesis is useful to obtain the vanadate host material (microwave-assisted synthesis has a reaction time of 30 minutes, the hydrothermal synthesis route has a reaction time of 24 hours). An increase in emission intensity was noted when the Eu-doped sample was co-doped with other lanthanide ions (Gd^{3+}, Y^{3+} and Lu^{3+}). All the different ions show an increase in intensity and except for the

high value of the 2 wt% Lu co-doped sample, no significant change between the different co-doped ions and doping percentages are found. This gives more evidence that the increase in emission intensity is due to the difference in size of the doped ion (all the doped ions are smaller than Eu^{3+} ions)

Acknowledgments

I would like to thank prof. Van Deun for giving me the opportunity to work on this project. Next, I would like to thank Dr. Anna Kaczmarek for being my supervisor during this project. Special thanks goes out to Tom Plankcaert, for all the powder XRD measurements, Olivier Janssens and Dr. Kaczmarek for the SEM measurements.

References

1. R. C. Ropp (1991), *Luminescence in the Solid State*. Amsterdam, Elsevier.
2. A. K. Levine and F. C. Papilla, *Electrochem. Tech.*,**4**, 16 (1966).
3. R. A. Fields, M. Birnbaum and C. L. Fincher, *Appl. Phys. Lett.*, **51**, 1885 (1987).
4. H. Wu, H. Xu, Q. Su, T. Chen and M. Wu, *J. Mat. Chem.*, **13**, 1223-1228 (2003).
5. J. R. DiMaio, B. Kokuoz and J. Ballato, *Optical Express*, **14**, 11412 (2006).
6. H. M. Zhang, J. B. Liu, H. Wang, W. X. Zhang and H. Yan, *J. Nanopart. Res.*, **10**, 767-774 (2008).
7. R. C. Ropp and R. Oakley, Ger. Pat., 2056172 (1971).
8. S. Erdei, *J. Mater. Sci.*, **30**, 4950 (1995).
9. S. Erdei, N. M. Rodriguez, F. W. Ainger, W. B. White, D. Ravichandran and L. E. Cross, *J. Mater. Chem.*, **8**, 99 (1998).
10. A. Huignard, T. Gacoin and J. P. Boilot, *Chem. Mater.*, **12**, 1090 (2000).
11. R. G. Chauduri and S. Paria, *Chem. Rev.*, **112**, 2373-2433 (2012).
12. J. C. Park, H. K. Moon, D. K. Kim, S. H. Byeon, B. C. Kim and K. S. Suh, *Appl. Phys. Lett.*, **77**, 2162 (2000).
13. T. Hatayama, S. Fukumoto and S. Ibuki, *Jpn. J. Appl. Phys.*, **31**, 3383 (1992).
14. H. K. Yang, K. S. Shim, B. K. Moon B. C. Choi, J. H. Jeong, S. S. Yi and J. H. Kim, *Thin Solid Films*, **516**, 5577-5581 (2006).
15. S. W. Park, H. K. Yang, J. W. Chung, B. K. Moon, B. C. Choi, J. H. Jeong, K. Jang, H. S. Lee and S. S. Yi, *J. Korean Physical Society*, **57**, 1764-1768 (2010).
16. J. S. Bae, S. S. Park, T. E. Hong, J. P. Kim, J. H. Yoon, E. D. Jeong, M. S. Won and J. H. Jeong, *Current Appl. Phys.*, **9**, S241-S244 (2009).
17. M. Maqbool, M. E. Kordesch and A. Kayani, *J. Opt. Soc. Am. B*, **26**, 998 (2009).
18. D. Ndagsi (2014), *Tuning the emission colour of rare-earth tungstate and vanadate material towards white light generation*, University of Ghent, Ghent, Belgium.
19. G. Lohmueller, G. Schmidt, B. Deppisch, V. Gramlich and C. Scheringer, *Acta Cryst. B*, **29**, 141-142 (1973).
20. W. O. Milligan and L. W. Vernon, *J. Phys. Chem.*, **56**, 145-147 (1952).
21. C. E. Rice and W. R. Robinson, *Acta Cryst. B*, **32**, 2232-2233 (1976).
22. Y. Oka, T. Yao and N. Yamamoto, *J. Solid State Chem.*, **152**, 486-491 (2000).

Table of Content

Akngowledgments

Firstly, I would like to thank prof. Van Deun for giving me the opportunity to do my thesis work in the Luminescent Lanthanide Lab. The past few months gave me an insight and knowledge on the subject of lanthanide luminescence of doped host materials. This proved to be an interesting topic and I am grateful to have been a part of it.

Secondly, I would like to thank Dr. Anna Kaczmarek, who was my supervisor during my thesis. She taught me some of the techniques which were indispensable for my research. Not only did she assist me in the procedures, she taught me to work more independently on the project, which is a crucial skill for my later career. Nevertheless, she was always ready to help and answer any questions I had. Next to the scientific part of the thesis, she created a lovely atmosphere at the office.

I would like to thank Tom Planckaert, who measured all the powder XRD samples I prepared, Olivier Janssens and Dr. Anna Kaczmarek for the SEM measurements.

I would also like to thank Dorine Ndagsi and Jason Serck, for the help with the data processing and any other questions I had for them. Together with the other thesis students, Florence Haepers and Tineke Mortier, they made coming to the office everyday always very pleasant.

A special thanks goes out to all my fellow students. The past few years created many memories that I will carry with me forever. Many of these memories were created with Bastiaan Dhanis, Dorien Van Lysebetten, Matthias van Zele and Mike Degraeve. They made my student days truly unforgettable and were always there to help me and listen to my complaints.

A final thanks goes out to my family. They were there in my best and worst days the last few years. Without them, I never would have been where I am now.

1. Introduction

Emission of light is a known phenomenon. The most known is emission by the sun, were not only visible light, but the entire electromagnetic spectrum is emitted. There are different ways in which light can be emitted: incandescent, luminescent …

Emission of light is caused by excitation. The excited material can then fall back to a lower lying electronic state, in which the energy produced by this process emitted out light. Luminescent emission is a process where no heat was used for excitation. Luminescence has found important applications, for example in light emitting diodes (LEDs). For example blue LEDs can be used to create white light. This application of luminescence is so important that it has been given the Nobel prize in physics in 2014. In comparison to incandescent light bulbs, LEDs are more energy efficient and have a longer lifetime. Environmental studies have shown that LEDs are more promising to replace incandescent lamps then compact fluorescent lamps[6]. But using pn-junctions (which is the case for LEDs) is not the only way to cause luminescent emission. In this thesis, luminescence is caused by absorption of photons, a process which is called photolumininescence.

The lanthanides are the 14 elements with atomic number from 57 to 71, and they are known for their excellent photoluminescent properties. The lanthanides have 4f-orbitals, which are gradually filled when going through the series of lanthanides. These 4f-orbitals are shielded from the environment due to the presence of the 5s- and 5p-orbitals, which lay more outwards than the 4f-orbitals. Because of this shielding, the 4f-orbitals cannot form any covalent bonds, since no overlap with ligand orbitals is possible. The favoured oxidations states of all the lanthanides is the 3+ state, but for some lanthanides other oxidations states are stable as well (for example, europium and samarium are stable in the 2+ state, while cerium and terbium are stable in the 4+ state). In this thesis, all the lanthanides will be used in their 3+ oxidation state. The luminescence properties of the trivalent lanthanide ions originate from the 4f-4f transitions for absorption and emission. However, these transitions are forbidden by Laporte's rule, which states that transitions between electronic states in which the parity remains unchanged are forbidden. For emission this problem can be overcome: if no other ways of de-excitation can occur, this will happen through emission. For absorption however this is a problem. This can be overcome in 2 ways: firstly by using a

high-power energy source for excitation (for example lasers) or by using organic ligands that can harvest the energy and transfer it to the lanthanide-ions. This process is called the antenna-effect[1]. This will make the transitions partially Laporte allowed.

In literature it is reported that yttrium orthovandate (YVO_4) is a good host lattice for different trivalent lanthanide ions[2]. When looking at the excitation spectra of different lanthanide doped YVO_4 they all have a V-O charge transfer band (see Figure 1). This charge transfer band will then transfer its energy to the lanthanide ions through resonance[3]. Not only YVO_4 had been used in this thesis, but some other vanadates ($LaVO_4$ and $GdVO_4$) well known for their ability to transfer energy to trivalent lanthanide ions were used as well. When comparing the excitation spectra of YVO_4 and $LaVO_4$, the same broad peak (although slightly shifted) can be seen. This shows that the energy transfer for both vanadate materials occurs through the V-O band[7].

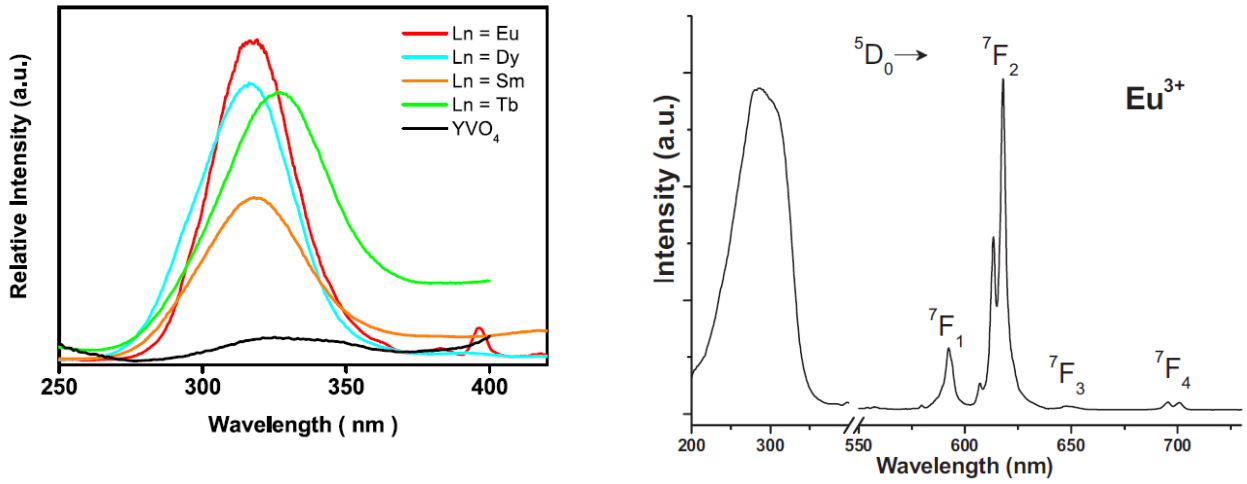

Figure 1. Left: Zoomed in region of the excitation spectrum for undoped and different doped YVO_4 nanoparticles. All show a broad band in the region between 300-350 nm. Since both the doped and undoped samples have a similar band, it is believed that they all have the same origin: the V-O stretch vibration[8]. Right: The excitation and emission spectrum of LaVO4:Eu nanoparticles[7].

The vanadate material needs to be nano-sized for this thesis in order to create core/shell structures. It is known that the properties of nanoparticles are different form their bulk materials and are often size and shape dependent. These different properties (for example different morphologies for the same material) will lead to different emission spectra of the doped lanthanide[4]. In our group, a thesis student from previous years already worked on fine-tuning the particle size for YVO_4 in a hydrothermal synthesis route, which then was used

for white light emitting materials[5]. The aim of this project was to fine tune the emission intensity of a vanadate material doped with Eu^{3+} into the matrix. This was done by using microwave-assisted syntheses. As green chemistry is gaining importance, this method is preferred due to the energy saving abilities of microwave-assisted syntheses compared to hydrothermal syntheses since the reaction time is cut significantly. This means that the energy consumption is a whole lot lower than for hydrothermal syntheses, making it a greener way of synthesis. The materials which were synthesized using a microwave furnace were further heat treated as was the case with the hydrothermal reaction. To increase the intensity, core-shell structures can be used to decrease the luminescence quenching.

2. Literature study

2.1. Lanthanides

The lanthanides belong to the rare-earth elements. They are a set of 14 elements going from cerium(Z= 58) to lutetium (Z=71). These elements all have electrons in their 4f-orbital, and this orbital is gradually filled up. Some sources may state that the lanthanides are actually comprised of 15 elements: lanthanum(Z= 57) is then classified as a lanthanide. Here we shall think of lanthanum as a lanthanoid, meaning that it has properties very similar as the lanthanides, but does not have any electrons in the 4f-orbital[1]. For lanthanum the 5d-orbital is energetically preferred since it is lower in energy than the 4f-orbital and it will have the electron configuration $[Xe]5d^16s^2$. Yttrium (Z=39) and scandium (Z=21) are other rare-earth elements with similar properties as the lanthanides but again do not have any electrons in a 4f-orbital. All of the lanthanide ions are stable in their trivalent state, additionally some lanthanides are stable in their divalent (samarium, europium, thullium and ytterbium) or even quadrivalent (cerium, praseodynium, neodymium, terbium and dysprosium) state.

Table1. The electronic configuration of trivalent ions of the rare earth[9]

Z	Element	Configuration of trivalent ions
21	Sc	[Ar]
39	Y	[Kr]
57	La	$[Xe]4f^0$
58	Ce	$[Xe]4f^1$
59	Pr	$[Xe]4f^2$
60	Nd	$[Xe]4f^3$
61	Pm	$[Xe]4f^4$
62	Sm	$[Xe]4f^5$
63	Eu	$[Xe]4f^6$
64	Gd	$[Xe]4f^7$
65	Tb	$[Xe]4f^8$
66	Dy	$[Xe]4f^9$
67	Ho	$[Xe]4f^{10}$
68	Er	$[Xe]4f^{11}$
69	Tm	$[Xe]4f^{12}$
70	Yb	$[Xe]4f^{13}$
71	Lu	$[Xe]4f^{14}$

The general configuration of the lanthanides is $[Xe]4f^n5d^16s^2$ were the [Xe] is the notation for the electronic configuration of xenon, a noble gas, and the n denotes the amount of electrons in the 4f-orbital of the lanthanide(0 for La to 14 for Lu). Since the most favoured oxidation state in aqueous solution is the 3+ oxidation state, the electronic configuration of

the trivalent lanthanide ions is of great importance. The electronic configuration of the rare earth elements is written down in table 1.

When passing through the series of lanthanides, a decrease in the atomic radii and the radii of the trivalent ion can be noticed. Due to the shielding of the 4f electrons by the 5s and 5p electrons, the 4f electrons show a core-like behaviour. This means that they are shielded from the ligands and cannot form any covalent bonds with them. But the 5s and 5p electrons are not shielded from the chemical environment, thus these feel the effects from the increasing effective nuclear charge. Because of this increasing of effective charge when the atomic number increases, the 5s and 5p orbitals will contract and the atomic radius will decrease. It has been shown that a small part of this contraction is due to relativistic effects[10,11].

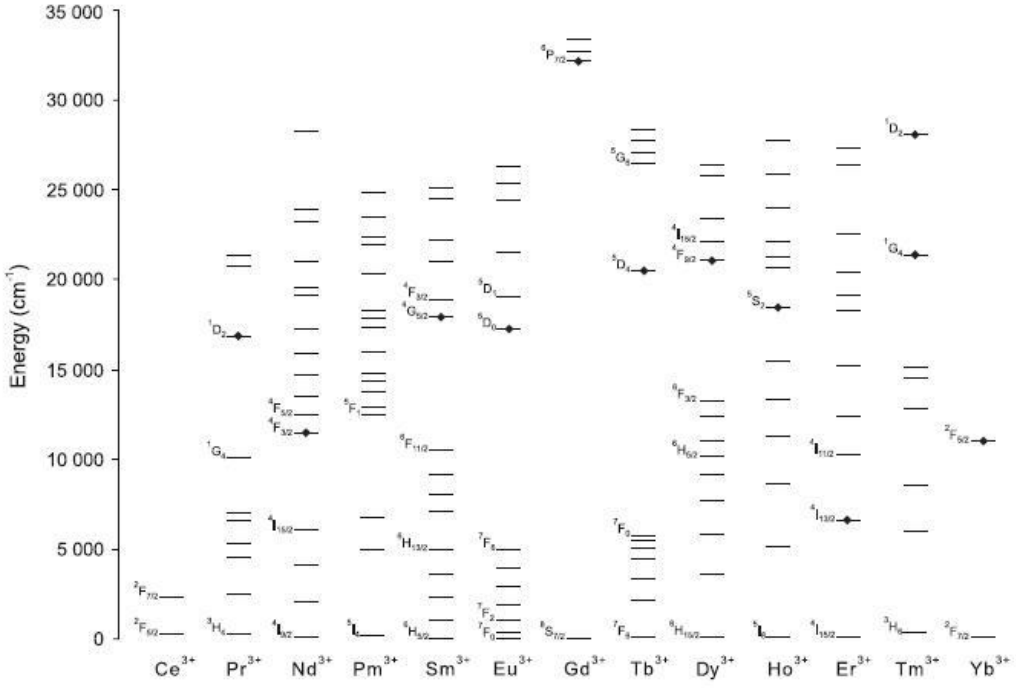

Figure 2. A Dieke diagram[9]

As stated in the introduction, lanthanides can absorb electromagnetic radiation and emit light via 4f-4f transitions. These are forbidden by Laporte's rules (4f-4f transitions are transitions which have the same parity) but can occur through ways explained in the introduction. In order to emit light different energy levels are needed. In Figure 2, a Dieke

diagram is shown, in which the different energy levels are shown. The energy levels which emit light commonly are marked with a diamond shape. Notice the fact that in the Dieke diagram lanthanum and lutetium are not present, this is because lanthanum does not have 4f electrons in its trivalent state and lutetium has a completely filled 4f subshell.

Unfortunately, the processes described in the introduction are described in the ideal situation. Different situations can occur during the transfer of the energy from the ligand to the lanthanide. Either singlet fluorescence, triplet phosphorescence or quenching are possible events that will lead to less intense emission of light. A schematic drawing of possible ways to lose the energy of the excited electron is given in Figure 3.

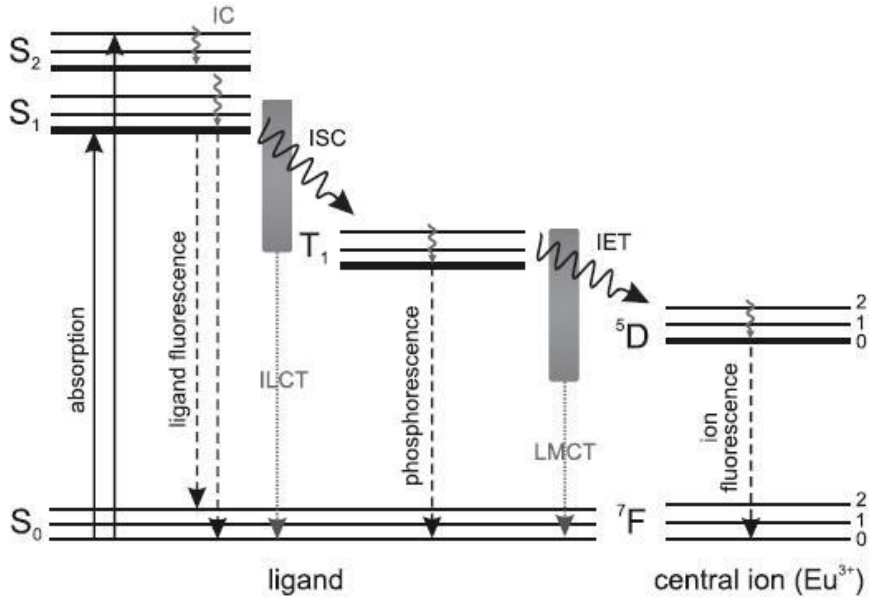

Figure 3. Possible ways for losing the energy of the excited state of a ligand-europium complex. [9]

First an ideal situation will be described using Figure 3. After the electrons are excited by absorption the energy of the phonons from the singlet ground state (S_0) to the excited singlet state (S_1 and S_2), the excited states will transfer its energy to a excited triplet state (T_1) by intersystem crossing (ISC). The energy of the excited triplet is then transferred to the lanthanide ion via intramolecular energy transfer (IET)[12, 13, 14]. This will lead to the luminescence of the lanthanide ion. Unfortunately, the excited singlet states can decrease their energy by radiatively fall back to a excited vibrational energy levels (thin horizontal lines in Figure 3) or the lowest excited electronic level (the electronic levels are the bold horizontal lines in Figure 3). This is called ligand fluorescence since there is no difference in

spin states between the ground and excited state. This process can also occur through intra-ligand charge transfer(ILCT) could also occur. Just like the excited singlet state, the excited triplet state can radiatively fall back to the singlet ground state. Because this transition occurs between different states (singlet and triplet) this process is called ligand phosphorescence[9]. For the excited triplet states, metal-to-ligand charge transfer (MLCT) can occur as well. Both the excited singlet and triplet state can non radiatively fall back to the ground state. Even if there is a high lanthanide luminescence fraction, the luminescence can still be diminished by quenching effects. This effect is caused by the coupling with vibrational overtones. There are quite a few functional groups known to have vibrational energy levels that will couple with the electronic energy levels of the lanthanide ions, such as O-H, C-H and N-H groups[15, 16]. This means that the quantum yield (the ratio of emitted photons over absorbed photons) will increase if the lanthanide complex is placed in D_2O instead of water[17].

2.2. Vanadate material

Since different vanadate materials were used in this thesis, a brief explanation will be given about each material.

2.2.1. Yttrium Orthovanadate

YVO_4 is a crystalline zircon-type vanadate material, this means that it has a tetragonal structure. It has been used in a lot of application, some which were for everyday use a few years back (as a host for Eu^{3+} in cathode ray tubes (CRTs) for colour television[18]) or some are for more high-end equipment (as a host material for lasers when doped with Nd^{3+}). YVO_4 has been synthesized in different ways either as a single crystal or as powders. Here the aim is to produce powders of nano-sized particles. In order to do this, literature recommends to use wet techniques[19-22]. A colloidal approached was used by Huignard *et al* in which they started from the work of Ropp and Carroll[23], who reported that not only YVO_4 was formed, but at lower pH values other material (YV_3O_9 or $Y_2V_{10}O_{28}$) could be detected as well. However, it is possible to get the pure YVO_4 phase at acidic conditions, but then the molar ratio of the yttrium and vanadium source has to be 1[24]. It is also known that YVO_4 can be synthesized in a basic or acidic medium[24], as can be seen in Figure 4. As the formed particles are nano/microparticles, changing the conditions of the reaction slightly can alter the morphologies, and thus even the luminescence properties, drastically.

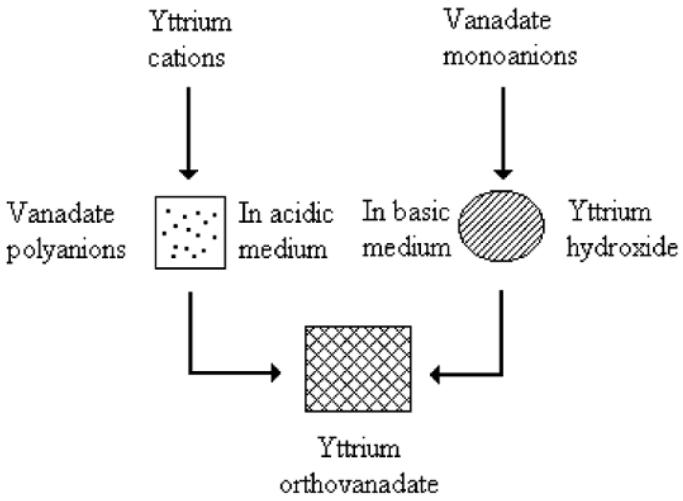

Figure 4. The reaction mechanism in acidic and basic conditions[24]

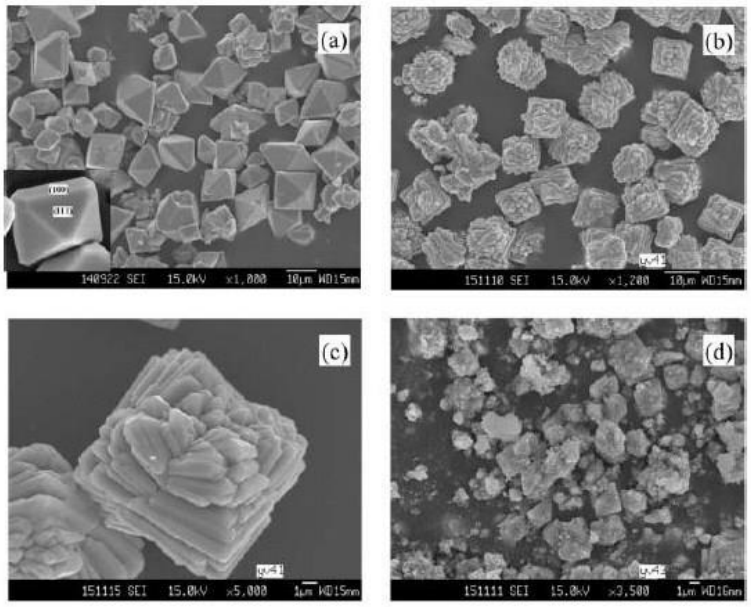

Figure 5. Changes in morphology when the reaction conditions are varied. A: Y_2O_3:V_2O_5:HNO_3:HCl = 1:1:2,5:2,5. B and C: Y_2O_3:NH_4VO_3:HNO_3:HCl =1:1:2,5:2,5 D: Y_2O_3:NH_4VO_3:HNO_3:HCl:NaOH = 1:1:2,5:2,5:2. In Figure A (and B and C), the difference in morphology due to a change in vanadium source can be seen. The difference between (B,C) and D is the addition of NaOH, which will cause the disappearance of the YVO_4 crystal facets, which will make the particles smaller[24].

Not only the shape of the nanoparticles can change when the conditions are changed (see Figure 5), but they can even start to aggregate into micro-sized particles (see Figure 6). To avoid this aggregation, capping agents can be used. Not only will the capping agents stop the aggregation, but they will make the nanoparticles more monodispersed. All this has an impact on the luminescence properties of the particles (see Figure 6)[8].

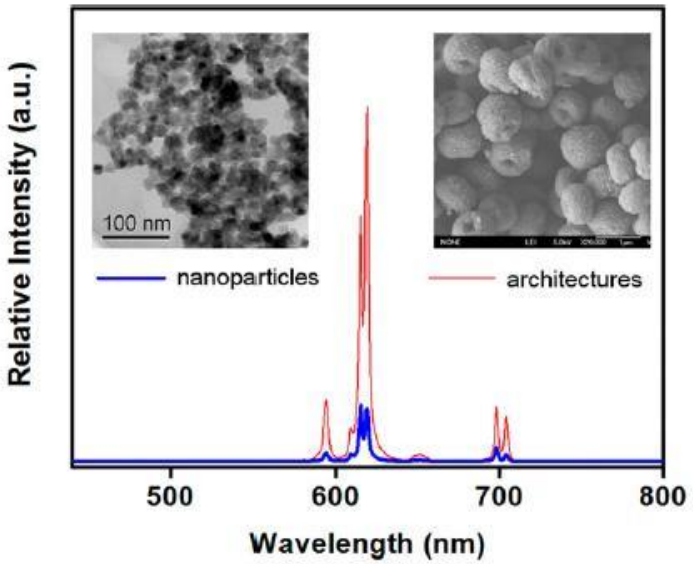

Figure 6. Top: SEM pictures of the colloidal nanoparticles (right) and the aggregated architecture (left). Bottom: difference In luminescence intensities of the colloidal and aggregated nanoparticles doped with Eu^{3+} ions [8].

2.2.2. Lanthanum Orthovanadate

The most stable form of lanthanum vanadate ($LaVO_4$) is de monazite type. Unfortunately, previous studies have shown that the intensity of the monazite type $LaVO_4$ host is considerably lower than for the metastable zircon type $LaVO_4$ host[25]. Nanoparticles of this zircon type $LaVO_4$ were already made and these particles had a structure similar to the bulk YVO_4[25], which is a suitable host for lanthanide luminescence. Metastable structures can be produced via mild conditions (for example lower temperatures)[25]. In literature this zircon type $LaVO_4$ is produced in a hydrothermal procedure where EDTA was used to speed up the procedure[25]. However, maybe very short reaction times in a microwave-assisted method could be used to create the zircon type: a transformation from one type to another in a microwave-assisted method has already been published[26]. In Figure 7 a comparison between the luminescence intensities of the monazite and zircon type $LaVO_4$ is given. It is very clear that the zircon type shows much better luminescence intensity.

As already mentioned for YVO_4, when the reaction conditions are changed different morphologies and luminescence properties have been reported. As an example of the change in morphology, SEM images of $LaVO_4$ at different reaction temperatures are shown in Figure 8. It is clear that the change in temperature influences the morphology from cuboid rods to cubes to cuboid rods which have been etched at the {001} facets. In Figure 9, the

luminescence properties of the different morphologies are shown. An increase in intensity is noticed when the cuboid rod morphology is formed[27]. Unfortunately, in literature different values of pH are reported in the synthesis of $LaVO_4$, which makes it more difficult to get the right synthesis at once. Some are basic[28] while others reported that the synthesis can occur at pH values as low as 4[29].

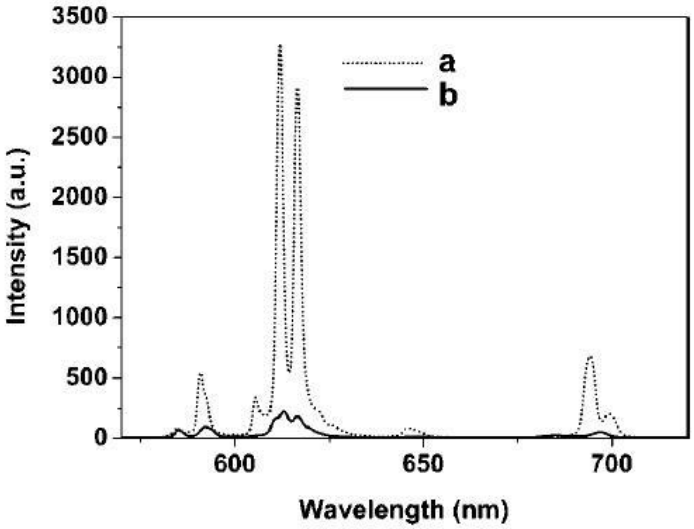

Figure 7. The luminescence intensity of the zircon type $LaVO_4:Eu^{3+}$ (dashed line) and the monazite type (full line)[25]

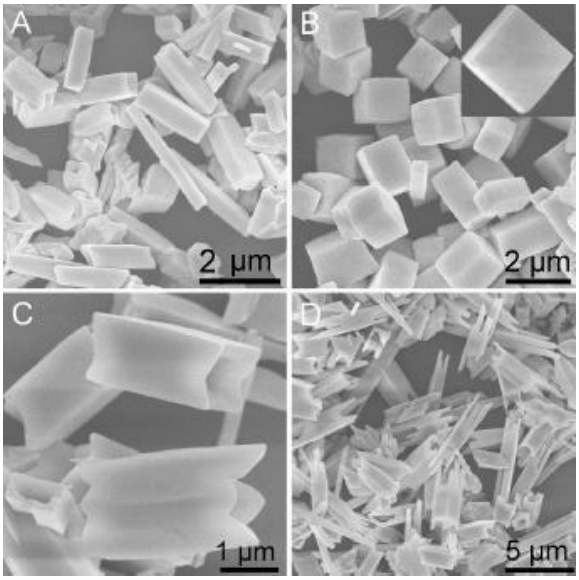

Figure 8. SEM of $LaVO_4$ synthesised at a fixed pH of 4 at different temperatures : A = 160°C, B = 180°C, C = 200°c and D = 220°C.[27]

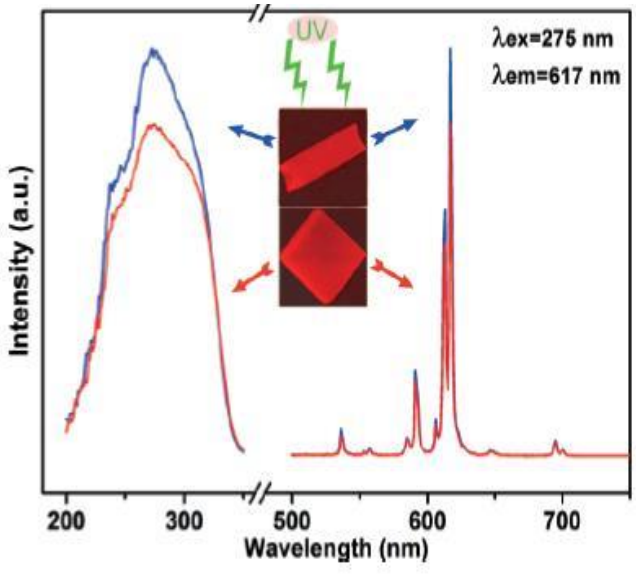

Figure 9. The luminescence intensities of $LaVO_4:Eu^{3+}$ of different morphologies[27]

2.2.3. Gadolinium Orthovanadate

Just like other vanadate host materials, gadolinium orthovanadate ($GdVO_4$) has a zircon-type crystal structure. As is the case with the other vanadates, the reaction conditions for the synthesis of the gadolinium vanadate are crucial for its morphology and properties. A study of the morphology and photoluminescent properties of Eu-doped $GdVO_4$ has already been carried out[30]. When the pH increased from 4-7 to 9-11, a change in the colour of the powders was noticed: the powders synthesised at pH 4.2 and 7.2 were pale yellow while the powders synthesised at pH 9.3 and 11.2 were white. Not only does the colour of the material change, but the shape of the particles went from homogenously distributed spherical particles (although the particles were smaller at pH around 4) to irregular short nanorods. As was expected, the properties of the materials were dependent on the morphology. In Figure 10 a change in the emission intensity of the particles can be seen. The emission intensities increase when the pH increases up to 7.2, but when it is changed to 9.3 a drop in intensity is noted whereas when the pH is furthermore increased, the intensity also increases. This drop in emission intensity could be explained in the change in morphology from pH 7.2 to 9.3.

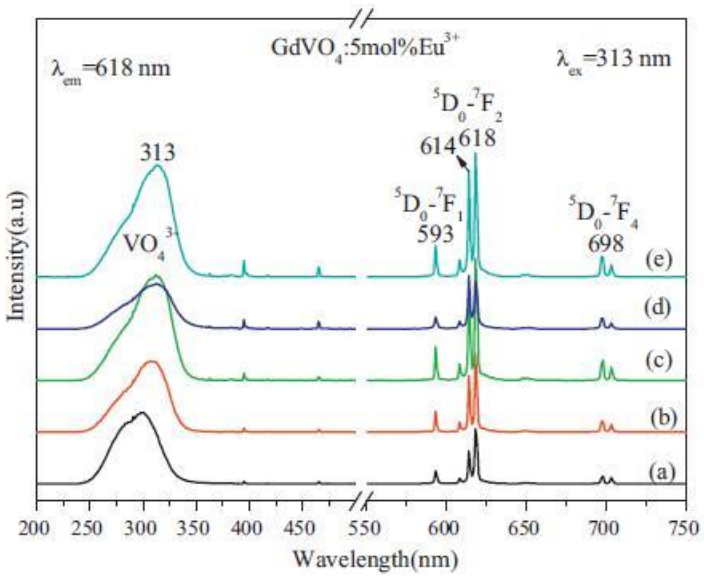

Figure 10. The luminescent intensity at different pH values: a)pH=2; b) pH=4.2; c) pH=7.2; d)pH=9.3 and e)pH=11.1[30]

2.3. Core/shell particles

From all the previously given information, the most simple way to tune the emission of a lanthanide doped nanoparticle vanadate is simply to change the reaction conditions. This will lead to a change in properties, however just changing these conditions may lead to an

undesired product. To actually fine-tune the properties in a controlled way (a) different method(s) must be applied.

It is known that for any type of phosphor there is a possibility of improved screen packing, brighter cathodoluminescence and high definition when the particles are uniform spheres[31-33]. An easy way of achieving uniform spherical particles is the use of silica. This material can be made uniformly with spherical particle sizes in the range of nano- to micrometer. This spherical silica can then be coated with the phosphor. Not only is silica easily made into controllable spheres, but this material is much cheaper than phosphors. The phosphor shell must be crystalline in order to have luminescence. Therefore, the core/shell structures must be heat treated afterwards.

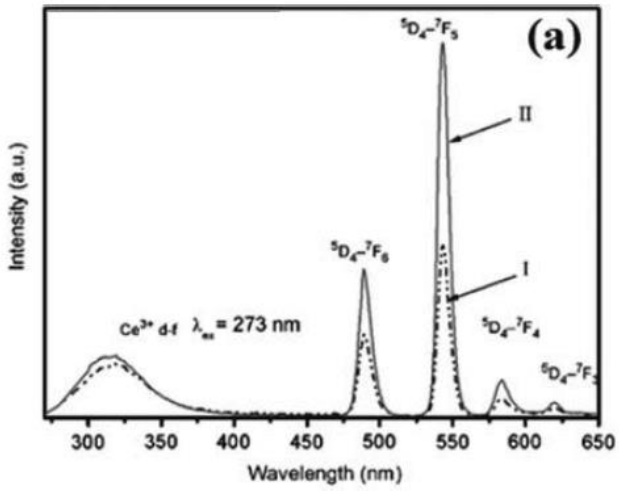

Figure 11. Emission spectrum of LaF_3: Ce^{3+}, Tb^{3+} (I) and LaF_3:Ce^{3+}, Tb^{3+}/LaF_3 (II)[34]

There are many types of core/shell structures: the inorganic/inorganic, the inorganic/organic, organic/inorganic, organic/organic and the core/multishell particles. For this thesis the inorganic/inorganic type of core/shell structures are important, because they contain the series of lanthanide nanoparticles. Since quantum dots, which have been studied a lot, seem to have problems with oxidation, quenching and even toxicity (especially when used as bio-labels) the use of lanthanide core/shell structures has been researched on their optical properties and stability[35-39]. These particles consist of a lanthanide doped core and a silica shell or even other lanthanide containing complex. These particles have a high emission efficiency, comparable to their bulk material and are soluble in common solvents. Some are even attachable to polymer matrices[40]. They are less toxic than the quantum dots, which makes them more applicable in bio-labels and other bio-applications. When studying

the intensity of LaF_3 doped with Ce^{3+} and Tb^{3+} is has been shown that the intensity increased almost 2-fold when around this particle a shell of LaF_3 has been produced[34], as can be seen in Figure 11.

Generally, core/shell particles are made in a 2 step process, where first the core is synthesized and afterwards the shell is synthesized. Procedures to synthesize core/shell particles can be separated in 2 classes: first, the separately synthesized core is incorporated in the system and proper surface modifications are done for coating the shell. Secondly, in situ created core particles which is followed by coating with the shell. The external creation of core particles must of course be first washed (for purification), dried and modified but has the advantage that the core particles are much more pure since less impurities can occur then during the in situ core particle generation[41].To have the desired properties, the shell must be uniform and the thickness must be able to be controlled. Different thicknesses will lead to different properties.

There are many different methods already reported for obtaining core/shell particles, for example precipitation, polymerization, microemulsion, sol-gel condensation, …[42-49]. Unfortunately, for all the researched techniques the proper control for the shell thickness and uniform coating is still not optimized. Problems that still occur are that sometimes the core particles agglomerate during the synthesis, the surface of the core is not completely covered by the shell material, instead of the formation of a coating the shell material will form particles and controlling the reaction rates[41].

As mentioned before, when external core particles are created surface modifications need to happen in order for the shell to be coated on the core. For this polymers and surface active groups can be used. These will affect the selectivity and surface charges of the core particles, which will allow the shell to be coated selectively on the surface of the core[41].

As mentioned, the lanthanide core/shell nanoparticles are part of the inorganic/inorganic structure, so only for this type of core/shell particles further information on the synthesis will be given. The core for the particles in this thesis subject will consist of a lanthanide doped vanadate. This type of core (metal salt) is usually made using a precipitation reaction. The shell will be the undoped vanadate. Unlike the core, which is made in a normal precipitation synthesis, the shell is made using the SILAR method. SILAR, which is short for

Successive Ionic Layer Adsorption and Reaction, has a few advantages when used for coating the core with the shell. First, independent nucleation of the shell material is prevented. This means that the core is coated with less crystals of the shell material is formed.

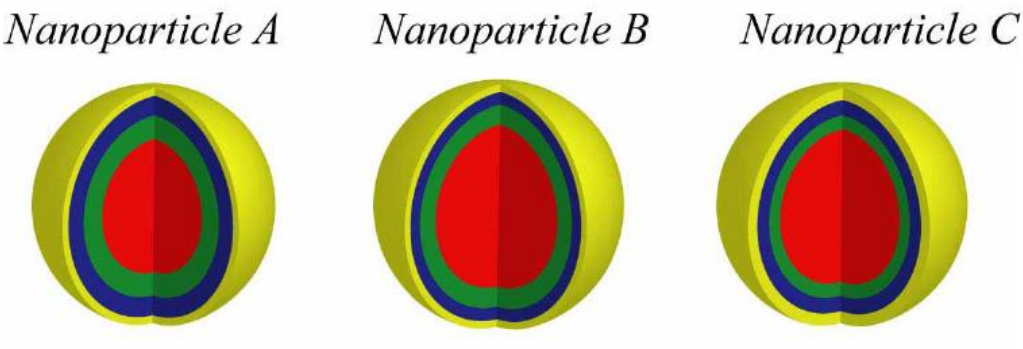

Figure 12. A core/multishell LaF_3 nanoparticle. The core consists of $LaF_3:Eu^{3+}$, the green layer of $LaF_3:Tb^{3+}$, the blue layer of $LaF_3:Tm^{3+}$ and the yellow layer is an undoped LaF_3[50]

Next, a more isotropic and uniform coating is created due to the low concentration of precursor. This low concentration is result of a slow adding of the reactants, as is normal for this synthesis. This isotropic, uniform coating will lead to spherical particles, which will lead to higher cathodoluminescence properties (see earlier). The last advantage is useful when depositing multiple shell layers. In between the depositions of the layers an annealing process takes place. This will prevent a bias of the composition, surface morphology, electrical and optical properties towards the different shell layers or core due to the longer reaction time of that specific shell layer. Since the core and the shell in this material have the same crystal structure (both are zircon-type materials), the shell will grow more easily on the vanadate core than on the silica core. As said above, the advantage of silica cores is that the particles will be spherical and uniform in size. The now emitting material will be coated on these particles and can be in contact with solvents. Many if (not all) solvents have C-H bonds. These bonds can cause a C-H vibrational overtone. These overtones can dissipate the energy of the excited lanthanide in a non-radiative way. This will quench the luminescence of the core/shell structure[1]. If however the core is now the emitting material and the shell(s) are a non-emitting variant of the core, luminescence is less likely quenched since the shell(s) now protect the core from these solvents.

It is possible to coat the core with more than one shell. Structures with different shells on the same core are called core/multilayer structures. These structures have already been investigated in applications for the generation of white light. White light can be generated when red, green and blue light are emitted at the same time. In Figure 12, core/multilayer nanoparticles are shown. The only difference between the three particles are the thicknesses of the layers. Here, the particles have a $LaF_3:Eu^{3+}$ core, a red emitting core. The green layer is $LaF_3:Tb^{3+}$, which is the green emitting shell. The blue layer is $LaF_3:Tm^{3+}$, which will be the blue emitting layer, since thulium has a blue luminescence when irradiated by UV-light. This means that the core and the two layers can provide white light. The most outer layer (the yellow) is an undoped LaF_3 layer that acts as an passive protective layer.[50]

2.4. Co-doping with other ions

Another known technique to increase the luminescence intensity is co-doping the material with Gd^{3+} ions. Literature showed that the luminescence intensity of holmium (Ho) in Ho doped (1%) aluminium nitride (AlN:Ho) increased when the amount of Gd^{3+} ions was increased[51]. When the ratio between Ho and Gd was increased, the luminescence intensity increased as well. However, when the ratio increased over 1:4, the luminescence intensity stayed constant. There are other ions than Gd^{3+} which are known to increase luminescence. Studies have shown that when lithium ions are incorporated into the crystal structure of a phosphor, an enhancement in the luminescence can be noticed[52, 53].The reason for this is that the Li^+ ions influence the crystallinity of the phosphor and luminescence can be (heavily) influenced by the crystallinity of the material. The incorporation of Li^+ was already described in literature for YVO_4[54], $LaVO_4$[55] and $GdVO_4$[56].

Results

3. Yttrium Orthovanadate

3.1. Synthesis

The main goal of this thesis was to synthesize vanadate nanoparticle in a microwave-assisted synthesis. In order to compare the materials made via this synthesis route, the materials were also hydrothermally synthesized.

3.1.1. Hydrothermal synthesis

The hydrothermal synthesis was performed in a process described by Ndagsi[5], a former thesis student of the L[3] group. In this process 1 mmol yttrium nitrate hexahydrate ($Y(NO_3)_3 \cdot 6H_2O$) was dissolved in 10 ml distilled water. To this solution a mixture of 20 ml glycerol dissolved in 10 ml distilled water was added. The glycerol acts like a capping agent. To this, 1 mmol sodium orthovanadate (Na_3VO_4) dissolved in 10 ml distilled water was added. When this was added, the solution changed from clear to a milky white solution. The pH was lowered to a value of 2. This caused the solution to become a clear bright yellow solution. The solution was then transferred to an autoclave and placed inside an oven for 24 hours at 200°C. After 24 hours, the product was left to cool down naturally for 24 hours. The product was then centrifuged at 7000 rpm for 5 minutes. The product was washed 3 times with distilled water and 3 times with ethanol. The product was dried overnight in a vacuum oven at 45°C. To increase the crystallinity of the product, remove water present in the product and any excess products, the product was heat treated for 3 hours at 900°C.

3.1.2. Microwave-assisted synthesis

The same procedure as the hydrothermal synthesis was used. Yet, unlike in the hydrothermal synthesis, the solution was now transferred to a 30 ml microwave tube. This tube was placed inside a microwave furnace at 180°C for 30 minutes. The same settings on the microwave furnace were used for all YVO_4 syntheses (180°C, 200W, 20 bar and no Powermax). Again the product was centrifuged at 7000 rpm for 5 minutes and washed several times with distilled water and ethanol. The product was left to dry overnight in a vacuum oven at 40°C. Afterward, the products were heat treated at 900°C for 3 hours. For the samples where ammonia methavanadate (NH_4VO_3) was used as a vanadium source, the

only thing different was the pH value. Here the pH was increased to value 10 using an ammonium hydroxide solution.

3.2. Reaction conditions

The reaction conditions for the different syntheses are presented in Table 2. Each reaction has been heat treated for 3 hours at 900°C.

Table 2. Reaction conditions of the different YVO_4 syntheses. In methods, H stands for hydrothermal reaction and M for microwave assisted reaction. The column adjustment pH describes which acid/base was used to change the pH.

Name	Method	Temperature	Time	pH	$Y(NO_3)_3.6H_2O$	Na_3VO_4	NH_4VO_3	Glycerol	Adjustment pH
1	H	200°C	24 hours	2	1 mmol	1mmol		20 ml	HCl
2	H	200°C	24 hours	2	1 mmol	1mmol		20 ml	HNO_3
3	M	180°C	15 minutes	2	1 mmol	1mmol		20 ml	HNO_3
4	M	180°C	30 minutes	2	1 mmol	1mmol		20 ml	HNO_3
5	M	180°C	15 minutes	10	1 mmol		1 mmol	20 ml	NH_4OH
6	M	180°C	30 minutes	10	1 mmol		1 mmol	20 ml	NH_4OH

3.3. Characterisation

3.3.1. Diffuse Reflectance Infrared Fourier Transform Spectra

For the characterisation of the samples, DRIFTS spectra were recorded. From the spectra (see Figure 13-14) it is quite clear that the peaks in the spectra of the heat treated samples are shifted to higher wavenumbers. The heat treated samples (red lines in the spectra) have less water present in the sample (broad band around 3500-3000 cm^{-1}). For sample 1, the peaks labelled a-c are peaks indicating the presence of glycerol[66] (see Figure C1 in the appendix). It is clear that these peaks are not visible for heat-treated sample 2, which might conclude that no glycerol is present on the particles after heat treatment. Both peak d (sample 1) and peak e (sample 2) are around 925 cm^{-1} and can be attributed to the V-O stretch vibration.

Name	Wavenumber	Vibration
a	1208 cm^{-1}	Glycerol
b	1120 cm^{-1}	Glycerol
c	1073 cm^{-1}	Glycerol
d	923 cm^{-1}	V-O
e	928 cm^{-1}	V-O

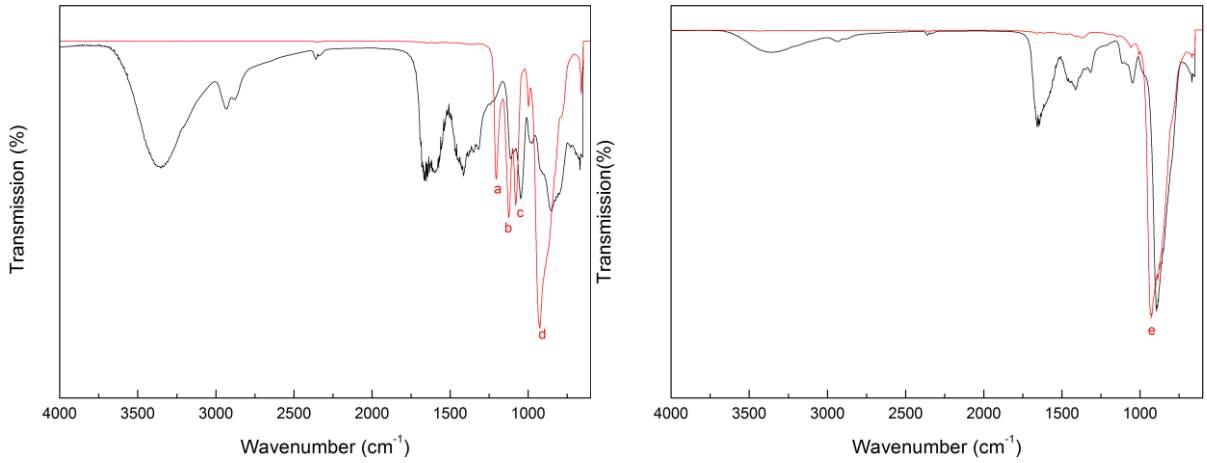

Figure 13. DRIFTS spectra of sample 1 (left) and sample 2 (right), both non-heat treated (black) and heat treated (red). Both products are synthesised hydrothermally.

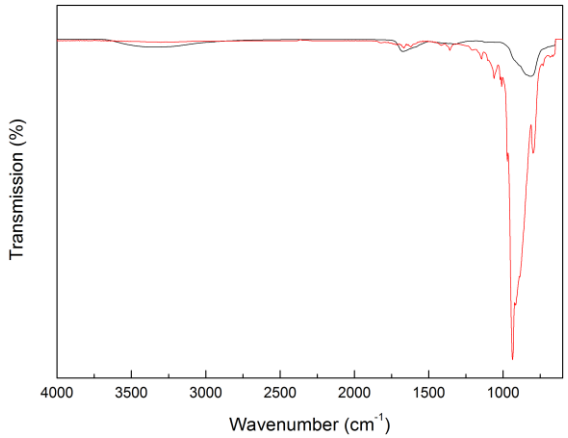

Figure 14. DRIFTS spectra of sample 4, both non-heat treated (black) and heat treated (red). The product was synthesised via a microwave-assisted synthesis.

In Figure 14 a DRIFTS spectrum of a microwave-assisted synthesised product is shown (sample 4). Again here it is clear that there is a peak shift towards higher wavenumbers when the product is a heat treated sample. Not only a peak shift is present, the heat treated samples have less contaminations present (see Figure 13 as well), the DRIFTS spectra of the other products will only show the heat treated sample. For this microwave-assisted synthesized product the most intense peak is as well situated around 938 cm^{-1}, which is characteristic for the V-O stretch vibration. There is no significant difference between the DRIFTS of the hydrothermal and microwave-assisted syntheses when the same conditions are used and therefore DRIFTS cannot be used to determine any difference between the different synthetic routes.

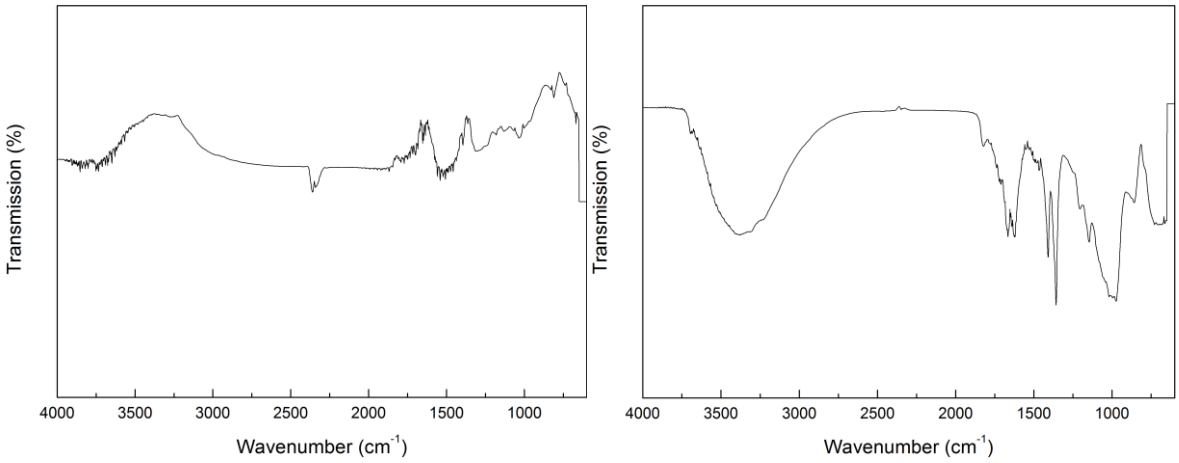

Figure 15. DRIFTS spectra of products synthesised for 15 minutes, in an acidic (left) and basic (right) environment.

The DRIFTS spectra of sample 3 (see Figure 15 left), which was similar to the synthesis of sample 4 (Figure 16 left), yet the reaction only lasted for 15 minutes, did not show this characteristic intense band, which suggests that the product is not formed or that the amount of water still present/glycerol is higher than the amount of the vanadate after 15 minutes in the acidic environment. When comparing this to a sample which was performed in a basic environment for 15 minutes (sample 5, Figure 15 right), it is clear that the product can be formed in a basic environment after a short reaction time, however in small yield, since the characteristic for the V-O stretch vibration is as intense as other peaks present in the sample.

To see if there is an influence on the product when different vanadium sources are used, a sample where the vanadium source was sodium orthovanadate (sample 4) and a sample were the vanadium source was ammonium metavanadate (sample 6) were synthesized. The DRIFTS spectra do not show any big differences, the V-O stretch is still present around the same wavenumber for both samples, as can be seen in Figure 16.

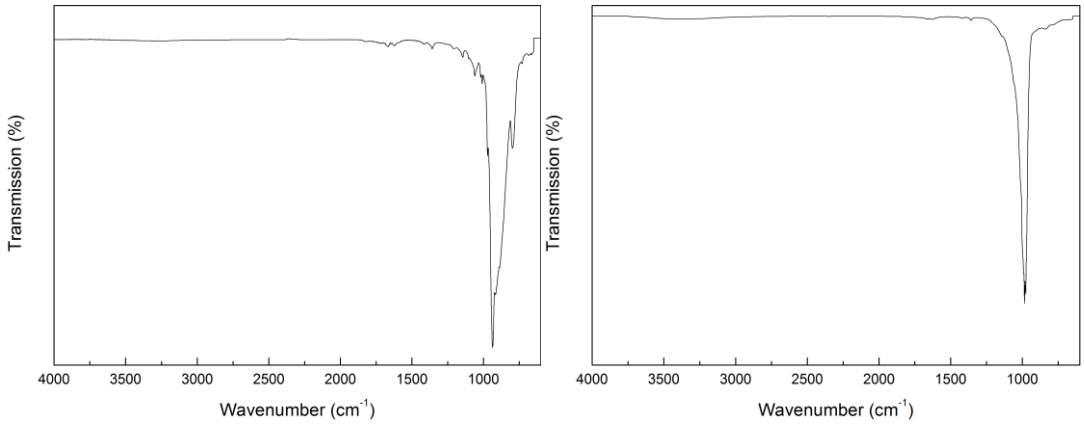

Figure 16. DRIFTS spectra of samples were the vanadium source was sodium orthovanadate (left) and ammonium metavanadate (right) after heat treatment at 900°C for 3 hours.

3.3.2. XRD diffractograms

The products were heat treated at 900°C for 3 hours to obtain a more crystalline material. The XRD diffractograms of the as prepared and heat treated material were made to identify the phase of the materials. Both the as prepared and heat treated sample show a pure tetragonal phase (36060-ICSD[62]). After heat treatment, the peaks in the diffractogram are more narrow then the peaks before heat treatment. This shows that the crystallinity increases after heat treatment. To see if there is phase differences when the vanadium source is changed, a new sample was synthesized where ammonium metavanadate (NH_4VO_3) was the vanadium source (samples 5 and 6). As can be seen in Figure 17, the non-heat treated samples show two broad peaks and for the hydrothermal samples, extra peaks can be seen (however, for sample 1, these contaminations can be the result of a different acid used to lower the pH). The diffractogram of sample 4 is slightly broader than for sample 3. This slight broadening is attributed to smaller particles. The same broadening can be seen in samples 5 and 6 and no phase change can be noticed between the sodium orhtovanadate (samples 3-4) and ammonium metavanadate (samples 5-6) as vanadium source.

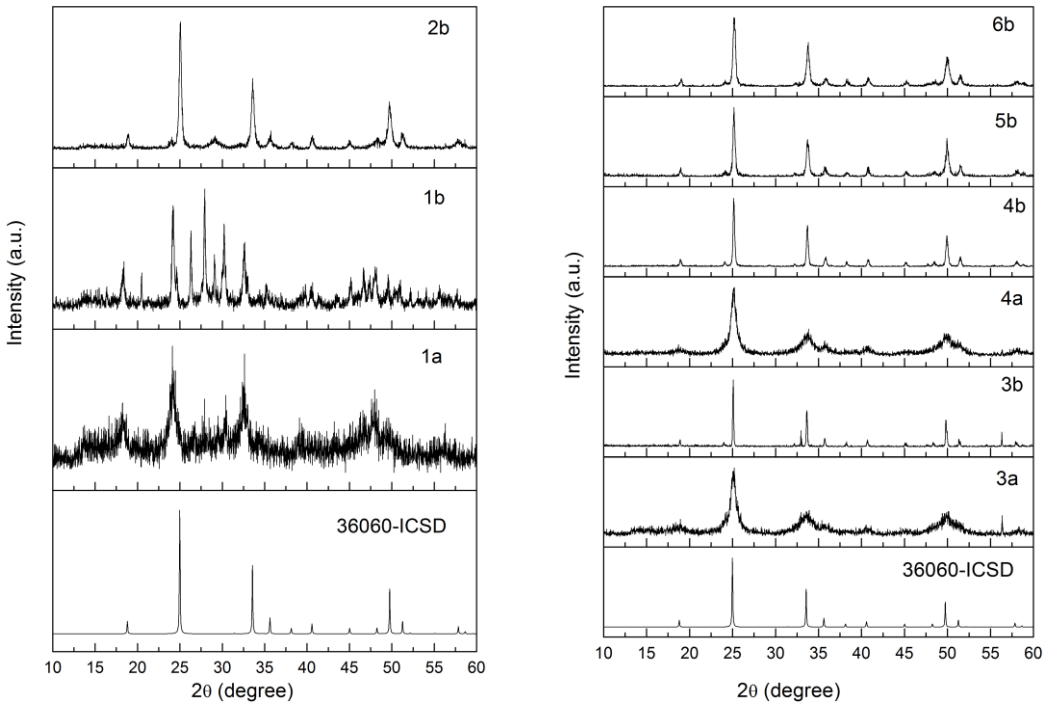

Figure 17. XRD diffractograms form YVO_4 made using hydrothermal (left) or microwave-assisted (right) synthesis. The a and b represent the non-heat treated and heat treated sample respectively.

3.4. Morphology

From literature it is known that the morphology of particles is influenced by the reaction conditions. In this work, the aim was to synthesize small, spherical and uniform particles. To obtain such particles, different reaction conditions were employed. The conditions to obtain crystalline, pure YVO_4 nanoparticles were already optimized[5]. In this work, the focus lied on making these particles smaller and more uniform. XRD measurements and SEM images of the obtained particles were performed to confirm the crystallinity and size of the particles These SEM images (see Figure 18) showed even at low magnification (top left) that the particles are quite uniform in their size. When the magnification was increased, it is clear that the particles are made out of agglomerated smaller particles. In the image of the highest magnification (bottom right), the particles which make up the bigger particles are not uniform in size. This means that the material cannot be used for core/shell like structures.

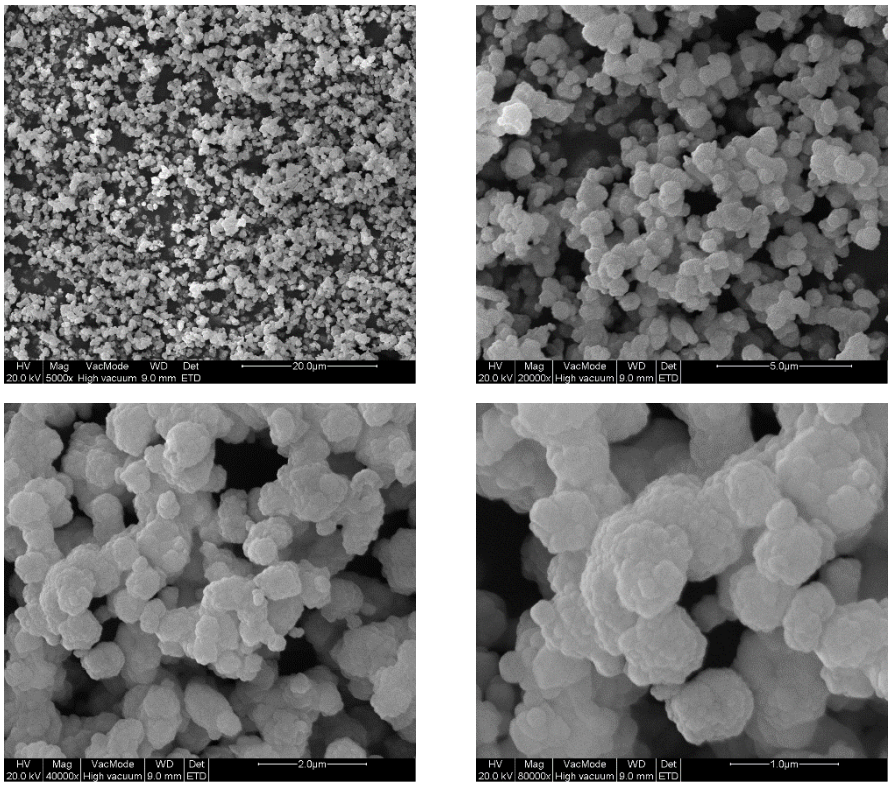

Figure18. SEM images sample 4, heat treated at 900°C for 3 hours. The different magnifications: Top left= 5000x, top right= 20000x, bottom left= 40000x and bottom right= 80000x

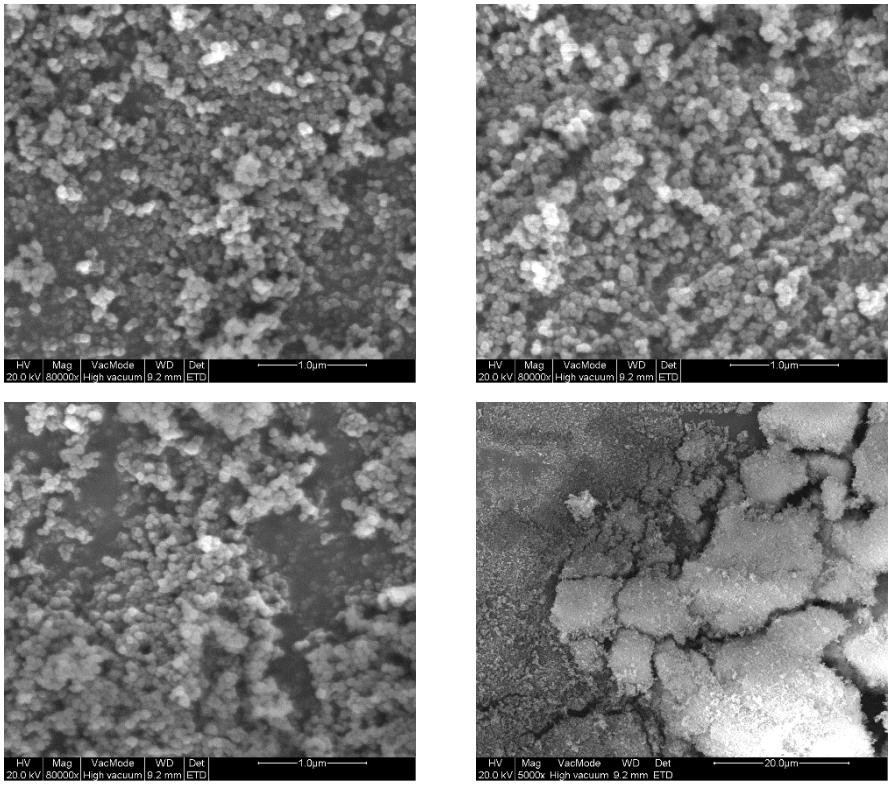

Figure 19. SEM images of sample 6, heat treated at 900°C for 3 hours. Top left: magnification 80.000x. Top right: magnification 80 000x. Bottom left: magnification 80 000x. Bottom right: magnification 5 000x.

Even though the resolution of the SEM images for the sample 6 (Figure 19) are quite low in comparison with sample 4 (Figure 18), it can be noticed that the sample with a different source of vanadium (the vanadium source is altered from sodium orthovanadate (sample 4) to ammonium metavanadate (sample 6)) shows relatively the same morphology. Just like sample 4, the morphology of sample 6 is an aggregation of spherical, nano-sized particles. Due to the low resolution (a lot of charge effects were observed when measuring these samples, therefore SEM images of better resolution were not possible to obtain), it is not entirely clear if the particles from sample 6 are more or less uniform in shape and size than the particles of sample 4.

4. Gadolinium Orthovanadate

4.1. Synthesis

As was in the case for YVO_4, the goal was to create spherical, uniform nano-sized particles which could be used for core/shell structures. The material was synthesised hydrothermally and in a microwave-assisted synthesis for comparison.

4.1.1. Hydrothermal synthesis

The hydrothermal synthesis of $GdVO_4$ was performed in the same procedure as for YVO_4. A solution of 1 mmol gadolinium nitrate hexahydrate ($Gd(NO_3)_3 \cdot 6H_2O$) dissolved in 10 ml distilled water was mixed with a solution of 20 ml glycerol dissolved in 10 ml distilled water. To this mixture, a solution of 1 mmol Na_3VO_4 dissolved in 10 ml distilled water was added. As was in the case of the YVO_4, the solution turned into a milky white solution. The pH of the solution was lowered to 2 using HCl and a clear yellow solution was obtained. The solution was transferred to an autoclave and placed inside an over for 24 hours at 200°C. The product was left to cool for 24 hours, centrifuged and washed several times with water and ethanol. The product was dried overnight in a vacuum oven at 40°C. The product was heat treated for 3 hours at 900°C

4.1.2. Microwave-assisted synthesis

The microwave-assisted synthesis was performed after the initial characterization of the products formed in the hydrothermal synthesis. Due to this, a difference in pH values between the hydrothermally synthesized products and the microwave-assisted products is noticed. The same procedure was followed as for the hydrothermal reaction (with exception of the pH value, which was increased with NaOH). The solution (no longer a clear, bright yellow solution, but a more pale yellow turbid solution was obtained) was transferred to a microwave tube and placed inside the microwave furnace for 15 and 30 minutes at 180°C. The settings for the microwave-assisted synthesis (Power = 200W, Pressure = 20 bar, Powermaxx = off and high stirring = on) remained the same for all the syntheses.

4.2. Reaction conditions

All the different reactions which were performed are presented in Table 3. The different reactions were performed to obtain a pure phased, spherically shaped and nano-sized

material. The different conditions used show their influences on the materials phase and morphology. The influence of the pH can be predicted by the literature study[30].

Table 3. Different reactions used in this thesis. In methods, H stands for hydrothermal reaction and M for microwave assisted reaction. The column adjustment pH describes which acid/base was used to change the pH.

Name	Method	Temperature	Time	pH	$Gd(NO_3)_3.6H_2O$	Na_3VO_4	Glycerol	Adjustment pH
7	H	200°C	24h	2	1mmol	1mmol	20 ml	HCL
8	H	200°C	24h	7	1mmol	1mmol	20 ml	NaOH
9	M	180°C	15min	7	1mmol	1mmol	20 ml	NaOH
10	M	180°C	30min	7	1mmol	1mmol	20 ml	NaOH
11	M	180°C	15min	10	1mmol	1mmol	20 ml	NaOH
12	M	180°C	30min	10	1mmol	1mmol	20 ml	NaOH
13	M	180°C	15min	7	1mmol	1mmol	10 ml	NaOH
14	M	180°C	30min	7	1mmol	1mmol	10 ml	NaOH
15	M	180°C	30min	10	1mmol	1mmol	10 ml	NaOH
16	M	180°C	30min	7	1mmol	1mmol	0 ml	NaOH
17	M	180°C	15min	10	1mmol	1mmol	0 ml	NaOH
18	M	180°C	30min	10	1mmol	1mmol	0 ml	NaOH

4.3. Characterisation

4.3.1. Diffuse Reflectance Infrared Fourier Transform Spectra

Just as is the case for YVO_4, DRIFTS spectra of the $GdVO_4$ samples were recorded. The DRIFTS spectra of the hydrothermally synthesised samples (sample 7 and 8) are shown in Figure 20. As was the case for YVO_4, the heat treated $GdVO_4$ samples show a better (without all the impurities) DRIFTS spectrum than the non-heat treated samples. For further characterisation, only the DRIFTS of the heat treated samples will be shown. For sample 7, the DRIFTS show the characteristic narrow peak, slightly shifted, of the V-O stretch vibration. This shows that a vanadate material was formed. Again, no distinction between the samples can be noticed from DRIFTS measurements, therefore other characterisation methods were necessary.

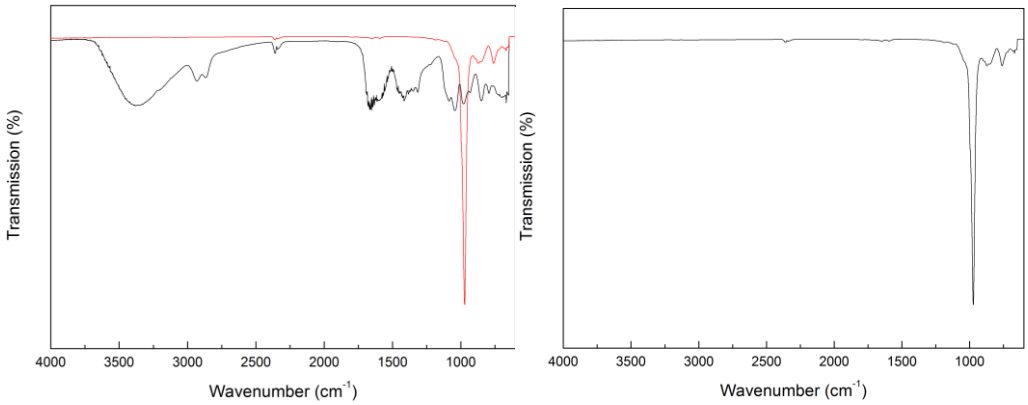

Figure 20. DRIFTS spectrum of sample 7 both non-heat treated (black) as heat treated (red) at 900°C for 3 hours (left) and sample 8 heat treated at 900°C for 3 hours (right).

The samples prepared using a microwave show varying DRIFTS measurements. Some show the narrow peak characteristic for the V-O stretch vibration, shifted in varying degrees, while others show more peaks (see Figure 21 and 22). This could mean that the samples showing these extra peaks are not pure enough or that for these conditions glycerol is present on the surface of the particles, resulting in the extra peaks (see Figure C1 in the appendix).

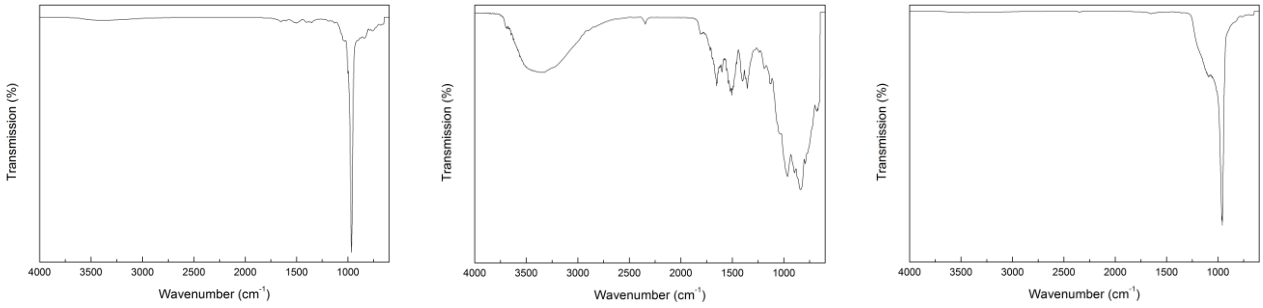

Figure 21. DRIFTS spectra of sample 13 (left), sample 14 (middle) and sample 15 (right). All samples were heat treated at 900°C for 3 hours.

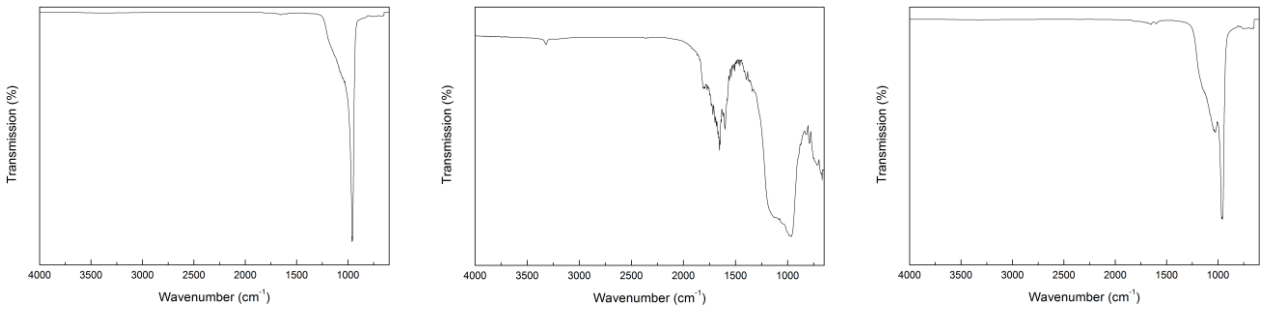

Figure 22. DRIFTS spectra of sample 16 (left), sample 17 (middle) and sample 18 (right). All samples were heat treated at 900°C for 3 hours.

4.3.2. XRD diffractograms

The XRD diffractograms of the syntheses are shown in Figure 23. For the hydrothermal reactions XRD diffractograms of both the non-heat treated and heat treated samples were measured. As was expected, the crystallinity of the samples improved after heat treatment. It is for this reason that only the heat treated microwave-assisted synthesized samples are measured. The diffractograms show that all the samples have the same tetragonal phase. However, some samples show little differences in their diffractograms. Samples 9 and 10 have the same pH value and therefore should show a very similar diffractogram. When comparing them, it can be noticed that the relative intensity of the peaks of sample 10 are quite different from the 15607 ICSD reference[63] and some peaks seem to blend in to the background. The only difference between these samples is the reaction time. This could mean that a phase change can occur if the reaction time is increased. In literature, a change of phase has been reported for $BiVO_4$ when using a microwave-assisted syntheses[26]: when the reaction mixture was irradiated for only 10 minutes, the product was pure tetragonal. When the reaction mixture was irradiated for 40 minutes, the product was pure monoclinic.

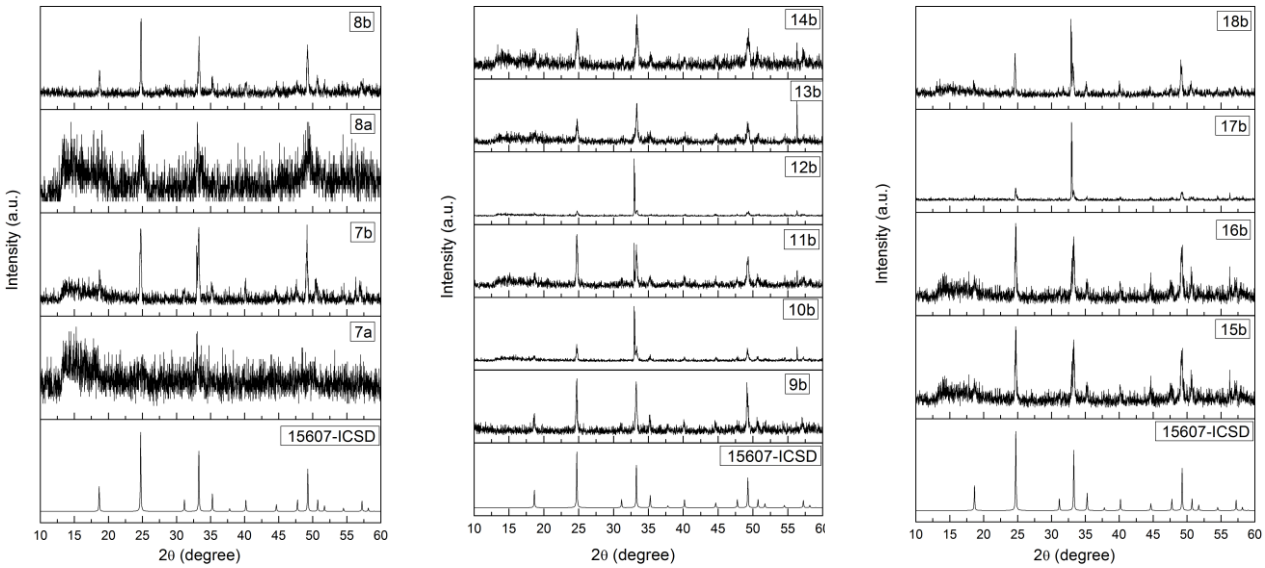

Figure 23. The XRD diffractograms of the $LaVO_4$ samples: left = hydrothermal synthesis, middle and right = microwave synthesis. In all diffractograms, a and b stand for non-heat treated and heat treated respectively.

An influence of the pH can also be noted from the XRD diffractograms. Comparing sample 9 with 11 (both 15 minutes of reaction and a pH of 7 and 10 respectively), it can be seen that the peaks of sample 11 still occupy the same place as the peaks of sample 9. In sample 11 there is a peak splitting at around 33°, which is a peak characteristic for the sample holder of

the XRD equipment. The same peak is present in samples 12-14 and samples 17 and 18. Samples 17 and 18 show the same pattern of peaks as the samples that did contain glycerol. This confirms that glycerol is an adequate capping agent and will not change the phase of the product. For more details on the efficiency of glycerol, SEM images needed to be recorded.

4.4. Morphology

To observe the morphology of the materials, SEM images were recorded. These can determine which material has the best size and uniformity to be used for doping with lanthanides. In Figure 24, the SEM images are shown. Not all the samples have SEM images, only the samples which showed a pure phase were chosen. When looking at the SEM images of sample 9, at the lowest magnification (20 000x) it seems quite uniform in size. However, just like in the case of YVO_4 in higher magnification (40 000x) it is clear that the nano-sized particles are not that uniform in shape and size. Therefore these materials are not quite suitable for core/shell like structures. Unfortunately, this was the only sample which showed non-aggregated particles (for truly non-aggregated particles, TEM images must be made). The images of sample 10 were taken at a lower resolution than the other samples, since there were problems with conductivity with that sample. These images show more or less the same morphology as the images of sample 9, which shows that the particles do not change their morphology when the reaction is performed for 30 minutes. The images of 11 show that although the particles are spherical, the particles are well aggregated and form a solid piece (third row of images in Figure 24). This means that for these conditions, more glycerol should be added to obtain non-aggregated particles. For sample 17 and 18, non-aggregated particles are expected since no glycerol was added. Together with the fact that no apparent change in phase in the XRD pattern is noticed if glycerol is added to the solution, the SEM images show that glycerol effectively caps the particles (this can be seen in the images on the row 1-3 in Figure 24).

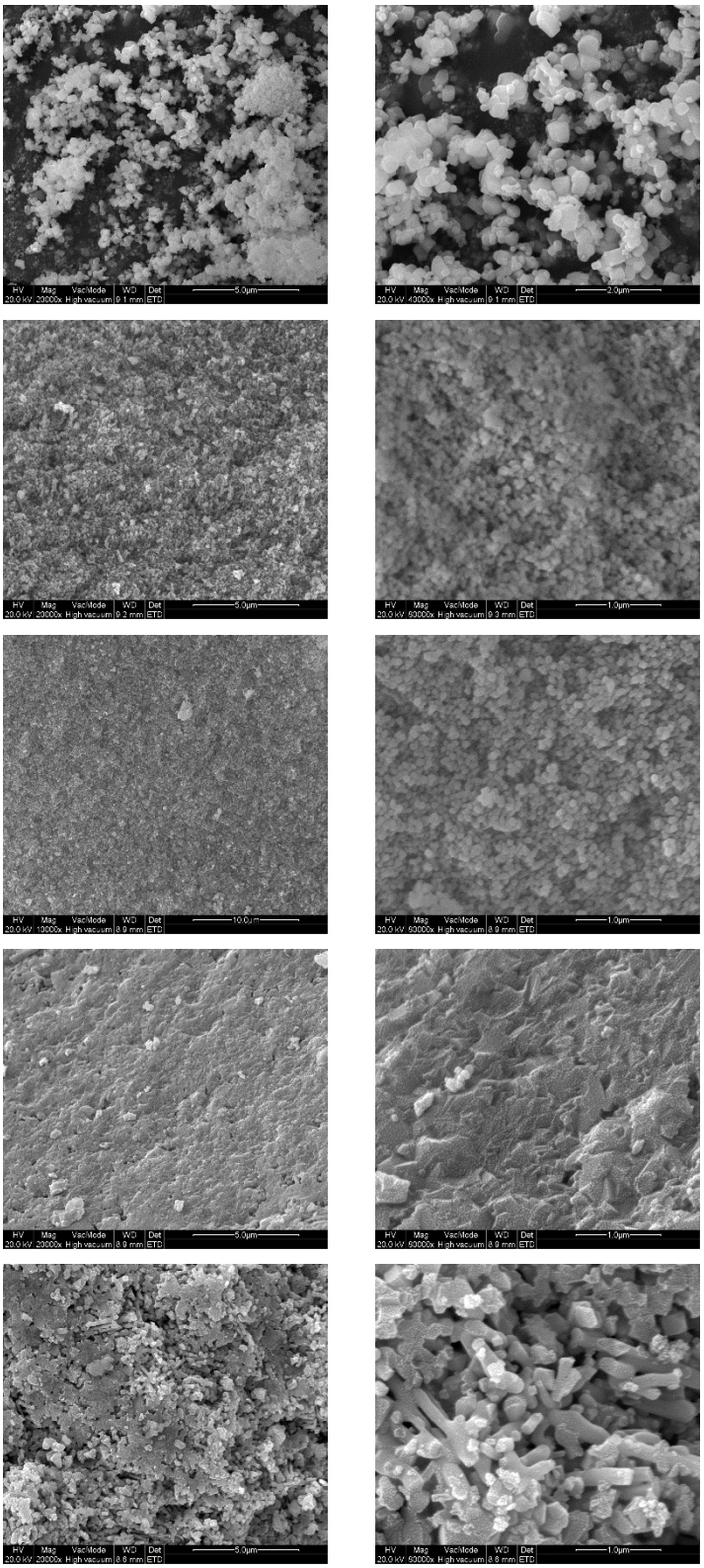

Figure 24. SEM images of $GdVO_4$ samples. The images: First row left: Sample 9 at magnification 20 000x; First row right sample 9 at magnification 40 000x; Second row left: sample 10 at magnification 20 000x; Second row right: sample 10 at magnification 80 000x; Third row left: sample 11 at magnification 10 000x; Third row right: sample 11 at magnification 80 000x; Fourth row left: sample 17 at magnification 20 000x; Fourth row right: sample 17 at magnification 80 000x; Fifth row left: sample 18 at magnification 20 000x and fifth row right: sample 18 at magnification 80 000x.

5. Lanthanum Orthovanadate

5.1. Synthesis

The synthesis of $LaVO_4$ was carried out in 2 ways, hydrothermally and microwave-assisted. The hydrothermal synthesis was performed like the first synthesis of YVO_4, and later was modified to obtain a pure phase. This modified synthesis was then performed using a microwave furnace. This synthesis was further modified to obtain the desired products.

5.1.1. Hydrothermal synthesis

For this synthesis, 1 mmol of lanthanum nitrate hexahydrate ($La(NO_3)_3.6H_2O$) and 1 mmol of Na_3VO4 were separately dissolved in 10 ml distilled water and stirred vigorously to ensure complete dissolution. A solution containing 20 ml glycerol was added to the lanthanum containing solution and stirred. The two mixtures were mixed and the pH was altered to the desired value. This solution was placed in a stainless steel autoclave for 24 hours at 200°C. The solution was naturally cooled to room temperature. The solution was then centrifuged to obtain the nanoparticles and these were washed 3 times with distilled water and ethanol. The product was then heat treated for 3 hours at 900°C. Later the pH was changed in order to create more uniform particles. XRD patterns showed that the product of this synthesis was monoclinic and not tetragonal.

5.1.2. Microwave-assisted synthesis

No literature was found on the synthesis of tetragonal $LaVO_4$ via a microwave assisted synthesis. In trying to obtain this, the conditions of the hydrothermal synthesis of monoclinic $LaVO_4$ were mimicked in the microwave assisted synthesis. Since tetragonal $LaVO_4$ has similar properties of bulk YVO_4, the reaction time for this synthesis was the same as for the YVO_4 powder. This means that 1 mmol of $La(NO_3)_3.6H_2O$ and 1 mmol of $NaVO_4$ were separately dissolved in 10 ml distilled water and stirred vigorously to ensure complete dissolution. A solution containing 20 ml glycerol was added to the $La(NO_3)_3$ solution and stirred. The two mixtures were mixed and the pH was altered to pH 4 using nitric acid. This mixture was placed inside a 30 ml microwave furnace tube and placed into the microwave for 30 minutes at 180 °C. The same conditions were used as in the synthesis of YVO_4 (180°C, 200W, 20 bar, high stirring and no Powermax).

5.2. Reaction conditions

The goal was to obtain the tetragonal $LaVO_4$. To do this, the reaction conditions were varied. The different syntheses are listed in Table 4. Some of the samples were heat treated. To indicate if the sample was heat treated, the name will be (sample name) b.

Table 4. Table of the syntheses $LaVO_4$. The M or H in method stands for Microwave-assisted synthesis and Hydrothermal synthesis respectively.

Name	Method	Temperature	Time	pH	$La(NO_3)_3 \cdot 6H_2O$	Na_3VO_4	Glycerol	Adjustment pH
19	H	200°C	24h	2	1mmol	1mmol	20 ml	HNO3
20	H	200°C	24h	6	1mmol	1mmol	20 ml	NaOH
21	M	180°C	30min	6	1mmol	1mmol	20 ml	NaOH
22	M	180°C	15min	6	1mmol	1mmol	10 ml	NaOH
23	M	175°C	15min	6	1mmol	1mmol	0 ml	NaOH
24	M	175°C	30min	6	1mmol	1mmol	0 ml	NaOH
25	M	180°C	15min	4	1mmol	1mmol	20 ml	HNO3
26	M	180°C	30min	4	1mmol	1mmol	20 ml	HNO3
27	M	180°C	15min	4	0,6mmol	0,6mmol	6 ml	HNO3
28	M	180°C	30min	4	0,6mmol	0,6mmol	6 ml	HNO3
29	M	180°C	15min	6	1mmol	1mmol	30 ml	NaOH
30	M	180°C	30min	6	1mmol	1mmol	30 ml	NaOH
31	M	180°C	15min	4	1mmol	1mmol	20 ml	HNO3
32	M	180°C	30min	4	1mmol	1mmol	20 ml	HNO3
33	M	180°C	15min	4	1mmol	1mmol	30 ml	HNO3
34	M	180°C	30min	4	1mmol	1mmol	30 ml	HNO3

5.3. Characterisation

5.3.1. Diffuse Reflectance Infrared Fourier Transform Spectra

When comparing the non-heat treated and heat treated material, the same remarks can be made as for the YVO_4 and $GdVO_4$ samples: there is a shift of the V-O stretch vibration and less impurities are seen (see Figure 25). Again, for that reason, only the heat treated DRIFTS spectra are shown for all samples that were heat treated. Sample 29-34 were non-heat treated samples. To obtain the tetragonal $LaVO_4$, mild conditions are advised. Therefore no heat treatment was performed on a few samples to see any differences.

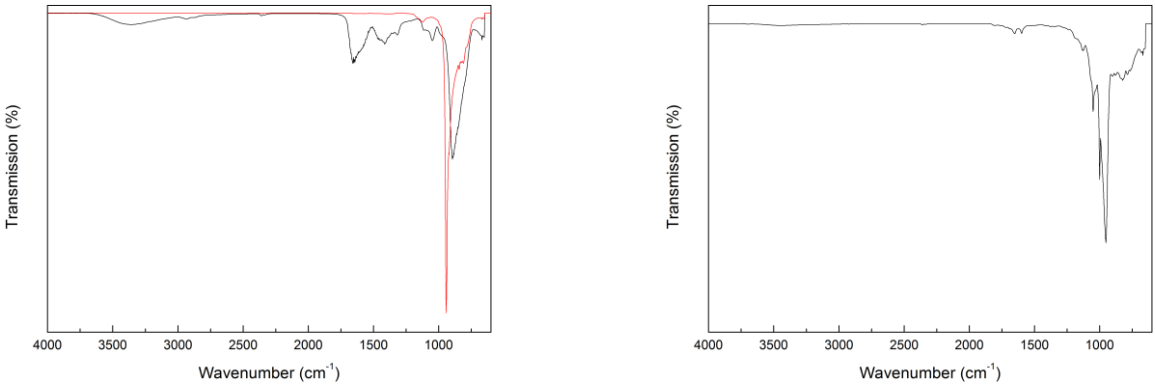

Figure 25. DRIFTS spectra of the hydrothermally synthesized products: sample 19 (left), both the non-heat treated (black) and heat treated (red), and sample 20 (right), heat treated. Heat treatment was performed at 900°C for 3 hours.

Many of the products obtained by the microwave-assisted synthesis show the characteristic V-O stretch vibration, although this peak is shifted in different degrees among the samples, as can be seen in Figure 26.

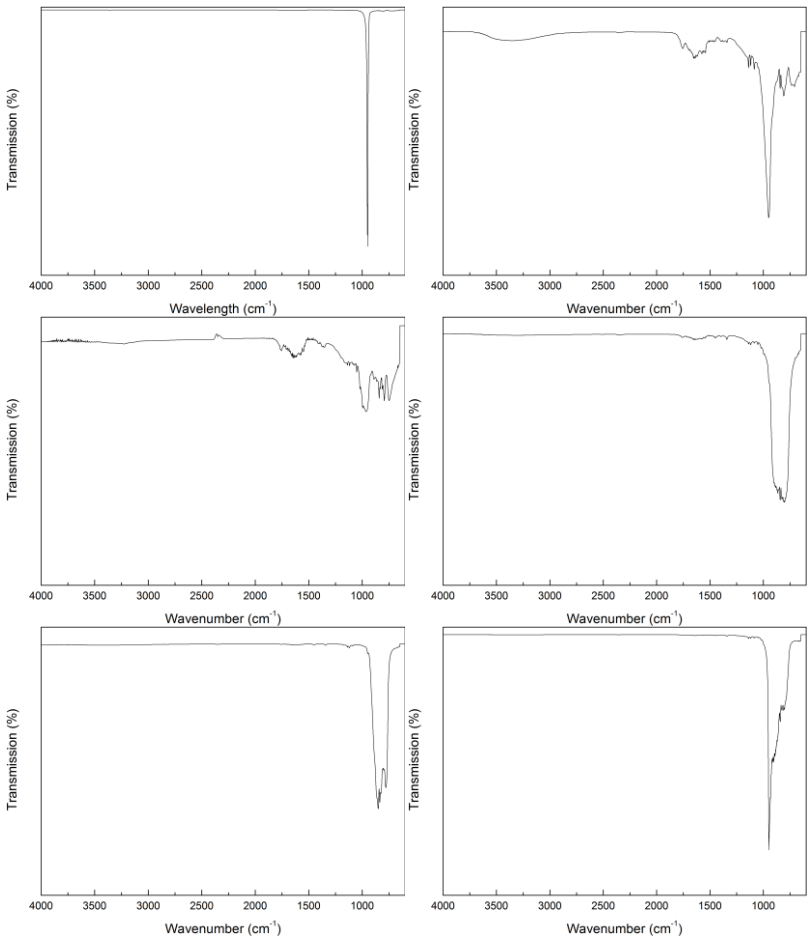

Figure 26. DRIFTS spectra of microwave-assisted synthesized products. Top row: sample 23 (left) and sample 24 (right). Middle row: sample 25 (left) and sample 26 (right). Bottom row: sample 27 (left) and sample 28 (right). All samples were heat treated at 900°C for 3 hours.

For the non-heat treated samples (29-34), a broad band around 3400 cm^{-1} can be expected (O-H vibration associated with water present in the sample) as well as other peaks which can be attributed to the C-H and/or O-H vibrations from glycerol still present (see Figure C1 in the appendix). The DRIFTS spectra of the non-heat treated samples can be found in Figure 27.

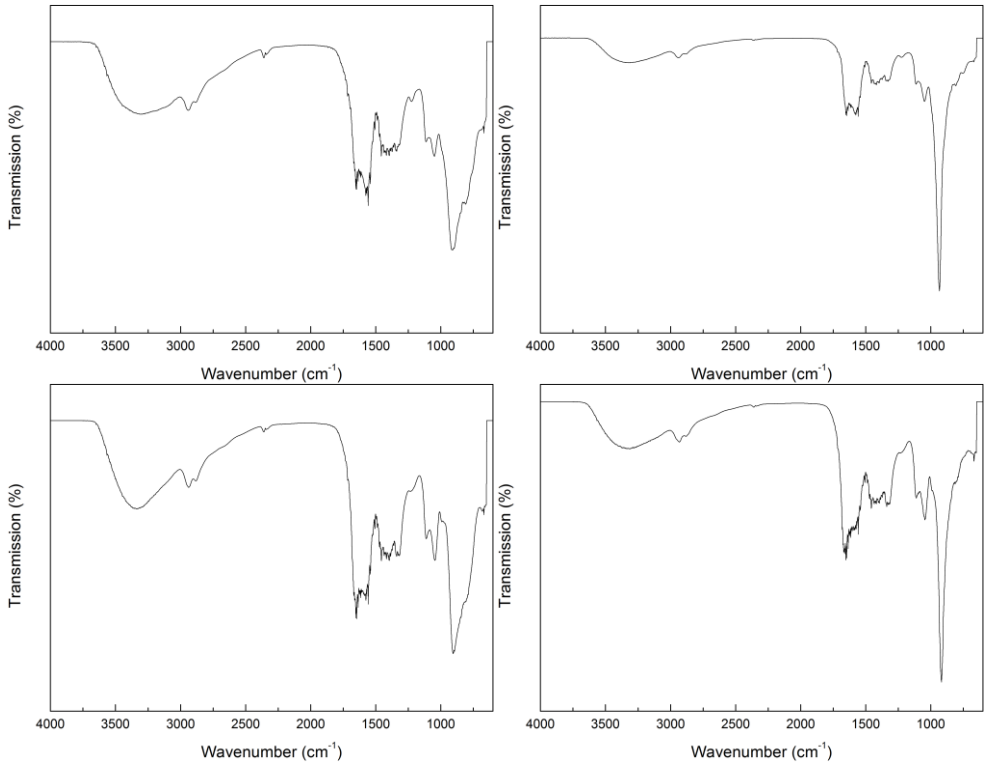

Figure 27. DRIFTS spectra of sample 31 (top left), sample 32 (top right), sample 33 (bottom left) and sample 34 (bottom right).

5.3.2. XRD diffractograms

The XRD diffractograms are presented in Figure 28. The hydrothermal reactions show the influence of the pH on the phase of the material. When the pH is 2 (sample 19) it is clear that the material has a monoclinic phase when heat treated (400-ISCD reference[64]), while the material synthesised in a solution of pH 6 (sample 20) shows a tetragonal phase when heat treated (411083-ISCD reference[65]), although the material is not completely pure phased. All next XRD diffractograms will only show the heat treated samples, since it has been shown for YVO_4, $GdVO_4$ and the hydrothermal samples of $LaVO_4$ that those are the only well-defined diffractograms. The same conditions of sample 20 were reproduced using a microwave-assisted synthesis. Surprisingly, the obtained sample (21) showed a monoclinic phase. In trying to obtain the tetragonal phase, some of the reaction parameters were

altered. However, all the samples synthesised using a microwave were in the monoclinic phase (with or without some impurities). The extra peak for sample 25 at 2θ = 33 is again the peak belonging to the sample holder of the XRD equipment.

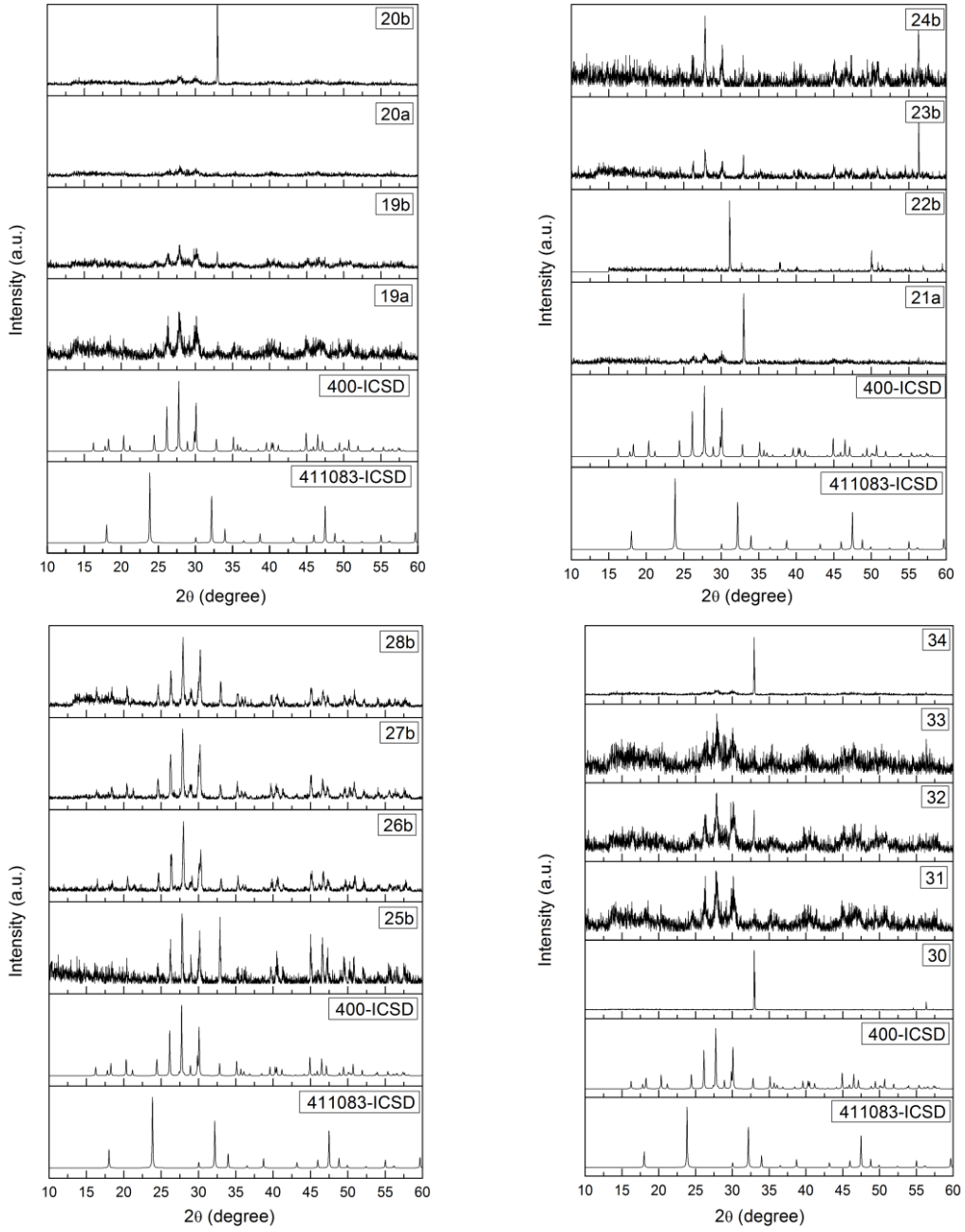

Figure 28. XRD diffractograms of the $LaVO_4$ samples prepared by a hydrothermal (upper left) or microwave-assisted synthesis (upper right and bottom). The a and b after the sample name stands for non-heat treated and heat treated at 900°C for 3 hours respectively. If the sample has no letter behind its name, the sample was not heat treated.

5.4. Morphology

As was the case for the other vanadate materials, only the samples with a pure phase, intense XRD diffractogram were sent to SEM to be analysed. In the case of $LaVO_4$, this were sample 26 and 33 Figure 29 shows the SEM images of sample 26, which is a heat treated sample and Figure 30 shows the SEM images of sample 33, a non-heat treated sample

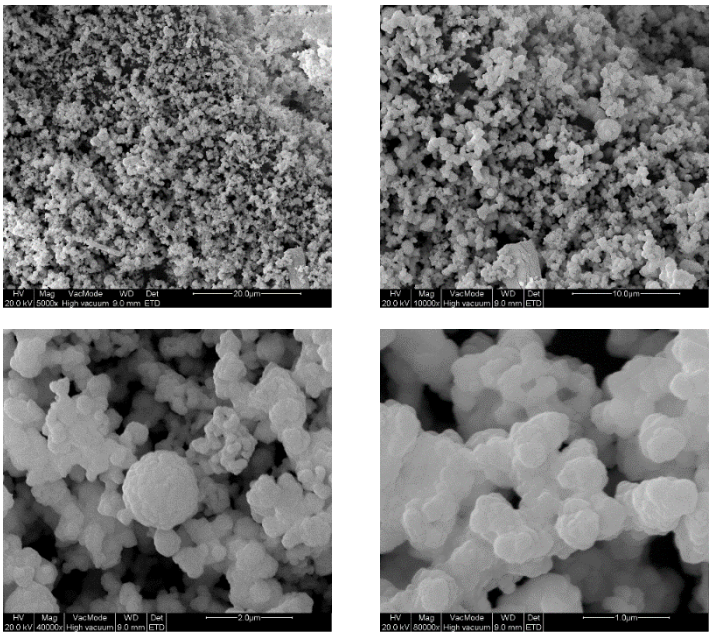

Figure 29. SEM images of sample 26 at magnification 5 000x (upper left), magnification 10 000x (upper right), magnification 40 000x (bottom left) and magnification 80 000x (bottom right).

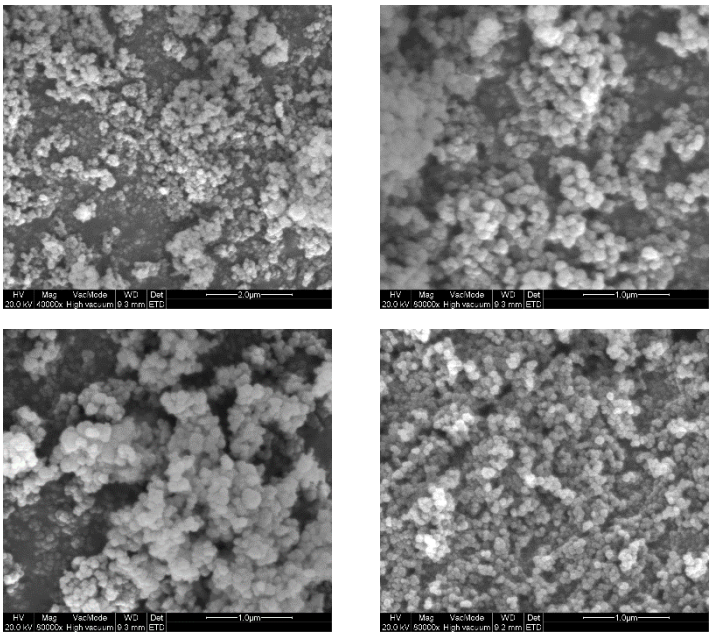

Figure 30. SEM images of sample 33 at magnification 40 000x (top left), magnification 80 000x (top right and bottom).

Again, the particles are quite small and fairly spherical, but not uniform enough to try to prepare core/shell particles. These particles were chosen to be further doped with Eu^{3+} ions

since Eu-doped $LaVO_4$ nanoparticles were the least investigated Eu-doped vanadate material used in this thesis.

6. Europium doped lanthanum orthovanadate

6.1. Synthesis

For the synthesis of the Eu^{3+} doped $LaVO_4$, the synthesis of $LaVO_4$ with the best XRD diffractogram was chosen. This is sample 26. This synthesis was repeated, and only the amount of $La(NO_3)_3{\cdot}6H_2O$ was altered. The general formula is now $La_{1-x}Eu_xVO_4$. This could be obtained by mixing $Eu(NO_3)_3{\cdot}6H_2O$ with the lanthanum nitrate. Different weight percentages were synthesised: 2.5 wt%, 5 wt%, 10 wt%, 12.5 wt% and 15 wt%.

The particles were harder to centrifuge than the non-doped particles. The doped particles were centrifuged at 9000 rpm for 10 minutes and dried overnight in a vacuum oven. After drying, the particles were heat treated at 900°C for 3 hours.

6.2. Characterization

To see if any changes in the phase occurred after the doping process, the samples needed to be characterized as well. Again, this was done using DRIFTS and XRD measurements.

6.2.1. Diffuse Reflectance Infrared Fourier Transform Spectra

To see any difference, the DRIFTS spectrum of the undoped sample is compared to the DRIFTS spectra of the Eu^{3+} doped samples. The comparison can be seen in Figure 31.

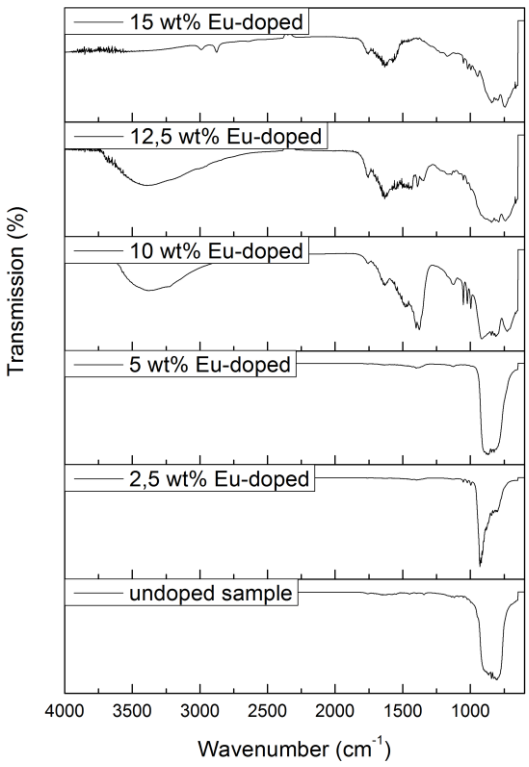

Figure 31. DRIFTS spectra of the undoped and Eu^{3+} doped samples.

For the doping percentage up to 5 wt%, no differences can be seen between the doped and undoped sample. From doping percentage 10 wt% to 15 wt%, it is clear that the sample contains more water (broad band around 3400 cm^{-1}) The other peaks present in these doping percentages are attributed to glycerol still present on the sample (see Figure C1 in the appendix). As was suspected, the intense peak around 925 cm^{-1} (V-O stretch bond) is present in the sample, which shows that the product was formed.

6.2.2. XRD diffractograms

The doped samples were compared to the same monoclinic and tetragonal references as sample 26. The XRD diffractograms are shown in Figure 32. The samples all have the monoclinic phase (400-ICSD), as was to be expected. This means that no significant change in phase occurred for doping percentages up to 10wt%.

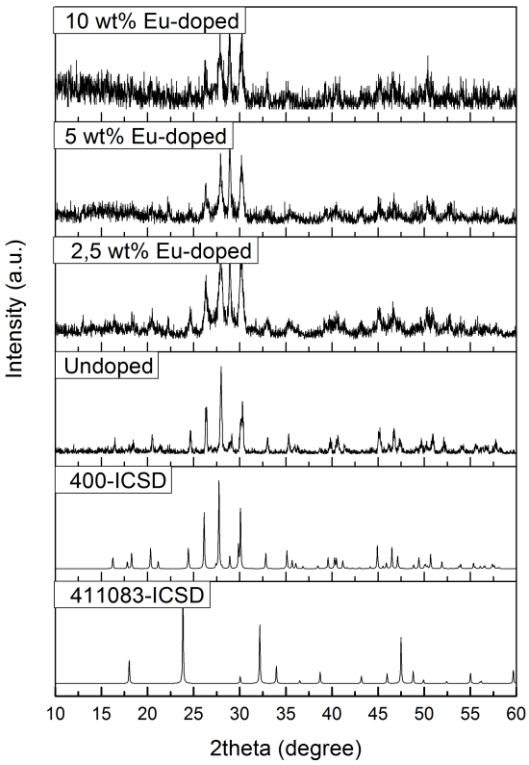

Figure 32. XRD diffractograms of the 2.5-10wt% Eu doped samples.

6.3. Morphology

The undoped sample is compared to the 10 wt% doped sample, to see if a significant difference in morphology can be detected. The SEM images are presented in Figure 33. Even though the resolution of the doped sample is much lower than for the undoped sample (there were a lot of charge effects and a better resolution could not be obtained), it is clear that the particles are much smaller. The aggregates of the undoped sample are bigger than the aggregates of the doped sample. This decrease in size when the sample is doped is consistent with the increase in rotations per minute needed for efficient centrifugation.

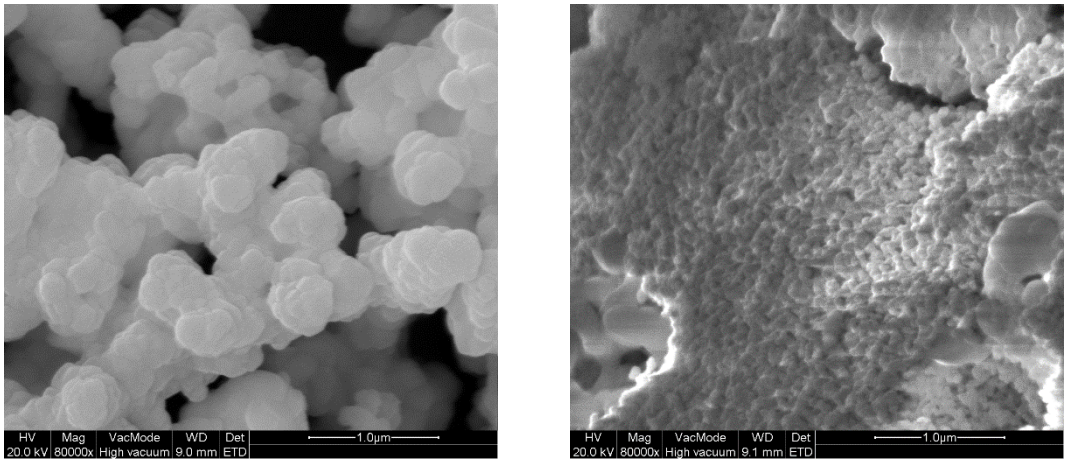

Figure 33. SEM images at magnification x 80.000 for an undoped (left) and 10 wt% Eu-doped (right) $LaVO_4$ sample

6.4. Luminescence data

In order to find out which molar percentage of europium doped in the monoclinic $LaVO_4$ host material would have the highest luminescence intensity and decay time, all the samples were measured with the same settings. For these samples the excitation wavelength was 316 nm and the emission wavelength was 614 nm. The spectra were measured with a step-size of 0.1 nm and a slit size of 0.5 nm to have well resolved spectra. The first sample measured was the 2.5 wt% Eu doped sample. In Figure 34, it can be noticed that the wavelength interval of the emission spectrum of this sample is different than for the rest of the samples. This was done to show that no emission of the vanadate host material was present during the measurements. Since all the samples only contain Eu^{3+}, all the peaks in the emission/excitation spectra of all the sample are in the same position and are assigned in Table 5. The excitation/emission spectra of the 10-15 wt% Eu-doped samples are presented in appendix D (Figure D1-D5). In the excitation spectra, the broad band, which is attributed to the V-O charger transfer band, is far more intense than the peaks belonging to the $^5L_6 \leftarrow {}^7F_0$ and $^5D_2 \leftarrow {}^7F_0$ transitions of the europium ions. This shows that the vanadium host material transfers the energy to the europium ion efficiently. Since the most intensive peak is the $^5D_0 \rightarrow {}^7F_2$ transition peak (at 614 nm) the products emit red light when excited with a UV-lamp at wavelength 302 nm.

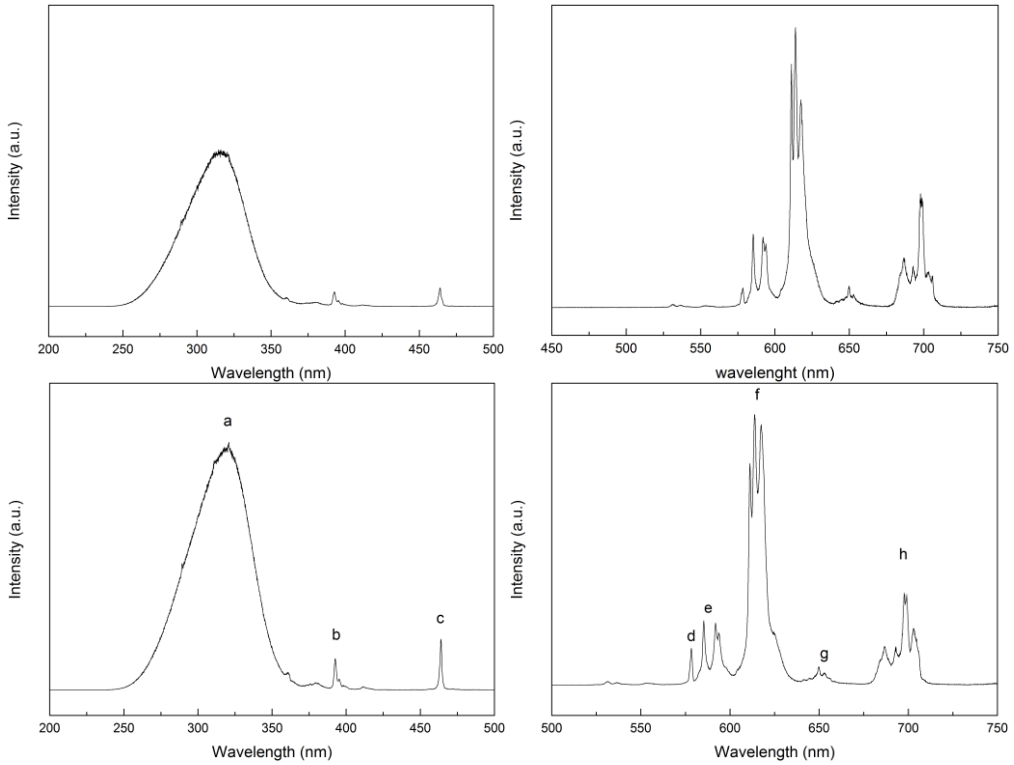

Figure 34. Luminescence measurments of the 2.5 wt% Eu-doped sample (top) and 5 wt% Eu-doped sample (bottom). The corrected excitation spectrum for both samples are shown on the left and the emission spectrum for both samples is shown on the right.

Table 5. Transitions of the peaks in the excitation and emission spectra of the Eu-doped $LaVO_4$ samples.

Label	Wavelength (nm)	Wavenumber (cm^{-1})	Transition
a			V-O charge transfer
b	392.6	25471	$^5L_6 \leftarrow {}^7F_0$
c	464.0	21552	$^5D_2 \leftarrow {}^7F_0$
d	578.3	17292	$^5D_0 \rightarrow {}^7F_0$
e	585.3	17085	$^5D_0 \rightarrow {}^7F_1$
f	614.0	16287	$^5D_0 \rightarrow {}^7F_2$
g	650.0	15385	$^5D_0 \rightarrow {}^7F_3$
h	697.8	14331	$^5D_0 \rightarrow {}^7F_4$

In accordance to literature[67], the 12.5 wt% Eu^{3+} sample showed the highest luminescence intensity and longest luminescence decay time (see Figure 35). The decay curves of the other Eu-doped samples can be found in Figure D6. The decay times of the different Eu-doped samples are presented in Table 6. In the literature, co-doping the samples with gadolinium ions increases the emission intensity[67]. To test this, the 12.5 wt% Eu doped sample was re-synthesized with a gadolinium co-doping percentage of 2 wt%, 5 wt% and 10 wt%. The idea

behind this co-doping is that the energy of the excited Gd^{3+} ions is transferred to the Eu^{3+} when excited. Due to the overlap between the excitation transitions of the Gd^{3+} ions and the V-O CTB, the Gd^{3+} will be excited around the same wavelength as the CTB. This means that both the CTB and the excited Gd^{3+} ions can transfer their energy to the Eu^{3+} ions. However, this increase in intensity can also be the effect of the change in ion size when Gd^{3+} is co-doped, which can form a defect in the crystal structure. Since the Gd^{3+} peak in the excitation spectrum overlaps with the V-O CTB, the effect which causes the increase in intensity cannot be defined. In order to define which effect took place, the 12.5 wt% Eu-doped sample was resynthesized with Y^{3+} (2, 5 and 10 wt%) and with Lu^{3+} (2, 5 and 10 wt%). If the increase in luminescent intensity is only due to the energy transfer between Gd^{3+} and Eu^{3+}, there should not be any increase/decrease in intensity for the Y/Lu co-doped samples (Y does not have any f orbitals, so no 4f-4f transition can occur. Lu has a completely filled f shell, so no 4f-4f transition can occur either).

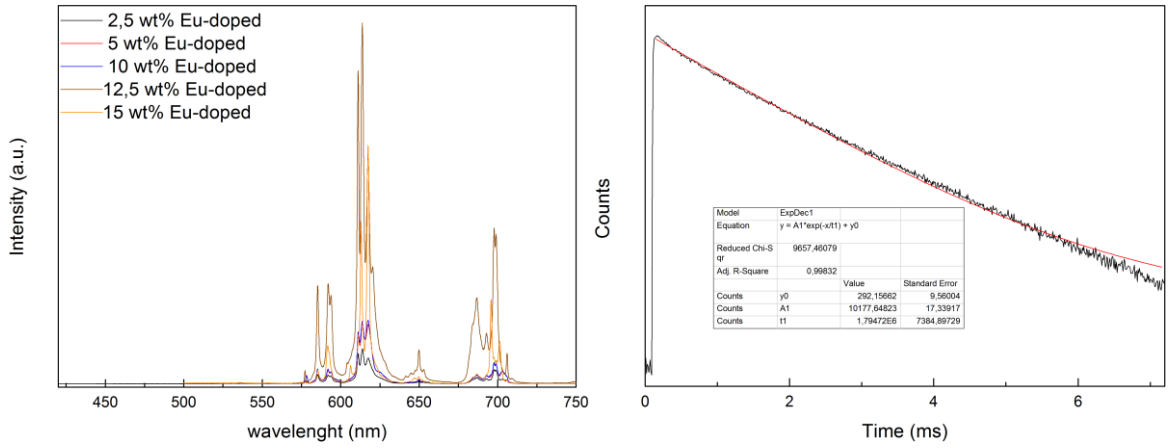

Figure 35. Left: the emission spectra of the 2.5 wt% Eu-doped (black), 5 wt% Eu-doped (red), 10 wt% Eu-doped (blue), 12.5 wt% Eu-doped (brown) and 15 wt% Eu-doped (orange) samples. Right: Decay curve of the 12.5 wt% Eu-doped sample.

Table 6. Decay time of the different Eu-doped samples

Doping percentage Eu	Decay time τ
2.5 wt%	0.98 ms
5 wt%	0.82 ms
10 wt%	0.87 ms
12.5 wt%	1.79 ms
15 wt%	0.62 ms

For all doping percentages, the $^5D_0 \rightarrow {}^7F_2$ peaks are more intense than the $^5D_0 \rightarrow {}^7F_1$ peaks. The $^5D_0 \rightarrow {}^7F_1$ transition is a magnetic dipole transition and this transition is almost not affected by any change in symmetry or ligand field strength. In sharp contrast to this, the $^5D_0 \rightarrow {}^7F_2$ transition (a hypersensitive transition) is an electric dipole transition and is heavily influenced by the presence/absence of an inversion centre at the trivalent europium site. By comparing the ratio of the integrated intensity of both peaks ($^5D_0 \rightarrow {}^7F_2$ / $^5D_0 \rightarrow {}^7F_1$), the symmetry can be estimated. A low value indicates a high symmetry, while a high ratio indicates a low symmetry. In this work, it is clear that the symmetry of the product is low.

6.5. Ln^{3+} Co-doping

The 12.5 wt% Eu-doped sample has been co-doped with Gd^{3+}, Y^{3+} and Lu^{3+} ions (2, 5 and 10 wt%). The synthesis is the same as for the synthesis with Eu^{3+}, but an extra amount of RE^{3+} ions were added to the lanthanide containing mixture. In Figure 36, the emission intensity of the co-doped samples were compared to each other. It is clear that for all different co-doped samples, the emission intensity increases when the doping percentage increases.

6.5.1. Gd^{3+} co-doping

The excitation and emission spectra of the 10 wt% Gd^{3+}/Y^{3+} co-doped samples are presented in Figure 37. For all the different doping percentages of Gd^{3+}, the peaks are on the same position and are labelled in Table 7.

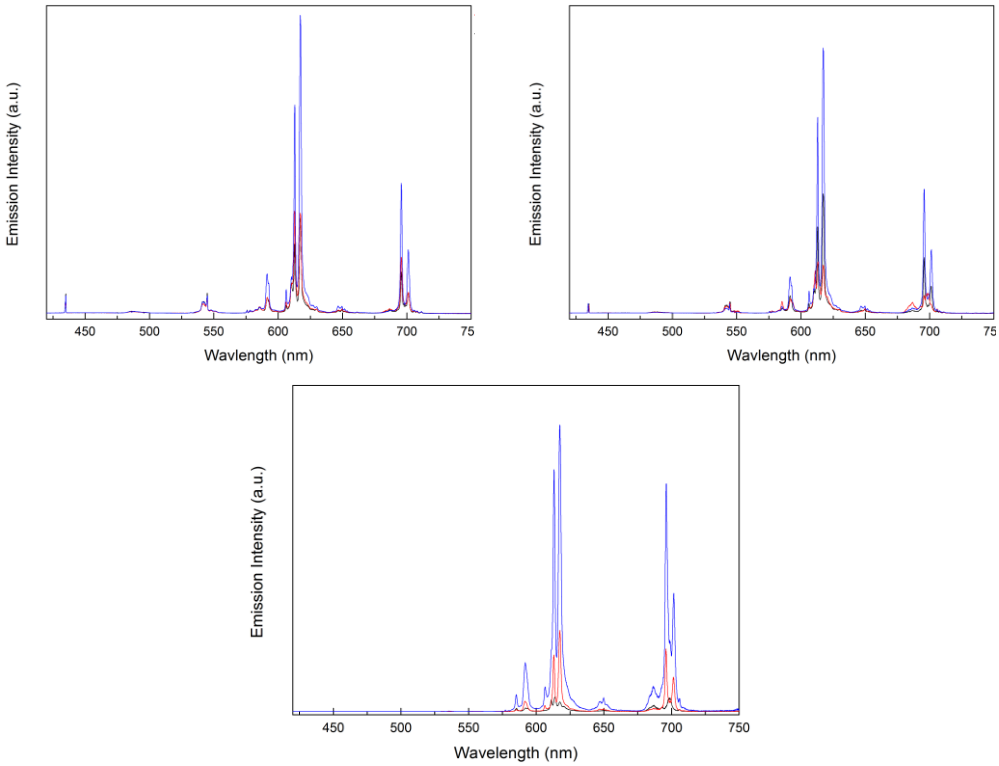

Figure 36. Comparison of the emission intensity of the 2 wt% (black), 5 wt% (red) and 10 wt% (blue) Gd^{3+} co-doped samples (top left), Y^{3+} co-doped samples (top right) and Lu^{3+} co-doped samples (bottom).

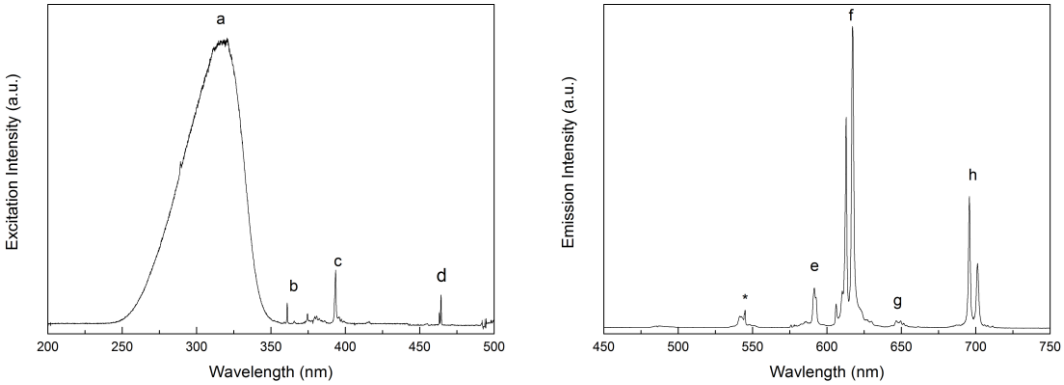

Figure 37. The uncorrected excitation (left) and emission (right) spectrum of the $La_{0.775}Eu_{0.125}Gd_{0.1}VO_4$ sample. The peak assigned with * is a peak of terbium contamination.

From Figure 37 it is clear that the charge transfer is efficient (V-O CTB is far more intense than the europium transition peaks). Since some of the La^{3+} ions were exchanged with Gd^{3+} ions, no apparent change in symmetry is expected. When looking at the emission spectrum, this is confirmed by the low ratio of $^5D_0 \rightarrow {}^7F_2$ / $^5D_0 \rightarrow {}^7F_1$. The only differences in the Gd^{3+} co-doped emission spectra is the peak splitting of the $^5D_0 \rightarrow {}^7F_4$ transition when compared to the non-co-doped sample. In the excitation spectra (Figure 37, left), an extra europium transition is noticed, the $^5D_4 \leftarrow {}^7F_0$. All the peaks have the same position in the other co-doping percentages (the other spectra are presented in Figure D7-D8). There is no significant difference in decay time of the different co-doping percentages of Gd^{3+}. The decay curve of

the 10 wt% Gd^{3+} co-doped sample is presented in Figure 38 and the different decay times are presented in Table 8. The other decay curves are presented in Figure D13.

Table 7. Labeling of the peaks of the Gd^{3+} co-doped samples

Label	Wavelength (nm)	Wavenumber (cm^{-1})	Transition
a			V-O CTB
b	360.9	27709	$^5D_4 \leftarrow {}^7F_0$
c	393.7	25400	$^5L_6 \leftarrow {}^7F_0$
d	464.5	21529	$^5D_2 \leftarrow {}^7F_0$
e	591.6	16903	$^5D_0 \rightarrow {}^7F_1$
f	617.3	16200	$^5D_0 \rightarrow {}^7F_2$
g	648.4	20644	$^5D_0 \rightarrow {}^7F_3$
h	695.7	14374	$^5D_0 \rightarrow {}^7F_4$

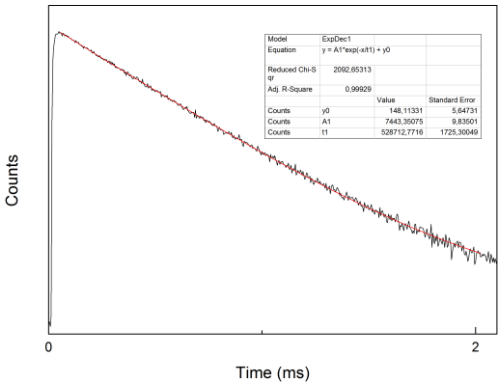

Figure 38. Decay curve of the 10 wt% Gd^{3+} co-doped sample

Table 8. The decay times of the different doping percentages Gd^{3+}

Doping Percentage Gd	Decay time τ
2 wt%	0.53 ms
5 wt%	0.50 ms
10 wt%	0.53 ms

6.5.2. Y^{3+} co-doping

The excitation and emission spectra of the 10 wt% Y^{3+} co-doped sample are presented in Figure 39. For all Y^{3+} co-doped samples, the peaks in the spectra are on the same position (the other luminescent spectra are presented in Figure D9- D10). The peaks are labelled in Table 9.

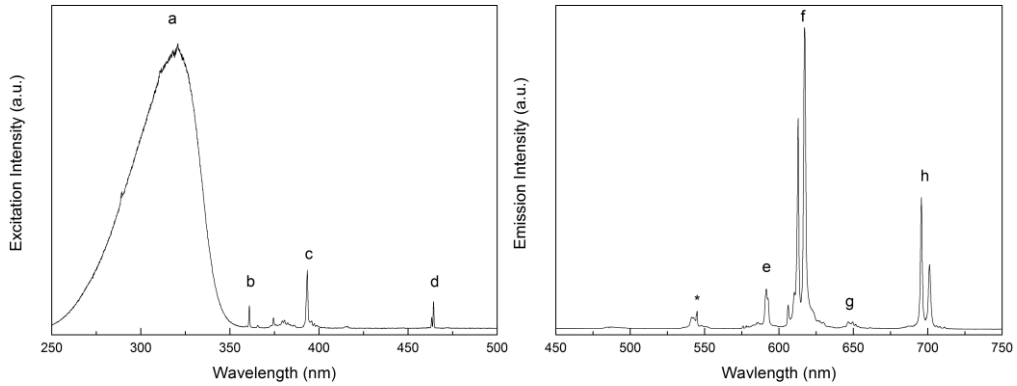

Fiigure 39. Uncorrected excitation (left) and emission spectrum (right) of the 10 wt% Y^{3+} co-doped sample. The peak assigned with * is a peak of terbium contamination.

Table 9. The labelling of the peaks of the Y^{3+} co-doped samples

Label	Wavelength (nm)	Wavenumber (cm^{-1})	Transition
a			V-O CTB
b	361.1	27693	$^5D_4 \leftarrow {}^7F_0$
c	393.6	25407	$^5L_6 \leftarrow {}^7F_0$
d	464.3	21538	$^5D_2 \leftarrow {}^7F_0$
e	591.5	16906	$^5D_0 \rightarrow {}^7F_1$
f	617.2	16202	$^5D_0 \rightarrow {}^7F_2$
g	648.4	20644	$^5D_0 \rightarrow {}^7F_3$
h	695.7	14374	$^5D_0 \rightarrow {}^7F_4$

In Figure 39, it is clear that the V-O CTB is far more intense than the peaks for the Eu^{3+} ion. This shows that this system has a good charge transfer effect and the Eu^{3+} ion is effectively excited. This system has a higher intensity of the $^5D_0 \rightarrow {}^7F_2$ transition than of the $^5D_0 \rightarrow {}^7F_1$ transition, meaning that this system has a low symmetry. The peak splitting of the $^5D_0 \rightarrow {}^7F_4$ is lower than the peak splitting of the non-co-doped (only 12.5 wt% Eu^{3+} doped) sample (see Figure 35). This means that a change in symmetry occurred when the sample was co-doped with Y^{3+} ions. As was the case for the Gd^{3+} co-doped samples, the decay time of the different doping percentages of Y^{3+} show no significant difference. The decay times are presented in Table 10 and the decay curve of the 10 wt% Y^{3+} co-doped sample is presented in Figure 40. The other decay curves are presented in Figure D14.

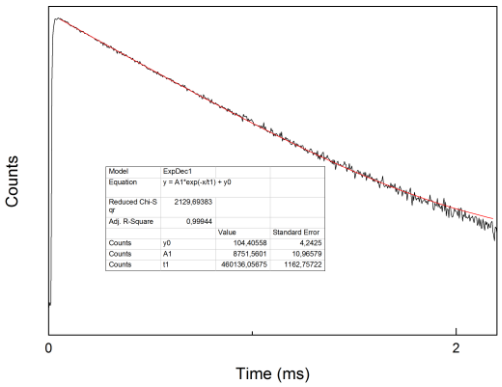

Figure 40. Decay curve of the 10 wt% Y^{3+} co-doped sample

Table 10. The decay times of the different doping percentages Y^{3+}

Doping Percentage Y^{3+}	Decay time τ
2 wt%	0.49 ms
5 wt%	0.46 ms
10 wt%	0.46 ms

6.5.3. Lu co-doping

The excitation and emission spectrum of the 10 wt% Lu^{3+} co-doped sample is presented in Figure 41. Just like the other co-doped ions, the peaks of the different transitions in the different doping percentages are on the same position. For this reason, the peaks are labelled in Figure 41 and Table 11. The other excitation and emission spectra are presented in Figure D11 and D12.

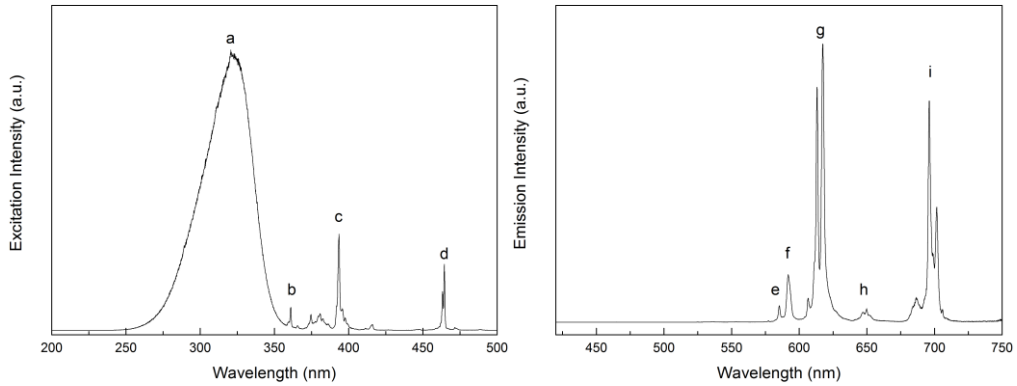

Figure 41. The uncorrected excitation (left) and emission spectrum (right) of the 10wt% Lu^{3+} co-doped sample.

For the Lu^{3+} co-doped samples, the $^5D_0 \rightarrow {}^7F_2$ transition is higher in intensity than the $^5D_0 \rightarrow {}^7F_1$ transition. This shows that these samples have a low symmetry. Since the $^5D_0 \rightarrow {}^7F_2$ transition has the highest emission intensity, the sample will emit a red light when excited under a UV-lamp. The peak splitting of the $^5D_0 \rightarrow {}^7F_4$ transition is again lower than for the only Eu^{3+} doped sample.

A comparison of the decay times of the different percentages of the co-doped ion is presented in Table 12. Only the 2 wt% Lu^{3+} co-doped sample shows a significant difference in decay time. The decay time is the highest for this doping percentages of Lu^{3+} ions. This is in

sharp contrast when compared to the emission intensity: the 2 wt% Lu^{3+} co-doped sample shows the lowest emission intensity. The decay curve of the 10 wt% Lu^{3+} co-doped sample is presented in Figure 42, the others are presented in the appendix (Figure D15).

Table 11. The labelling of the peaks of the Lu^{3+} co-doped samples

Label	Wavelength (nm)	Wavenumber (cm^{-1})	Transition
a			V-O CTB
b	361.0	27701	$^5D_4 \leftarrow {}^7F_0$
c	393.5	25413	$^5L_6 \leftarrow {}^7F_0$
d	464.5	21529	$^5D_2 \leftarrow {}^7F_0$
e	585.1	17091	$^5D_0 \rightarrow {}^7F_0$
f	592.1	16889	$^5D_0 \rightarrow {}^7F_1$
g	617.4	16202	$^5D_0 \rightarrow {}^7F_2$
h	649.8	15389	$^5D_0 \rightarrow {}^7F_3$
i	696.1	14366	$^5D_0 \rightarrow {}^7F_4$

Table 12. The decay times of the different Lu^{3+} co-doping percentages.

Doping Percentage Lu	Decay time τ
2 wt%	1.53 ms
5 wt%	0.53 ms
10 wt%	0.54 ms

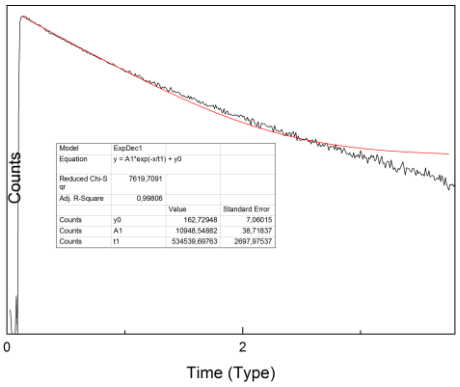

Figure 42. Decay curve of the 10 wt% Lu^{3+} co-doped sample.

7. Conclusions

A microwave-assisted synthesis route decreases the synthesis time quite drastically. In this work, it showed that the microwave-assisted route can be performed in 30 minutes, while the hydrothermal synthesis needs to be performed in 24 hours or more. However, for the $LaVO_4$ samples the tetragonal phase was never synthesized with the microwave-assisted route. Changing the reaction conditions according to literature (see the section literature study), which lead to the tetragonal product in a hydrothermal route, did not lead to a tetragonal product in the microwave-assisted synthesis route. This suggest that further research is needed to obtain the tetragonal product via a microwave-assisted synthesis. Doping the vanadate material with lanthanides is possible via a microwave-assisted synthesis. Increasing the intensity of the Eu^{3+}-doped samples was possible when co-doped with another rare-earth ion. In this work, 3 different ions were co-doped in the Eu^{3+}-doped samples, Gd^{3+} ions, Y^{3+} ions and Lu^{3+} ions. Each different ion showed an increase in emission intensity when the doping percentage was increased. Between the different ions, there was no significant change in decay time, even when the doping percentage was increased. The co-doped ions were all smaller in size than the Eu^{3+} ions. This meant that smaller ions occupied bigger holes in the crystal lattice. This causes a specific defect to be present in the crystal lattice, which can influences the emission intensity.

References

1. R. Van Deun, Advanced Inorganic Chemistry, 2014.

2. R. C. Ropp (1991), *Luminescence in the Solid State*. Amsterdam, Elsevier.

3. R. K. Datta, *Trans. Metal. Soc.AIME.,* **1967**, *239*, 355.

4. B. Shao, Q. Zhao, N. Guo, Y. Jia, W. Lv, M. Jiao, W. Lü and H. You ,*CrystEngComm*, **2014**, *16*, 152.

5. D. Ndagsi (2014), *Tuning the emission colour of rare-earth tungstate and vanadate material towards white light generation,* University of Ghent, Ghent, Belgium.

6. S.-R. Lim, D. Kang, O. A. Ogunseitan and J. M. Schoenung, Environ. Sci. Technol., **2013**, *47*, 1040.

7. J. Liu and Y. Li, *Adv. Mater.*, **2007**, *19*, 1118.

8. L. Li, M. Zhao, W. Tong, X. Guan, G. Li and L. Yang, *Nanotechnology,* **2010**, *21*, 195601.

9. J. Vuojola and T. Soukka, Methods Appl. Fluoresc., 2014, 2, 012001.

10. A. F. Wells (1984), *Structural Inorganic Chemistry, 5th ed*.; Clarendon Press: Oxford.

11. M. Seth, M. Dolg, P. Fulde and P. Swherdtfeger, *J. Am. Chem. Soc.*, **1995**, *117*, 6597.

12. S. I. Weissman, *J. Chem. Phys*., **1942**, *10*, 214.

13. G. A. Crosby, R. E. Whan and R. M. Alire, *J. Chem. Phys*., **1961**, *34*, 743.

14. M. H. Werts, M. A. Duin, J. W. Hofstraat and J. W. Verhoeven, *Chem. Commun.*, **1999**, *1999*, 799.

15. Beeby A et al, *J. Chem. Soc., Perkin Trans.,* **1999**, *2*, 493.

16. S. Lis, *J. Alloys Compounds*, **2002**, *341*, 45.

17. A. Huignard, T. Gacoin and J. P. Boilot, *Chem. Mater.*, **2000**, *12*, 1090.

18. A. K. Levine and F. C. Papilla, *Electrochem. Tech.*, **1966**, *4*, 16.

19. R. C. Ropp and R. Oakley, Ger. Pat., 2056172, 1971.

20. S. Erdei, *J. Mater. Sci.*, **1995**, *30*, 4950.

21. S. Erdei, N. M. Rodriguez, F. W. Ainger, W. B. White, D. Ravichandran and L. E. Cross, *J. Mater. Chem.*, **1998**, *8*, 99.

22. A. Huignard, T. Gacoin and J. P. Boilot, *Chem. Mater.*, **2000**, *12*, 1090.

23. R. C. Ropp, B. Carroll, *J. Inorg. Nucl. Chem.***1977**, *39*, 1303.

24. H. Wu, H. Xu, Q. Su, T. Chen and M. Wu, *J. Mat. Chem.*, **2003**, *13*, 1223.

25. C.- J. Jia, L. D. Sun, F. Luo, X. C. Jiang, L. H. Wei and C. H. Yan, *Applied Phyics Letters,* **2004**, *84,* 5305.

26. H. M. Zhang, J. B. Liu, H. Wang, W. X. Zhang and H. Yan, *J. Nanopart. Res.,* **2008**, *10,* 767.

27. B. Shao, Q. Zhao, N. Guo, Y. Jia, W. Lv, M. Jiao, W. Lü and H. You, *Cryst. Eng. Comm.,* **2014**, *16,* 152.

28. A. A. Ansari, M. Alam, J. P. Labis, S. A. Alrokayan, G. Shafi, T. N. Hasan, N. A. Syed and A. A. Alshatwi, *J. Mater. Chem.,* **2011**, *21,* 19310.

29. L.-P. Wang and L.-M. Chen, *Materials Characterization*, **2012**, *69*, 108.

30. S. Tang, M. Huang, F. Wang, F. Yu, G. Shang and J. Wu, *Journal of Alloys and Compounds,* **2012**, *513,* 474.

31. A. Vecht, C. Gibbons, D. Davies, X. Jing, P. Marsh, T. G. Ireland, J. Silver and A. Newport, *J. Vac. Sci. Technol. B,***1999**, *17*, 750.

32. Y. D. Jaing, Z. Wang, F. Zhang, H. G. Paris and C. J. Summers, *J. Mater. Res.,***1998**, *13*, 2950.

33. H. Lu, G. Yi, S. Zhao, D. Chen, L. Guo and J. Cheng, *J. Mater. Chem,***2004**, *14*, 1336.

34. R. G Chauduri and S. Paria,*Chem Rev.*, **2012**, *112*, 2373.

35. K. Kömpe, H. Borchert, J. Storz, A. Lobo, S. Adam, T. Möller and M. Haase, *Angw. Chem. Int. Ed.*, **2003**, *42*, 5513.

36. J. R. DiMaio, C. Sabatier, B. Kodouz and J. Ballato, *J. Proc. Natl. Acad. Sci. U.S.A., **2008**, 105,* 1809.

37. Y. Wang, L. Tu, J. Zhao, Y. Sun, X. Kong and H. Zhang*, J. Phys. Chem., **2009**, 113,* 7164.

38. . S. S. Yi, J. S. Bae, B. K. Moon, J. H. Jeong and J. H. Kim*, Opt. Mater., **2006**, 28,* 610.

39. J. Ballato, R. E. Riman and E. Snitzer, *Opt. Lett.*, **1997**, *22*, 691.

40. M.- Y. Xie, L. Yu, H. He, X.-F. Yu, *J. Solid State Chem,* **2009**, *182*, 597.

41. A. Imhof, *Langmuir*, **2001**, *17*, 3579.

42. M. Ocana, W. P. Hsu and E. Matijevic, *Langmuir*, **1991**, *7*, 2911.

43. P. A. Dresco, V. S. Zaitsev, R. J. Gambino and B. Chu, *Langmuir*, **1999**, *15*, 1945.

44. H. Zou, S. Wu and J. Shen, *Chem Rev.*, **2008**, *108*, 3393.

45. G. Hota, S. Idage and K. C. Khilar, *Colloids Surf. A*, **2007**, *293*, 5.

46. M. Y. Han, W. Huang C. H. Chew, L. M. Gan, X. J. Zhang and W. Ji, *J. Phys. Chem. B*, **1998**, *102*, 1884.

47. T. Li, J. Moon, A. A. Morrone, J. J. Mecholsky, D. R. Talham and J. H Adair, *Langmuir*, **1999**, *15*, 4328.

48. C. Song, W. Yu, B. Zhao, H. Zhang, C. Tang, K. Sun, X. Wu, L. Dong and Y. Chen, *Catal. Commun.*, **2009**, *10*, 650.

49. U. Rambabu, D. P. Amalnerkar, B. B. Kale, and S. Buddhudu, *Mater. Res. Bull.*, **2000**, *35*, 929.

50. J. R. DiMaio, B. Kokuoz and J. Ballato, *Optical Express,* **2006**, *14*, 11412..

51. M. Maqbool, M. E. Kordesch and A. Kayani, *J. Opt. Soc. Am. B*, **2009**, *26*, 998.

52. J. C. Park, H. K. Moon, D. K. Kim, S. H. Byeon, B. C. Kim and K. S. Suh, *Appl. Phys. Lett.*, **2000**, *77*, 2162.

53. T. Hatayama, S. Fukumoto and S. Ibuki, *Jpn. J. Appl. Phys.*, **1992**, *31*, 3383.

54. H. K. Yang, K. S. Shim, B. K. Moon B. C. Choi, J. H. Jeong, S. S. Yi and J. H. Kim, *Thin Solid Films*, **2006**, *516*, 5577.

55. S. W. Park, H. K. Yang, J. W. Chung, B. K. Moon, B. C. Choi, J. H. Jeong, K. Jang, H. S. Lee and S. S. Yi, *J. Korean Physical Society*, **2010**, *57*, 1764.

56. J. S. Bae, S. S. Park, T. E. Hong, J. P. Kim, J. H. Yoon, E. D. Jeong, M. S. Won and J. H. Jeong, *Current Appl. Phys.*, **2009**, *9*, S241.

57. C.-P. Sherman Hsu, Ph.D., *Handbook of Instrumental Techniques for Analytical Chemistry*, Prentice-Hall, New Jersey, **1997**, 262.

58. Z. Hens, I. Van Driessche and P. Van der Voort, Solid State Chemistry, 2013.

59. D. Depla, Kristalchemie, 2011.

60. A. Adriaens and H. Teryn, Surface analysis, 2012.

61. Burgess, Jeremy (1987). *Under the Microscope: A Hidden World Revealed*. CUP Archive. p. 11. ISBN 0521399408.

62. G. Lohmueller, G. Schmidt, B. Deppisch, V. Gramlich and C. Scheringer, *Acta Cryst. B*, **1973**, *29*, 141.

63. W. O. Milligan and L. W. Vernon, *J. Phys. Chem.*, **1952**, *56*, 145.

64. C. E. Rice and W. R. Robinson, *Acta Cryst. B*, **1976**, *32*, 2232.

65. Y. Oka, T. Yao and N. Yamamoto, *J. Solid State Chem.*, **2000**, *152,* 486.

66. *IR spectrum of Glycerine*. Retrieved from http://tera.chem.ut.ee/IR_spectra/index.php?option=com_content&view=article&id=109&Itemid=76.

67. C.-J. Jia, L.-D. Sun, Z.-G. Yan, Y.-C. Pang, S.-Z. Lü and C.-H. Yan, *Eur. J. Inorg. Chem.*, **2010**, 2626.

Appendix A. Used Chemicals

The used chemicals are yttrium nitrate ($Y(NO_3)_3.6H_2O$, 99.9%, Sigma Aldrich), gadolinium nitrate ($Gd(NO_3)_3.6H_2O$, 99.9%, Sigma Aldrich), lanthanum nitrate ($La(NO_3)_3{\cdot}6H_2O$, >98%, Acros Organics), lanthanum nitrate ($La(NO_3)_3.6H_2O$, 99.9%, Merck), europium nitrate ($Eu(NO_3)_3.6H_2O$, 99.9% Alfa Aesar), lutetium nitrate ($Lu(NO_3)_3{\cdot}6H_2O$, 99.9%, Sigma Aldrich), sodium orthovanadate (Na_3VO_4, 99.98%, Sigma Aldrich), ammonium orhtovanadate (NH_4VO_3, >99.0%, Sigma Aldrich), glycerol (99.9%, BDH Laboratory Supplies), nitric acid (69%, Merck), nitric acid (65%, Acros Organics), ammonia solution (28-30%, NH_3 basis), ethanol (96%, VWR Chemicals) and sodium hydroxide (pellets, Laborimpex).

Appendix B. Equipment and Techniques

1. Diffuse Reflectance Infrared Fourier Transform Spectroscopy (DRIFTS)[57, 58]

This is a spectroscopic technique, meaning that the absorbance or transmittance of the light is measured in function of the used frequency of the light. Spectroscopic techniques can be used to identify the sample since all the atoms have a specific wavelength for which they absorb the light. This absorbance/transmittance can be measured for each wavelength sequentially. This technique is called a dispersive technique, which is used in traditional IR measurements. This is rather slow compared to Fourier transform techniques, which measure the absorbance/transmittance of all the wavelengths simultaneously. The light will not only transmit through the sample but will also reflect of the surface. There are two types of reflections: specular and diffuse reflection. Unlike the specular reflection, were the light is reflected at one specific angle (which can be described like a mirror-like reflection), diffuse reflection occurs at different angles.

In this technique, powder samples can be measured. These samples do not need any preparation prior to the measurement. To obtain a good background, this sample is mixed with potassium bromide, a non-absorbing support material. The power sample has a rough surface, therefor diffuse reflection will occur. These reflection will be collected using mirrors. The light source in DRIFTS is polychromatic and to obtain isolated wavelengths, a Michelson Interferometer is used.

In order for the most molecules to be in their lowest vibrational state, the measurement was performed under vacuum and at room temperature. A Thermo Scientific FT-IR spectrometer (type Nicolet 6700) equipped with a DRIFTS cell was used. The measurement range was 650-4000 cm^{-1} with a resolution of 4 cm^{-1}.

2. Powder X-Ray Diffraction(powder XRD)[59, 60]

In this technique the powder samples are irradiated with X-rays. The X-rays are generated by an X-ray tube. This is a vacuum tube in which electrons are generated by applying a high voltage to a cathode filament. The temperature of the cathode will increase due to the voltage, and at a certain point will eject electrons. These electrons are then accelerated to the anode material (cupper is mostly used for crystallography) with a high velocity. Upon collision, these high velocity electrons will then generate the X-rays. The generated X-rays can be divided into classes dependant on the processes of X-ray generation: characteristic X-

rays and Bremsstrahlung. The characteristic X-rays are generated when the high velocity electron knock out an electron out of a valence shell on the anode material. The name of each line can be named and depends on the valence shell in which an electron is knocked out. An electron from upper shells needs to fall back and this process will generate an X-ray. When an electron is kicked out from the K-shell, the generated X-rays are called K lines. When the electron is kicked out of the L- shell, these X-rays are called L lines and so on. These lines are dependent on the kind of anode material used. Bremsstrahlung is generated when the high velocity electron is deflected by the nuclei of the atom. This will cause the electrons to lose some of their kinetic energy. This lost energy is converted into X-rays which have a continuous spectrum, unlike the characteristic X-rays.

Crystalline materials have well defined lattice parameters and are ordered in two or three dimensions. When X-rays are irradiated onto the surface of such a material, part of these rays will be scattered on the surface. The other part can penetrate the material and will scatter on atoms in the next atom layer. This can cause diffraction of the X-rays to happen. The diffraction pattern is dependent on the crystal structure of the sample. For diffraction to actually happen, the scattered X-rays from different atom layers must be in phase (constructive interference). This constructive interference, and by extend the diffraction of the X-rays, can only happen when Bragg's Law is fulfilled ($\sin\theta = n\lambda/2d$ where θ is the angle of the incident X-ray, n is the order of diffraction (an integer), λ is the wavelength of the X-ray and d is the spacing between atom layers). As one can see in Bragg's Law, diffraction will happen when the material has a regular structure. This means that only crystalline material will have these characteristic diffraction patterns. In a powder XRD, the relative intensities are plotted in function of 2θ. This spectrum can be used to identify the crystal structure of the material: databases were made which recorded the spectra of known pure-phased materials. The database used to compare the samples with in order do find the right phase was the ICSD crystallographic database.

The XRD patterns were recorded by a Thermo Scientific ARL X'TRA diffractometer with a CuKα source (with a wavelength of 1.5405 Å), a goniometer and a Peltier cooled Si(Li) solid state detector.

3. Scanning electron microscopy (SEM)[60, 61]

Scanning Electron Microscopy can be used to look at the samples with very high magnifications. The sample is scanned with a focused beam of electrons in a raster-like way. This technique is very similar to an optical microscope, but here the lenses are electromagnetic lenses to focus the electrons and cause the magnification. Electrons can interact in different manners with matter, which will give different types of information on the sample. Since X-rays can be generated, SEM can be used not only as microscope, but it can give a chemical analysis of the sample. Still SEM is mostly used for imaging. To obtain an image, the sample first needs to undergo preparations. First, the sample must be able to be placed in the holder, therefore the sample must be small enough, or fine enough if a powder is used. Secondly, if the surface of the sample is not conductive, it must be coated with a conductive layer. This can be done with various materials, but gold is still the most used material to form the conductive layer. To form the image, the secondary electrons generated by the electron beam are detected. These secondary electrons have low energies. This means that these electrons come of the first few nm of the surface, otherwise more higher energies are required.

The SEM images were recorded by a FEI Quanta 200 F SEM and a FEI Nova 600 Nanolab Dual-Beam focused ion beam in secondary electron mode.

4. Luminescence setup[1]

To measure the luminescence properties of the materials, a luminescence setup was used. The setup for steady-state measurements uses a xenon-lamp as source of excitation. For time resolved measurements, a pulsed beam at a fixed wavelength was used as the excitation source. Since a xenon-lamp emits a continuous spectrum and in order to filter one specific wavelength out of it, monochromators are used. The setup comes with different monochromators which can be used for different wavelengths. Different detectors are also available (dector for Vis and NIR) depending on the emitting wavelength of the measured lanthanide.

To record an excitation spectrum, the emission monochromator is fixed at a certain wavelength. This wavelength is normally the most intense emission peak. To find this peak, a quick scan is made in the wavelength range where this peak is to be expected (the wavelength of the emission peaks of lanthanide can predicted, since the lanthanides 4f

electrons are shielded and therefore are little influenced by the environment). This quick scan will determine the wavelength of the most emissive peak and a full scan can be made.

The same principle applies to the emission spectrum, but here the excitation monochromator is fixed at a certain wavelength. First the quick scan is made to determine at which wavelength the monochromator must be fixed at and then a full scan is made.

To determine the decay time of the luminescence, a short-lived excitation source is used. The material is thus irradiated for a short amount of time and the photons of a certain wavelength are measured in function of time. The decay was measured for 60 seconds. To obtain the decay time, the obtained curve needs to be fitted, either to single or higher exponential equation.

Single exponential tail fit $I = A_0 e^{-\frac{t}{\tau}}$

Double exponential tail fit $I = A_1 e^{-\frac{t}{\tau 1}} + A_2 e^{-\frac{t}{\tau 2}}$

The average life time $< \tau > = \frac{(A_1 {\tau_1}^2 + A_2 {\tau_2}^2)}{(A_1 \tau_1 + A_2 \tau_2)}$

With *I* for the intensity at time t, A_0 the intensity at time t = 0 and τ the lifetime of the material.

As explained in the literature study, the f-f transitions needed to excite the lanthanide are Laporte forbidden. Therefore other means of excitation are often chosen. This can be done by using the charge transfer effect from our ligand. For vanadates, there is a broad charge transfer band from the 2p orbitals of the oxygen to the 5d orbitals of the vanadium. This broad peak has its maximum intensity around 320 nm. This means, that the material can be excited through this charge transfer band.

Luminescent measurements were performed on an Edinburgh Instruments FLP920 spectrometer. Steady-state measurements can be performed in the range 250-1700 nm. This was done with a 450W xenon lamp and with a Hamamatsu R928P PMT detector for the 200-870 nm range. Time-resolved measurements of 100 µs – several seconds were recorded with a µF920H 60W microsecond xenon flash-lamp: 0.1-100 Hz, pulse width ± 2 µs and the same photomultiplier detector.

Appendix C. DRIFTS

The capping agent in this work was glycerol. Some of the DRIFTS spectra in this work often showed peaks of glycerol. Here, a DRIFTS spectrum of glycerol is presented for the ease of comparing these extra peaks with the peaks of pure glycerol.

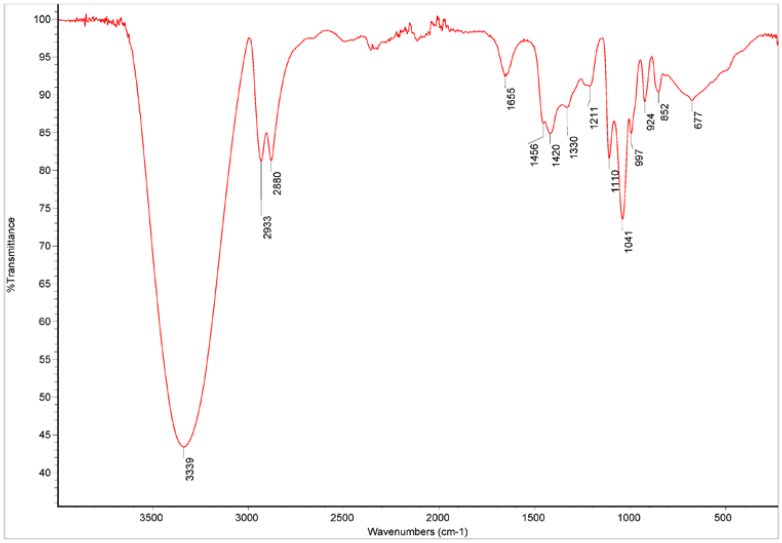

Figure C1. DRIFTS spectrum of glycerol

Appendix D. Luminescence measurements

All the samples which were measured by the luminescence setup were heat treated at 900°C for 3 hours.

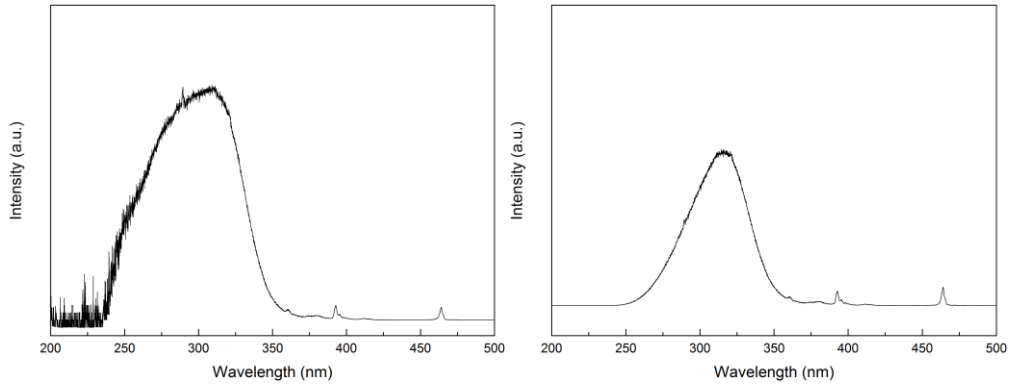

Figure D1. The corrected (left) and uncorrected (right) excitation spectrum of the 2.5 wt% Eu^{3+}-doped sample.

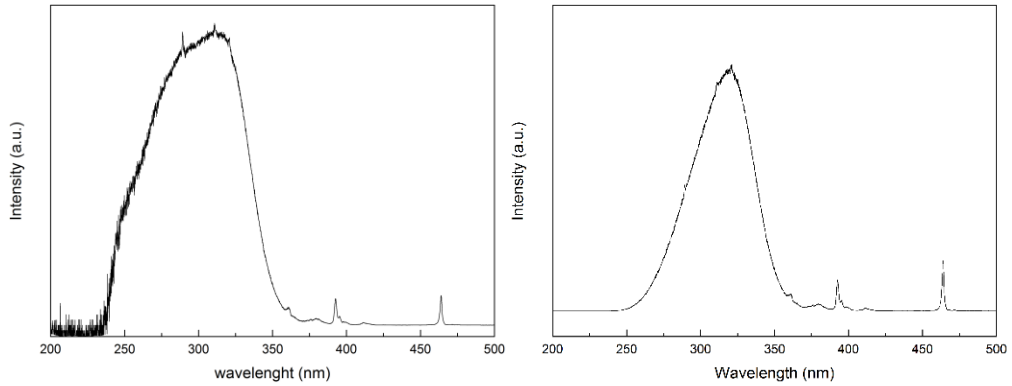

Figure D2. The corrected (left) and uncorrected (right) excitation spectrum of the 5 wt% Eu^{3+}-doped sample.

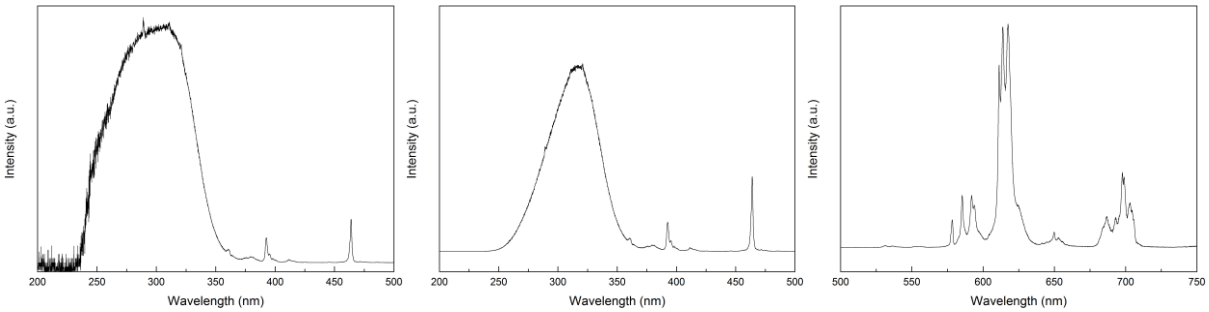

Figure D3. The corrected (left) and uncorrected (middle) excitation spectrum and the emission spectrum (right) of the 10 wt% Eu^{3+}-doped sample.

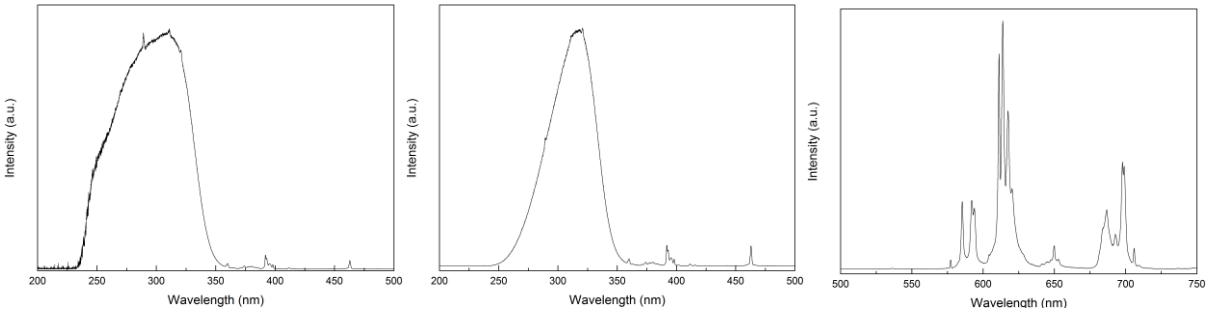

Figure D4. The corrected (left) and uncorrected (middle) excitation spectrum and the emission spectrum (right) of the 12.5 wt% Eu^{3+}-doped sample.

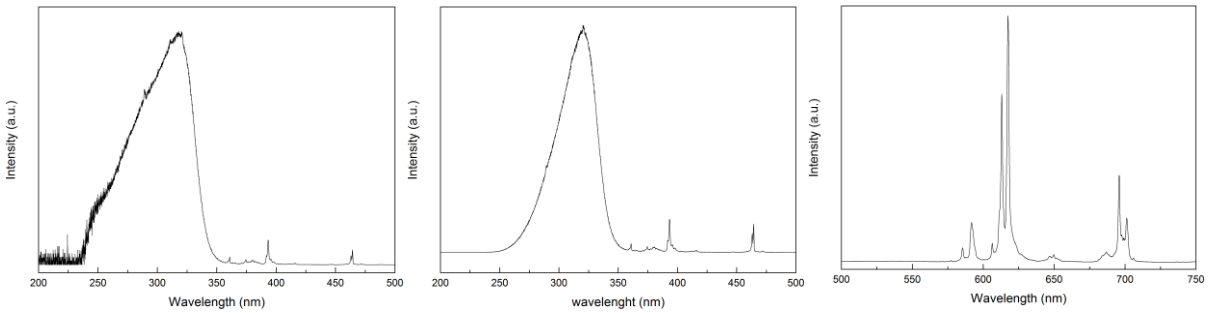

Figure D5. The corrected (left) and uncorrected (middle) excitation spectrum and the emission spectrum (right) of the 15 wt% Eu^{3+}-doped sample.

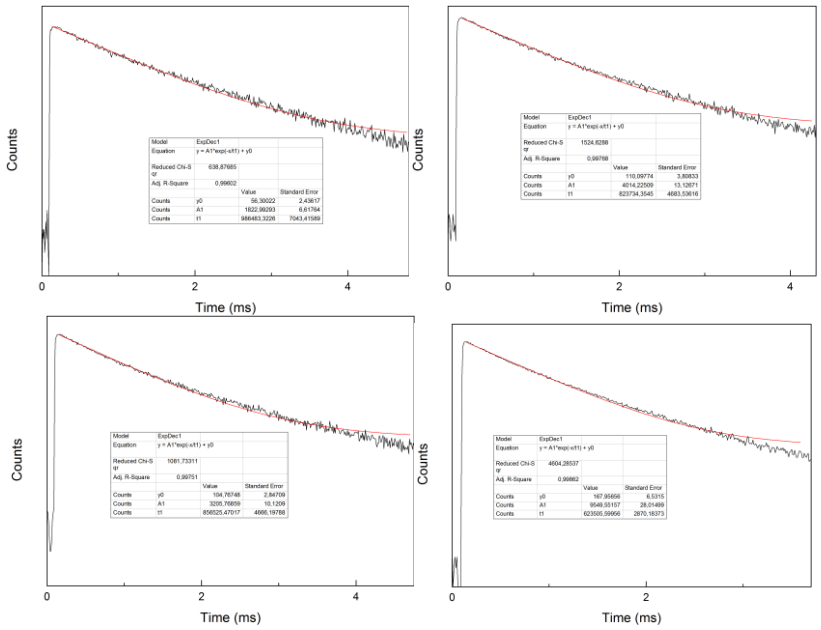

Figure D6. Decay curves of the 2.5 wt% (top left), 5 wt% (top right), 10 wt% (bottom left) and 15 wt% Eu-doped samples (bottom right).

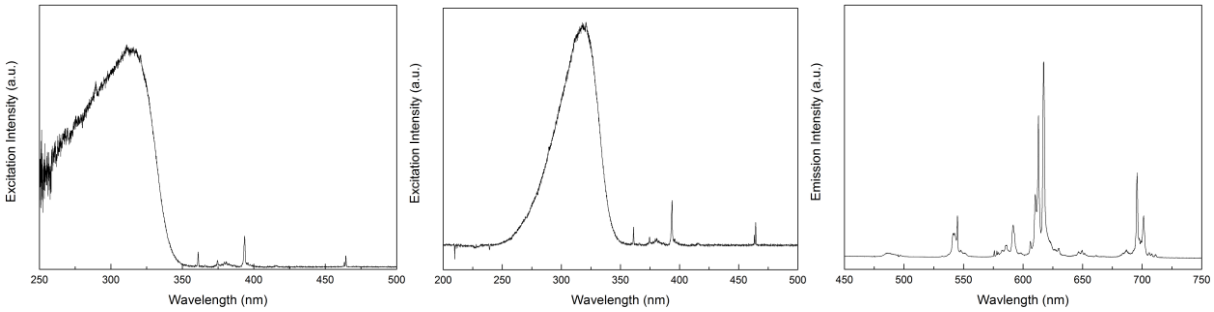

Figure D7. The corrected excitation (left), uncorrected excitation (middle) and emission spectra (right) of the 2 wt% Gd^{3+} co-doped sample.

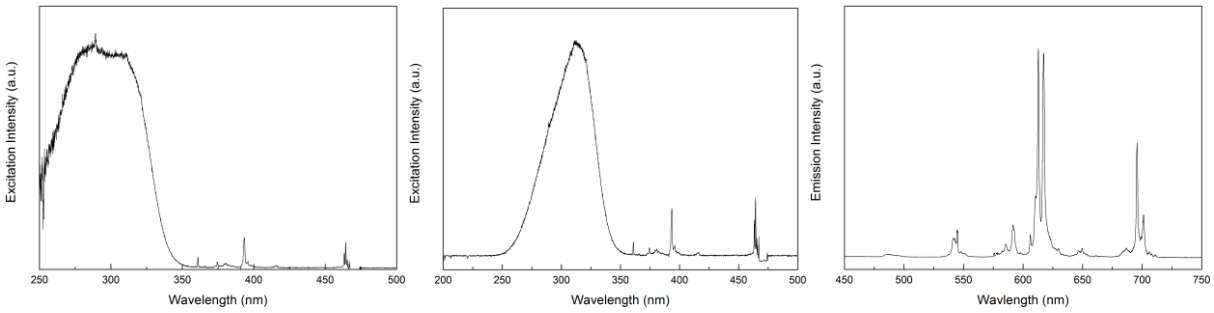

Figure D8. The corrected excitation (left), uncorrected excitation (middle) and emission spectra (right) of the 5 wt% Gd^{3+} co-doped sample.

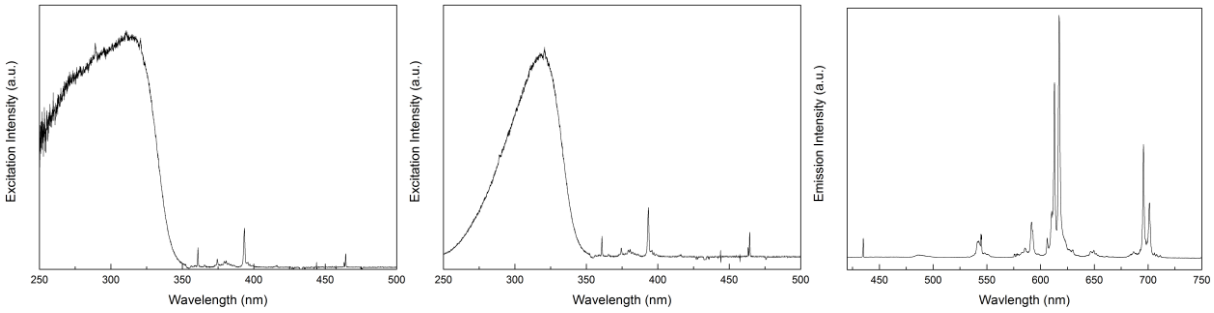

Figure D9. The corrected excitation (left), uncorrected excitation (middle) and emission spectra (right) of the 2 wt% Y^{3+} co-doped sample.

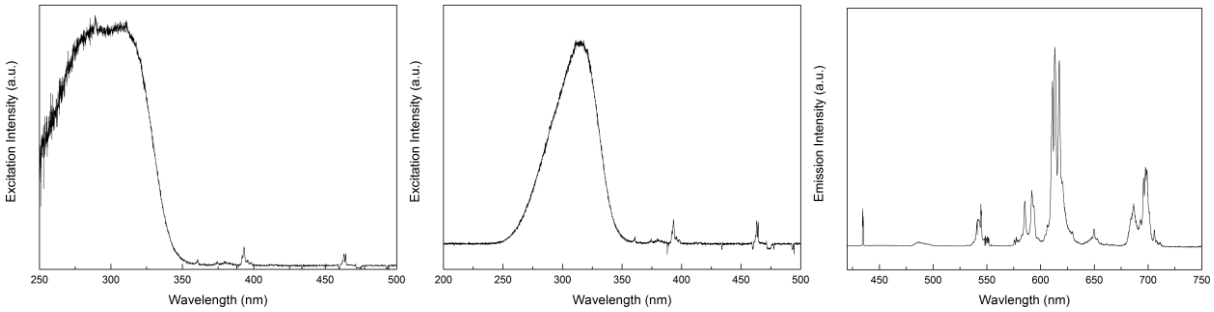

Figure D10. The corrected excitation (left), uncorrected excitation (middle) and emission spectra (right) of the 5 wt% Y^{3+} co-doped sample.

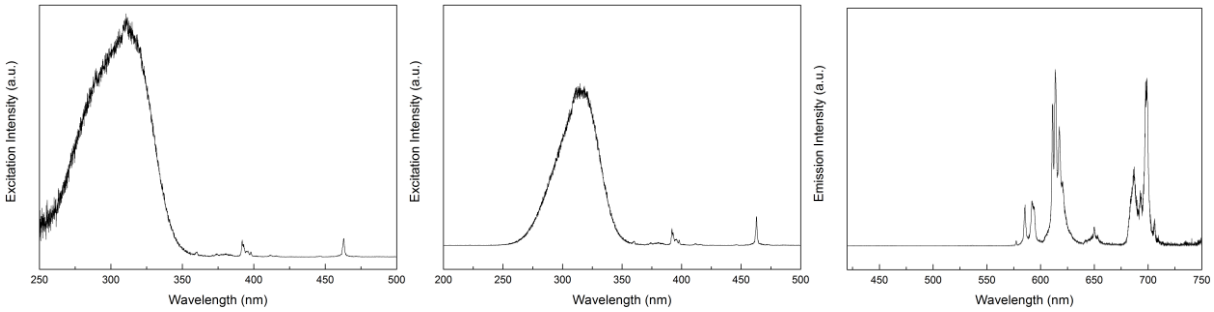

Figure D11. The corrected excitation (left), uncorrected excitation (middle) and emission spectra of the 2 wt% Lu^{3+} co-doped sample.

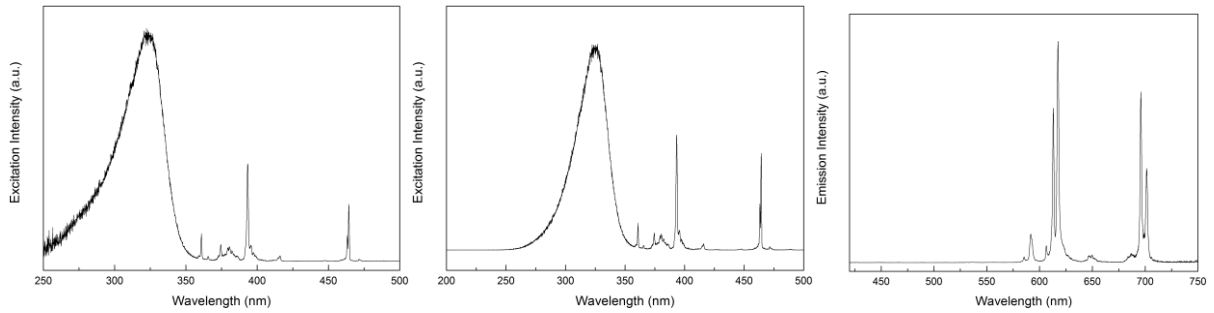

Figure D12. The corrected excitation (left), uncorrected excitation (middle) and emission spectrum of the 5 wt% Lu^{3+} co-doped sample.

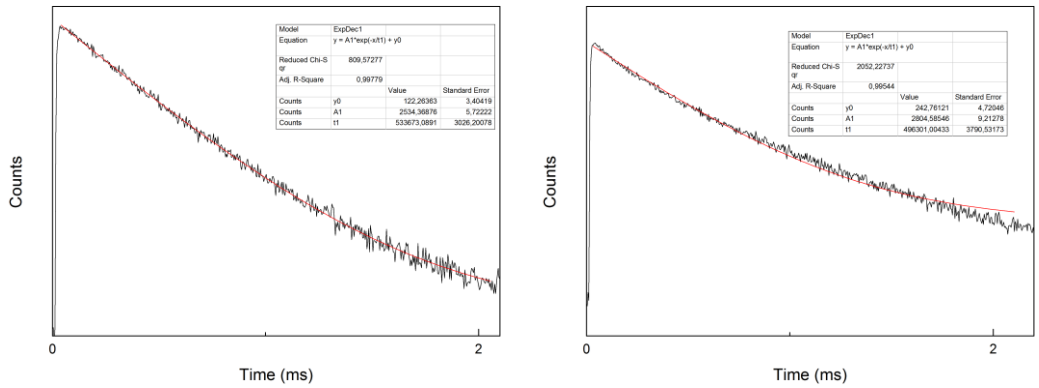

Figure D13. The decay curves of the 2 wt% (left) and 5 wt% Gd^{3+} co-doped sample.

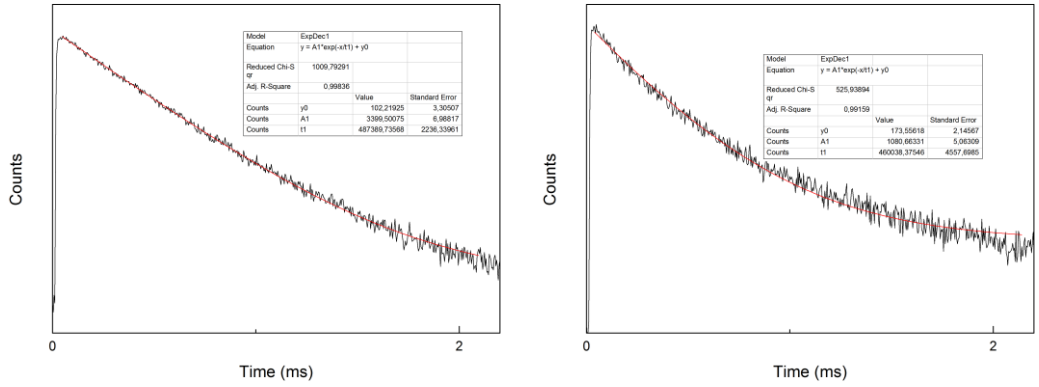

Figure D14. The decay curves of the 2 wt% (left) and 5 wt% Y^{3+} co-doped sample.

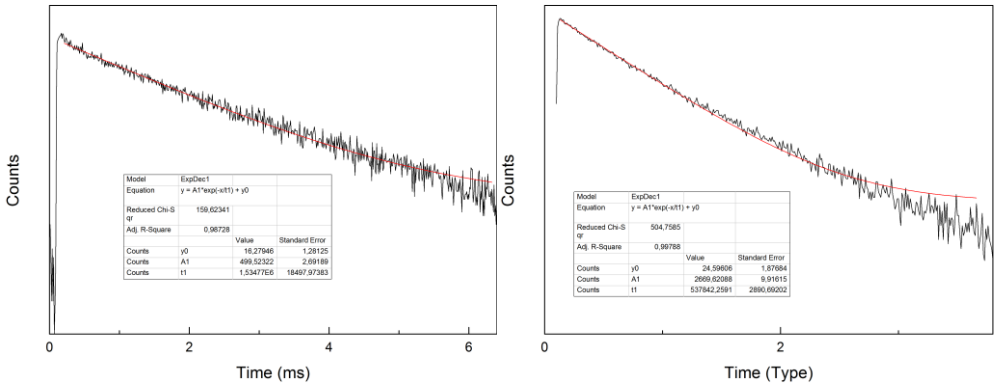

Figure D15. The decay curves of the 2 wt% (left) and 5wt% (right) Lu^{3+} co-doped sample.